
The C¹⁸O core mass function toward Orion A: Single-dish observations

Hideaki TAKEMURA^{1,2}, Fumitaka NAKAMURA^{1,2,3}, Shun ISHII^{1,2}, Yoshito SHIMAJIRI², Patricio SANHUEZA^{1, 2}, Takashi TSUKAGOSHI², Ryohei KAWABE^{1,2}, Tomoya HIROTA^{1,2}, Akimasa KATAOKA^{1,2}

¹The Graduate University for Advanced Studies (SOKENDAI), 2-21-1 Osawa, Mitaka, Tokyo 181-0015, Japan

²National Astronomical Observatory of Japan, 2-21-1 Osawa, Mitaka, Tokyo 181-8588, Japan

³Department of Astronomy, The University of Tokyo, Hongo, Tokyo 113-0033, Japan

Received (reception date); Accepted (acceptation date)

Abstract

We have performed an unbiased dense core survey toward the Orion A Giant Molecular Cloud in the C¹⁸O ($J = 1-0$) emission line taken with the Nobeyama Radio Observatory (NRO) 45-m telescope. The effective angular resolution of the map is $26''$, which corresponds to ~ 0.05 pc at a distance of 414 pc. By using the *Herschel–Planck* H₂ column density map, we calculate the C¹⁸O fractional abundance and find that it is roughly constant over the column density range of $\lesssim 5 \times 10^{22}$ cm⁻³, although a trend of C¹⁸O depletion is determined toward higher column density. Therefore, C¹⁸O intensity can follow the cloud structure reasonably well. The mean C¹⁸O abundance in Orion A is estimated to be 5.7×10^{-7} , which is about 3 times larger than the fiducial value. We identified 746 C¹⁸O cores with *astrodendro* and classified 709 cores as starless cores. We compute the core masses by decomposing the *Herschel–Planck* dust column density using the relative proportions of the C¹⁸O integrated intensities of line-of-sight components. Applying this procedure, we attempt to remove the contribution of the background emission, i.e., the ambient gas outside the cores. Then, we derived mass function for starless cores and found that it resembles the stellar initial mass function (IMF). The CMF for starless cores, dN/dM , is fitted with a power-law relation of M^α

with a power index of $\alpha = -2.25 \pm 0.16$ at the high-mass slope ($\gtrsim 0.44 M_{\odot}$). We also found that the ratio of each core mass to the total mass integrated along the line of sight is significantly large. Therefore, in the previous studies, the core masses derived from the dust image are likely to be overestimated at least by a factor of a few. Accordingly, such previous studies may underestimate the star formation efficiency of individual cores.

1 Introduction

Stars are formed in dense cores embedded in molecular clouds. Therefore, it is important to understand how dense cores form from parental molecular clouds. Previous studies of nearby low-mass star-forming regions have suggested that a typical dense core has its mass of 1–10 M_{\odot} , size of 0.01–0.1 pc, and density of 10^{4-5} cm^{-3} (Bergin & Tafalla 2007). Since the evolutionary processes of stars are partly determined by their masses at birth, it is important to reveal the origin of the mass distribution of dense cores in molecular clouds. Thus, the mass functions of dense cores (Core Mass Functions, CMFs) are expected to imprint some information on their formation and evolution processes. Salpeter (1955) derived the stellar initial mass function (IMF) for nearby stars and he discovered that the IMF has a power-law shape of $dN/dM \propto M^{-2.35}$ at the high-mass end ($\gtrsim 1 M_{\odot}$).

Both the CMF and IMF are often characterized by their slopes at the high-mass ends ($\gtrsim 1 M_{\odot}$) and the turnover masses at the low-mass part of the distributions. Many previous studies toward nearby star-forming regions have suggested that the CMF has a Salpeter-like slope at the high-mass end and resembles the IMF (Motte et al. 1998; Alves et al. 2007; Könyves et al. 2010). This resemblance of the CMF and IMF appears to suggest that the identified cores are the immediate precursors of stars. One fundamental difference, however, between the CMF and the IMF is the turnover mass, i.e., the peak at the low-mass part. Observed CMFs usually have larger turnover masses than observed IMFs (Alves et al. 2007; Nutter & Ward-Thompson 2007; Könyves et al. 2010). The previous studies proposed that this difference is consistent with the idea that about half of each core mass is blown out by stellar feedback such as protostellar outflows and stellar winds (Matzner & McKee 2000; Alves et al. 2007). However, recent observations of CMF in the W43-MM1 high-mass star-forming region revealed a CMF with a shallower slope. This might indicate that the CMFs evolve with time (Motte et al. 2018). On the other hand, Bontemps et al. (2001) revealed that the CMF in ρ Oph has

a turnover mass similar to that of the mass function of Class II objects in this region. This indicates that almost all the core masses should go into the stars formed. Ikeda et al. (2007) discussed the effect of confusion among cores on CMF in Orion A, especially to the low-mass part. They claimed that there is no turnover in confusion-corrected CMF and the observed turnover is not made by any physical processes.

Most of the previous studies on the CMFs have used the dust continuum emission (Motte et al. 1998; Alves et al. 2007; Nutter & Ward-Thompson 2007; Könyves et al. 2010; Motte et al. 2018; Liu et al. 2018; Kong 2019; Sanhueza et al. 2019). In general, the dust emission is optically thin on the cloud scale and thus it is an excellent tracer of the cloud column density since the spatial variation of the dust-to-gas mass ratio is believed to be small. However, a core is a dense structure embedded in the parent cloud. Thus, it seems to be very difficult to accurately estimate the core masses from the 2D dust emission maps. In other words, it is crucial to estimate the core masses by removing the ambient gas outside the core. In this paper, we call gas components that are not associated with the core along the line of sight as ambient gas. In this sense, the previous studies of the CMFs based on the dust emission and extinction maps tend to overestimate the core masses.

In this paper, toward a full understanding of the relationship between the CMF and IMF, we attempt to identify the cores in the Orion A Giant Molecular Cloud using 3D position-position-velocity data of a wide-field C18O mapping and estimate the core masses using the *Herschel–Planck* column density map (Lombardi et al. 2014) by removing the contribution of the ambient gas. It is worth noting that previous studies have demonstrated that real structures in molecular clouds are reasonably related to the structures identified in the position-position-velocity data (Williams et al. 1994; Rosolowsky et al. 2008; Goodman et al. 2009).

Orion A is the most studied giant molecular cloud (Bally et al. 1987; Genzel & Stutzki 1989; Hillenbrand 1997; Ikeda et al. 2007; Shimajiri et al. 2011; Nakamura et al. 2012; Tatematsu et al. 2016; Hacar et al. 2017). The distance to the cloud is derived to be 414 pc based on the VLBI observations (Menten et al. 2007). Thus, it is one of the nearest GMCs. Orion A also contains the nearest ongoing high-mass star formation site in Orion Nebula Cluster. Near-infrared observations also indicate that younger populations are more abundant, i.e., star formation is accelerated (Palla & Stahler 1999). Recently, we have obtained wide-field maps of this region in ^{12}CO ($J=1-0$), ^{13}CO ($J=1-0$), and C^{18}O ($J=1-0$) with the Nobeyama 45-m telescope (Feddersen et al. 2018; Nakamura et al. 2019; Ishii et al. 2019; Tanabe et al. 2019). Among the three CO isotopologues, the C^{18}O emission is expected to trace denser structures with densities of $\sim 10^4 \text{ cm}^{-3}$. Recent studies by Pety et al. (2017) and Gratier et al. (2020)

also demonstrated that the C¹⁸O emission reasonably traces the high-column density molecular gas with $N_{\text{H}_2} \sim 10^{22} \text{ cm}^{-3}$. The wide-field H₂ column density map obtained from the *Herschel* observations, which is derived from the dust emission, is also available (Lombardi et al. 2014). Thus, Orion A is one of the suitable star-forming clouds to assess the contribution of the ambient gas mass to the core mass estimate.

This paper is organized as follows. In section 2, we present the details of the observations and data. In section 3, we describe the global distribution of the dense molecular gas with the C¹⁸O data. Then, we show the results of the core identification in section 4. Here, we adopt Dendrogram and define a leaf as a core, following the previous studies. In section 5, we present the CMF derived from the C¹⁸O data. We also compare our results with previous studies of the CMF in Orion A. In section 6, we compare the CMF derived from the C¹⁸O data and dust continuum emission (Nutter & Ward-Thompson 2007). Finally, we briefly summarize our results in section 7.

2 Observations and data

2.1 C¹⁸O ($J=1-0$)

We carried out On-The-Fly (OTF) mapping observations of C¹⁸O ($J = 1-0$, 109.782182 GHz) toward Orion A using the FOREST (Minamidani et al. 2016) receivers mounted on the NRO 45-m telescope. Our map covers 1×2 square degree area which contains OMC-1/2/3/4, L1641N, and V380 Ori. Figure 1 shows the observed area of the C¹⁸O emission overlaid on the H₂ column density map obtained with the procedure described in the next subsection.

The details of the FOREST observations are described in Nakamura et al. (2019). In brief, the observations were done in the period from 2016 March to 2017 March. The telescope beam size (HPBW) is $\sim 15''$ at 110 GHz and the typical pointing accuracy was $3''$. The effective angular resolution of the data product is $\sim 21''$ (FWHM) after convolving by a spherical function with a spatial grid size of $7.''5$. In this paper, the data was additionally smoothed to reduce the noise level of the map. The C¹⁸O map has an effective resolution of $\sim 26.''4$ (FWHM), corresponding to ~ 0.05 pc at a distance of 414 pc, and a velocity resolution of $\sim 0.1 \text{ km s}^{-1}$. The typical rms noise level of the C¹⁸O data is $1\sigma = 0.33 \text{ K}$ in the unit of T_{MB} . It is worth noting that the original map provides a higher angular resolution of $\sim 21''$, but we smoothed the data to a lower angular resolution to reduce the noise level. We used the data taken only with the FOREST receiver in this paper. Ikeda & Kitamura (2009) derived CMF in a square degree area of Orion A from C¹⁸O ($J=1-0$) observations with the comparable

resolution taken by the same telescope. We compare the result of our analysis with (Ikeda & Kitamura 2009) in section 5.3. Our observations cover a larger area of $1 \times 2^\circ$ than that of Ikeda & Kitamura (2009), who conducted the mapping observations toward the Orion Nebula Cluster region in a full-beam sampling mode with a previous receiver, BEARS, and the noise level of our map (0.33 K) is better than theirs (0.45K). The velocity resolution of $\sim 0.1 \text{ km s}^{-1}$ is almost similar to each other. The integrated intensity map of the C^{18}O ($J = 1-0$) emission is shown in figure 2 (a).

2.2 H_2 column density data

We also used the *Herschel-Planck* H_2 column density map (Lombardi et al. 2014; Stutz & Kainulainen 2015) to calculate the core masses. The original Herschel data have an effective angular resolutions of 18 and $36''$ at the 250 and 500 μm , respectively. The temperature map with $36''$ and 250 μm continuum emission map with $18''$ are used to make the column density map. See Stutz & Kainulainen (2015) for the actual procedure.

Then, we smoothed the $18''$ data to match the C^{18}O effective angular resolution of $26''.4$, with a grid of $7''.5$.

2.3 Catalog of young stellar objects (YSOs)

In order to distinguish starless cores from protostellar cores, we used a catalog of YSOs from the Herschel Orion Protostar (HOP) Survey (Furlan et al. 2016). This catalog contains 36 Class 0 sources and 38 Class I sources in our observed area. In this paper, we use the 74 Class 0 and Class I sources as HOPS YSOs.

3 Global distribution of the C^{18}O emission

Figure 2 (b) and (c) show the maps of the intensity weighted velocity and the velocity dispersion of Orion A. The C^{18}O emission well follows the long filamentary structure, which includes the OMC-1/2/3/4 regions, called the Intengral-shaped Filament (ISF). Also, there is a velocity gradient along the ISF. The northern region has a velocity of $\sim 12 \text{ km s}^{-1}$ and the southern region such as L1641N has a velocity of $\sim 5 \text{ km s}^{-1}$. The moment-1 map [figure 2 (b)] also shows a sudden jump in the velocity from $\sim 9 \text{ km s}^{-1}$ to $\sim 5 \text{ km s}^{-1}$ around the L1641N region, and V380 Ori region has a velocity of $\sim 9 \text{ km s}^{-1}$. In other words, two components with different velocities appear to overlap along the line-of-sight. Nakamura et al. (2012) suggested that these components may be colliding (see also Lim et al. 2020). In fact, some faint extended emission

with intermediate velocities appears to connect with the two components in the position-velocity diagrams (see figure 8 in Nakamura et al. (2012)). The OMC-1 region has a very complicated velocity structure, which presumably is affected by stellar feedback or global gravitational contraction along the ISF (Hacar et al. 2017; Ishii et al. 2019) and cloud-cloud collision (Fukui et al. 2018). The moment-2 map [figure 2 (c)] indicates that the velocity dispersion tends to be larger toward brighter regions inside the ISF.

Figure 3 shows the optical depth of C¹⁸O in Orion A. Here, we adopted Equation (6) in Nakamura et al. (2019) with the excitation temperature derived with their Equation (3). The maximum optical depth is about 0.2 and thus we assume that the C¹⁸O emission is optically thin in the entire area.

4 Core identification

There are at least two main approaches to identify the dense cores in molecular clouds. One is to use dust emission or extinction maps (e.g., Motte et al. 1998; Alves et al. 2007; Nutter & Ward-Thompson 2007; Cheng et al. 2018; Sanhueza et al. 2019). The other is to use molecular emission line data (e.g., Ikeda et al. 2007; Ikeda & Kitamura 2009; Maruta et al. 2010). The dust emission is considered to be an excellent tracer of the column density of molecular clouds or interstellar medium (ISM). However, the dust cores, which have a three-dimensional structure in nature, are identified on the basis of the two-dimensional position-position maps. It is difficult to distinguish the structures overlapped along the line of sight.

The structure identification using molecular line emission allows to distinguish overlapping structures along the line of sight by taking advantage of the three-dimensional position-position-velocity (p-p-v) data. This method assumes that the coherent structures in p-p-v space are closely related to actual structures in position-position-position (p-p-p) space. However, the fractional abundances of the interstellar molecules relative to the hydrogen gas often vary even in single clouds (Savva et al. 2003). Thus, the mass estimation would be significantly influenced by the spatial variation of the fractional abundances. In this sense, using these two tracers is complimentary for the structure identification in molecular clouds.

In this paper, we use the advantages of the two tracers for core identification. We first identify the dense cores using our C¹⁸O ($J = 1-0$) data cube with a velocity resolution of 0.1 km s⁻¹. Then, we use the *Herschel-Planck* H₂ column density map to estimate the masses of the cores identified from the C¹⁸O ($J = 1-0$) data. To evaluate the masses of the cores, we attempt to remove the contribution of the ambient gas to the core mass estimation using the C¹⁸O ($J =$

1–0) data. As shown above, the C¹⁸O emission is optically-thin. However, the C¹⁸O molecule tends to be sometimes depleted in cold dense regions with $T \lesssim 20$ K (Caselli et al. 1999). In the presence of strong far UV radiation, selective dissociation changes the fractional abundances of CO and its isotopologue (Lada et al. 1994; Shimajiri et al. 2014; Lin et al. 2016; Ishii et al. 2019). These effects tend to destroy the linear relationship between the intensities of the dust emission and the optically-thin C¹⁸O emission.

4.1 Dendrogram and dense cores

We applied `astrodendro` ver. 0.2.0¹ to the three-dimensional (p-p-v) C¹⁸O data. The algorithm searches the hierarchical structures in the two-dimensional data (position-position) or three-dimensional data for given parameters. The `astrodendro` has three input parameters, (1) `min_value`, (2) `min_delta`, and (3) `min_npix`. It keeps searching the local peaks from the highest value of the data to the lowest value specified by `min_value` in the interval of `min_delta`. The local peak is called `leaf` in the algorithm. In addition, the number of pixels contained in a leaf should be greater than `min_npix`.

Two leaves are merged into one structure called `branch` when the bottoms of both leaves are larger than `min_value`. After that, two branches are merged into a new branch or a `trunk` which is the lowest structure. Then, the result of the identification is depicted with a tree-like diagram. A more detailed description and discussion about the algorithm are given in Rosolowsky et al. (2008). See also Goodman et al. (2009) for the application to the 3D molecular line data. In this study, we adopted `min_delta` = 2σ , `min_value` = 2σ and `min_npix` = 30 which corresponds to the volume of 1 beam times 3 channels for our structure identification. We define a leaf as a dense core of the molecular cloud. We note that this core definition is reasonably verified by the synthetic observations of the turbulent cloud simulations (Burkhart et al. 2013; Beaumont et al. 2013), although the structures identified in the real p-p-p space do not perfectly match with those identified in the p-p-p space. In addition, the structure identification in the p-p-p space also depends on cloud environments.

Since the observations were carried out in various atmospheric conditions for a couple of years, the rms noise level of the map is not uniform over the observed area. The value of `min_value` does not always correspond to twice the noise level. To minimize the effect of the non-uniform noise levels in the core identification, we imposed the following three conditions for identified leaves with the parameters mentioned above. Condition (1): the peak intensity of

¹ <https://dendrograms.readthedocs.io/en/stable/>

the identified leaf should be four times larger than the local rms noise level at the corresponding spatial position. Condition (2): More than three successive channels ($\sim 0.3 \text{ km s}^{-1}$) should contain more than 9 pixels for each channel. This threshold pixel number of 9 is equivalent to one effective angular resolution of the map ($\approx 26.''4$). Condition (3): an identified core should not contain any pixels located at the boundaries of the observation area. In total, we identified 746 cores.

Then, we classified the identified cores into two groups using the HOPS catalog, starless and protostellar cores. If an identified core overlaps spatially with at least one HOP object on the plane of the sky, we classified it as a protostellar core. Here we classified an identified core as a protostellar core when it contains more than one HOP object within the projected area onto the plane of the sky. A core without the overlapped HOP objects is categorized as a starless core.

As a result, we identified 709 starless cores and 37 protostellar cores (table 1). Figure 4 shows the result of the core identification. The starless cores and the protostellar cores are plotted onto the integrated intensity map of the C^{18}O emission and most cores are distributed along ISF. Among the 74 HOPS Class 0/I objects, 34 ($\sim 46\%$) objects were not identified as our protostellar cores. However, most of the HOPS Class 0/I objects are associated with local C^{18}O peaks and they are excluded from our samples by the additional thresholds of core identification. To identify these protostellar cores, we need data with better sensitivities.

4.2 Derivation of the core physical quantities

4.2.1 Core radius, aspect ratio, and velocity dispersion

We define the physical quantities of the identified cores as follows. The positions and the line-of-sight velocity of a core are determined by the mean positions of the structure identified and the intensity-weighted first-moment velocity, respectively. The core radius is defined as

$$R_{\text{core}} = \left(\frac{A}{\pi} \right)^{1/2}, \quad (1)$$

where A is the exact area of the core projected onto the plane of the sky. The aspect ratio of the core is calculated as the ratio of the major and minor axes. The major and minor axes in half width at half maximum (HWHM) are computed from the intensity-weighted second moment in the direction of greatest elongation and perpendicular to the major axis, respectively, in the plane of the sky. The position angle of the core is determined counter-clockwise from the +R.A. axis. The velocity width in full width at half maximum (FWHM), dV_{core} is obtained by multiplying the intensity-weighted second moment of velocity by a factor of $2\sqrt{2\ln 2}$. Figure 5

(a), (b) and (c) show the histograms of the diameter, aspect ratio and velocity width in FWHM. The minimum, maximum, mean value and standard deviation of each physical properties of identified cores are summarised in table 2. The mean values of standard deviations of diameter, aspect ratio, and velocity width in FWHM of identified cores are 0.16 ± 0.06 pc, 0.58 ± 0.16 , 0.33 ± 0.14 km s⁻¹, respectively. Starless cores tend to have a small diameter and velocity width compare to protostellar cores. There are no clear differences between the aspect ratios of starless cores and protostellar cores.

4.2.2 Core mass and virial mass

To estimate the core mass with minimizing the effect of the CO depletion, we used the *Herschel–Planck* H₂ column density data different from previous studies on the core identification based on C¹⁸O observations (Ikeda et al. 2007; Ikeda & Kitamura 2009; Shimajiri et al. 2015). We determined the core mass by integrating the *Herschel–Planck* H₂ mass over the projected area of the core on the plane of the sky defined by Dendrogram on the C¹⁸O image. The dendrogram analysis allows us to distinguish between the cores and other structures. In other words, we can estimate the contribution of the emission associated with cores on the integrated intensity (see also figure 4 (left) and Sect 4.1.2 in (Rosolowsky et al. 2008)). When multiple pixels belonged to the different cores are overlapped along the line of sight at a pixel, we divide the *Herschel–Planck* H₂ mass between cores in proportion to the integrated intensity of C¹⁸O emission after removing the contribution of the ambient gas. Thus, the mass of the k -th core is calculated as

$$M_{\text{core}}^k = \mu m_H \times \sum_i \left(N_{\text{H}_2, i} \times F_i^k \right) \quad (2)$$

where $F_i^k = I_i^k / T_i$ is the intensity fraction at the i -th pixel for the k -th core to sum of emission of all trunks, I_i^k is the C¹⁸O integrated intensity at the i -th pixel for the k -th core, and $T_i (= \int_{\text{trunk}} I_i dv)$ is the total velocity-integrated intensity at the i -th pixel in all trunk, $\mu = 2.3$ is the mean molecular weight, m_H is the mass of a hydrogen atom, $N_{\text{H}_2, i}$ is the *Herschel–Planck* H₂ mass contained in the i -th pixel. We discuss the influence of the warm ambient gas (trunk) to this method in appendix 1. About 60% of identified cores overlaps with more than one core (see appendix 2 for detail). Here we classified a pair of identified cores as overlapped cores when they overlaps more than one pixel along the line of sight. The above expression can be rewritten as

$$M_{\text{core}}^k = 4.15 \times 10^{-2} \left(\frac{\theta}{7.''5} \right)^2 \left(\frac{D}{414 \text{ pc}} \right)^2 \left(\frac{\sum_i N_{\text{H}_2, i, k} \times F_i^k}{10^{22} \text{ cm}^{-2}} \right) M_{\odot} \quad (3)$$

The virial mass of a core is estimated as

$$M_{\text{vir}} = 210 \left(\frac{R_{\text{core}}}{\text{pc}} \right) \left(\frac{dV_{\text{core}}}{\text{km s}^{-1}} \right)^2 M_{\odot} \quad (4)$$

where dV_{core} is the FWHM velocity width and the core is assumed to be an uniform sphere and magnetic fields and external pressures are neglected for dynamical support. The virial ratio is defined as

$$\alpha_{\text{vir}} = \frac{M_{\text{vir}}}{M_{\text{core}}} . \quad (5)$$

We note that for a centrally-condensed sphere with $\rho \propto r^{-2}$, the virial ratio becomes smaller by a factor of 5/3 than the above definition. The cloud shape also influences the actual value of the virial parameter (Bertoldi & McKee 1992). If the CO depletion is significant particularly in cold dense regions, the estimates of the line-widths in the cold starless cores may be somewhat affected.

In this paper, we define the core whose virial ratio is smaller than 2 as a gravitationally bounded core. Then, we identified 684 bound starless cores and 25 unbound starless cores, respectively. All protostellar cores are likely to be bounded by gravity. Figure 6, the virial ratio–mass relation, shows the clear trend that more massive cores tend to have smaller virial ratios. The minimum, maximum, mean value, and the standard deviation of each physical properties of identified cores derived in this section are also summarised in table 2. The mean values of standard deviations of the mass, number density and virial ratio of identified cores are $1.08 \pm 2.42 M_{\odot}$, $(0.87 \pm 1.92) \times 10^4 \text{ cm}^{-3}$ and 0.64 ± 0.89 , respectively.

We assumed the local thermodynamic equilibrium (LTE) condition and optically thin emission of the C¹⁸O ($J=1-0$) to derive the mean column densities of the C¹⁸O of individual cores. Here, we assigned individual excitation temperature derived from ¹²CO observation (see Nakamura et al. 2019) to each core. The mean excitation temperature of projected areas of cores is 33 K. Then we calculate the fractional abundance of C¹⁸O, $X_{\text{C}^{18}\text{O}}$, for each core as a ratio of the column density of the C¹⁸O and H₂. The mean value is $\overline{X_{\text{C}^{18}\text{O}}} = 5.7 \times 10^{-7}$, which is 3 times larger than the representative value of 1.7×10^{-7} (Frerking et al. 1982). Also, the number density of a core is obtained by assuming that the core has a constant density with a radius R_{core} . The physical properties of the identified starless and protostellar cores such as core mass, virial ratio, density, and C¹⁸O fractional abundance are summarized in tables 3 and 4, respectively.

Figures 5 (d), (e) and (f) show the histograms of mass, virial ratio, and number density of the C¹⁸O cores. It is clear that protostellar cores are more massive and denser than starless cores. A large fraction of identified cores have a virial ratio of smaller than 2 and protostellar

cores tend to have smaller virial ratios.

5 Discussion

5.1 Comparison between the C¹⁸O emission and dust emission

Figure 7 shows the relationship between the H₂ column density derived directly from the C¹⁸O integrated intensity, $N_{\text{H}_2, \text{C}^{18}\text{O}}$, and the *Herschel–Planck* H₂ column density, $N_{\text{H}_2, \text{Herschel}}$, in Orion A. The relationship is shown as a two-dimensional histogram of PDF (probability distribution function) in figure (a) and contour in figure (b), respectively. Here, we obtained the C¹⁸O column density under the assumption of LTE and optically-thin condition as Ikeda & Kitamura 2009 and Shimajiri et al. 2015. The excitation temperature of C¹⁸O was assumed to be the same as the peak intensity of ¹²CO emission. We have calculated the C¹⁸O column density of pixels which integrated intensity is larger than 15 local rms noise included in the projection of all trunks to the plane of the sky. Then we converted the C¹⁸O column density to the H₂ column density with a constant fractional abundance of C¹⁸O to H₂ of $X_{\text{C}^{18}\text{O}} = 5.7 \times 10^{-7}$. The plot indicates that the column density of C¹⁸O is roughly proportional to the *Herschel–Planck* H₂ column density below $N_{\text{H}_2} \lesssim 5 \times 10^{22} \text{ cm}^{-2}$. In figure 7 (a), the two dashed lines show $N_{\text{H}_2, \text{C}^{18}\text{O}} = 0.5 N_{\text{H}_2, \text{Herschel}}$ and $N_{\text{H}_2, \text{C}^{18}\text{O}} = 2 N_{\text{H}_2, \text{Herschel}}$. For larger H₂ column density ($n \gtrsim 10^5 \text{ cm}^{-3}$), the C¹⁸O column density tends to level off for larger column density. The number of such pixels is only 18.2 %. In figure 7 (b), the identified cores are plotted onto the contour. For most of the cores identified, the C¹⁸O column density is more or less proportional to the *Herschel–Planck* H₂ column density. Thus, the C¹⁸O is likely to be a reliable tracer of the molecular hydrogen mass with the exception of cold and dense regions with $N_{\text{H}_2} \gtrsim 5 \times 10^{22} \text{ cm}^{-2}$.

For dense regions, C¹⁸O appears to be less abundant. Therefore, the cores located in the dense regions may not be well traced by C¹⁸O emission. However, the number fraction of such cores is likely to be small for the entire Orion A. There may be at least two reasons why C¹⁸O abundance is lower toward denser regions. One is the CO depletion on to the grain surfaces for cold ($T \lesssim 20 \text{ K}$), dense ($n \gtrsim 10^5 \text{ cm}^{-3}$) parts. Another is the dissociation due to FUV radiation (Shimajiri et al. 2014; Lin et al. 2016; Ishii et al. 2019). In Orion A, several massive stars, mainly located in the OMC-1 region, emit strong UV radiation, which can dissociate C¹⁸O in dense regions where ¹²CO and ¹³CO emissions become optically thick.

Our result is consistent with that of Ripple et al. (2013) with ¹³CO. They showed that the effect of CO freeze out is limited to regions with $N_{\text{H}_2} \gtrsim 10^{22} \text{ cm}^{-2}$ ($A_V \gtrsim 10 \text{ mag}$) and gas

temperatures less than ~ 20 K for Orion.

5.2 Consideration of the effect of the ambient gas to mass estimation

In this section, we compare the core masses calculated with two different approaches. One is the core mass weighted by the C^{18}O emission (M_{core}) defined by equation (2) in section 4.2.2. The other ($M_{\text{projection}}$) is derived by summing up all *Herschel–Planck* H_2 column density included in the projected area of a core to the plane of the sky without removing the ambient components of the gas. This is essentially the same as the mass estimation based on some core identification schemes such as `clumpfind` (Williams et al. 1994) and Fellwaker (Berry 2015). When multiple cores overlap along the line-of-sight, we distribute the *Herschel–Planck* H_2 column density to each core. The assigned H_2 column density of each core is proportional to the C^{18}O intensity of a core. The difference between M_{core} and $M_{\text{projection}}$ is the treatment of ambient gas of the dense core. $M_{\text{projection}}$ is a sum of M_{core} and mass of the ambient gas along the line of sight. Then we calculated mass ratio, $M_{\text{core}}/M_{\text{projection}}$ and show the mass ratio – *Herschel–Planck* H_2 column density relation in figure 8. As shown in this figure, an identified core with a higher H_2 column density tends to have a smaller mass ratio. This suggests that such cores have more ambient gas and the core mass derived from dust observations tends to be more overestimated. A large fraction of core has mass ratios of smaller than 0.5 and the mean mass ratio and standard deviation are 0.35 ± 0.21 . Then, more than 50% of H_2 column density seems to come from the ambient gas in the dense regions whose H_2 column density is $\gtrsim 10^{22} \text{ cm}^{-2}$. In other words, the mass estimated only from the 2D dust emission map is about 3 times larger than the actual mass evaluated in 3D. This implies that the core masses estimated with the dust emission and extinction are significantly larger than the actual values. For further discussion, we need more observations with other molecular lines.

5.3 Core mass function in Orion A

In this section, we derive the CMF in Orion A using the cores identified above and M_{core} and then discuss their properties. Here, the CMF is defined as the number of cores with masses in a mass range from M_{core} to $M_{\text{core}} + dM_{\text{core}}$.

Figure 9 shows the CMFs for all identified cores, starless cores, and gravitationally bound cores. Since almost all identified cores seem to be bounded by gravity as shown in Section 4.2.2, we do not classify bound and unbound cores to derive CMFs in this paper. The mass detection limit for our analysis is $\sim 0.03M_{\odot}$. This mass is derived from the minimum intensity and

size to pass the core identification conditions described in section 4 and assumptions of LTE condition and optically thin emission of C¹⁸O ($J=1-0$) emission. Here we applied $T_{\text{ex}}=33$ K and $X_{\text{C}^{18}\text{O}}=5.7\times 10^{-7}$. Both CMFs have turnovers at $\sim 0.3 M_{\odot}$ and power-law like shape above them. The best-fit power-law indexes of CMFs for all cores, starless cores, and gravitationally bound cores are -2.08 , -2.25 , and -2.24 , respectively. The best-fit power-law indices are in agreement with that of the Salpeter IMF (-2.35 , Salpeter 1955). The slopes in the CMFs are also consistent with the previous study (Ikeda & Kitamura 2009) that identified C¹⁸O cores with a different core identification scheme `clumpfind` in a much smaller area including the OMC-1 region ($\sim 2.4 \text{ pc} \times 2.4 \text{ pc}$). Their C¹⁸O data have the same effective angular resolution and velocity resolution as ours. However, a turnover mass of their CMF for the OMC-1 region, $\sim 5M_{\odot}$, is about three times larger than our value. This difference mainly comes from the usage of the different core identification schemes. For the Ikeda et al. (2007)'s scheme, i.e., `clumpfind`, the core mass tends to be larger than that obtained based on Dendrogram since for the former, all the pixels located inside the closed contour which contains cores are assigned to the adjacent core.

In order to estimate the completeness of core identification, we derived the detection probability as a function of the core mass by putting the artificial cores generated as follows.

1. We decided the mass of each artificial core as the central value of each mass bin on the log scale.
2. With the assumptions of the LTE condition and optically thin emission of the C¹⁸O ($J=1-0$), we converted the mass of each artificial core to the integrated intensity of C¹⁸O emission using $T_{\text{ex}}=33$ K and $X_{\text{C}^{18}\text{O}}=5.7\times 10^{-7}$.
3. We calculated the radius and velocity width of each core using the radius – mass and velocity width in rms – mass relations, which are derived by fitting for all identified cores. Here we derived radius as the geometric mean of major and minor axes of identified cores. The mean values of major and minor axes are shown in table 3.
4. We made a modified dataset by inserting the artificial cores that have the three-dimensional Gaussian shape in the p-p-v space with sizes and velocity widths derived above. Here we just added the artificial cores to the observed data. The positions and the system velocities of the artificial cores that correspond with individual mass bins are given randomly in the trunks which are the lowest structures of the Dendrogram's hierarchies.
5. We applied the same core identification method to the modified data and checked whether the artificial core is identified or not.

6. We repeated this procedure N_{trial} times for each each mass bin in the CMF plot and calculated the possibility that the artificial cores are identified as independent cores $F(M_{\text{LTE}}/M_{\odot})$ with equation (6).

To calculate the probability that the artificial cores are identified as independent cores, first, we prepared two data; the original observed data and modified data which contains the artificial core. We applied the same core identification method described in Section 4. Then, we counted the number of identified cores within 1σ from the center of the artificial core in observed data n_{observed} and modified data $n_{\text{artificial}}$. We summed up the number of the case of $n_{\text{artificial}} - n_{\text{observed}} \geq 1$ for $N_{\text{trial}} = 100$ trials as $n_{\text{identified}}$. Finally, the probability function that the artificial cores are identified as independent cores is derived as

$$P(M_{\text{LTE}}/M_{\odot}) = \frac{n_{\text{identified}}(M_{\text{LTE}}/M_{\odot})}{N_{\text{trial}}} \quad (6)$$

Then, the corrected number of cores in each mass bin $N_{\text{corrected}}$ is calculated with the observed number of cores N_{observed} as

$$N_{\text{corrected}} = \frac{N_{\text{observed}}}{P(M_{\text{LTE}}/M_{\odot})} \quad (7)$$

Figure 10 shows the observed and compensated CMFs. The shape of the compensated CMF at the high-mass end is essentially the same as the observed one. In contrast, we see significant differences between the distribution at low-mass parts of observed CMF and compensated CMF. The number of low-mass cores in observed CMF is smaller than that in compensated CMF and such cores are likely to be missed in observed CMF. We find no clear turnover in the compensated CMF. Thus, it is difficult to conclude that the CMFs have a turnover at the low-mass part from our observations. This is consistent with the argument by Ikeda et al. (2007). This fact suggests that the spatial resolution of our data is not enough to confirm whether a CMF has a turnover and we need a higher spatial resolution to address this point.

6 Comparison with the CMF derived from the dust emission

In section 5.2, we pointed out that the masses derived from the dust emission map tend to be significantly overestimated due to the contribution of the ambient gas. Here, we attempt to assess how this overestimation affects previous results by using Nutter & Ward-Thompson (2007)'s core catalog. Figure 11 shows the CMF derived from the SCUBA 850 μm emission map with an angular resolution of $\sim 15''$. The core identification scheme of Nutter & Ward-Thompson (2007) is also different from ours. They used not a hierarchy but a signal-to-noise ratio and a detailed explanation are in the paper. The authors set the distance of Orion A as 400 pc and we

recalculated the core masses with a distance of 414 pc. As a result, the turnover mass derived from the dust emission ($\sim 0.5 M_{\odot}$) appears to be comparable to our value obtained from the $C^{18}O$ emission. However, the dust mass tends to be overestimated the core mass since the dust mass sums up both the core mass and the ambient gas overlapped along the line of sight. This is one of the disadvantages to estimate the core masses only from the dust observations. It is worth noting that in the SCUBA dust image, the structures larger than ~ 1.5 are removed during the data reduction process. This artificial effect leads to underestimates of the dust emission.

In addition, the cores overlapped along the line of sight are difficult to be distinguished only from the dust map. In fact, the most massive dust core in Nutter & Ward-Thompson (2007) has a mass of $\sim 1062 M_{\odot}$, located in OMC-1. In our $C^{18}O$ case, the most massive core has a mass of $\sim 42 M_{\odot}$. In the area containing the most massive dust core, our $C^{18}O$ data indicate the existence of the multiple cores overlapped and/or a lot of ambient gas surrounding cores. This effect makes massive cores more massive and the slope of the CMF shallower toward the high-mass part, and this is another disadvantage for the dust observations. Figure 12 shows the histograms of physical properties of dust cores such as the core diameter, aspect ratio, mass, and density. Although the mass ranges of $C^{18}O$ cores and dust cores are similar, dust cores tend to be smaller than $C^{18}O$ cores. Then, dust cores are likely to be denser than $C^{18}O$ cores. There are no big differences in aspect ratio between the two cores.

As derived in section 5.2, the dust mass may be overestimated by a factor of 3 from our data. If we apply this correction factor to their CMF, the turnover mass becomes small at 0.1–0.2 M_{\odot} . This turnover mass is comparable to that of the stellar IMF in Orion Nebular Cluster (Hillenbrand 1997; Da Rio et al. 2012). If we apply the same discussion of Alves et al. (2007), this may indicate that star formation efficiency (SFE) of individual cores is much higher than the prediction of the theoretical studies (Matzner & McKee 2000; Machida & Matsumoto 2012), in which SFE is estimated to be 30–50% since the protostellar outflows blow out of a significant amount of core mass. Such a high SFE appears to be consistent with the result by Bontemps et al. (2001). We note that recent numerical simulations have suggested that the mass infall from the surrounding play an important role in the evolution of the core mass (Vázquez-Semadeni et al. 2019; Padoan et al. 2020). Such processes also affect the peak masses of CMFs i.e., the turnover mass would evolve over time due to the mass accretion.

Considering the overestimation, the turnover mass is expected to be $\sim 0.1 M_{\odot}$, and observations with a higher angular resolution are needed to confirm it. In a forthcoming paper, we attempt to identify $C^{18}O$ cores in Orion A using the CARMA-NRO combined data (Kong

et al. 2018) with a much higher angular resolution ($\sim 8''$) to reveal the shape of the CMF at low mass part.

7 Summary

We conducted an unbiased dense core survey in Orion A with the C¹⁸O data taken by Nobeyama 45-m telescope. The main conclusions are summarized as follows.

1. The C¹⁸O($J=1-0$) emission is likely to be a reliable tracer of molecular mass toward the regions with $N \lesssim 5 \times 10^{22} \text{ cm}^{-2}$. The average abundance of C¹⁸O relative to H₂ is obtained to be 5.7×10^{-7} . Its abundance tends to be smaller for the denser region within a factor of a few.
2. Applying Dendrogram, we conducted hierarchical structure analysis of the Orion A cloud and define leaves as cores. As a result, we identified 746 cores. With the HOPS catalog, we classified the cores into two groups: 709 starless cores and 37 protostellar cores.
3. We derived the masses of the cores identified from the *Herschel-Planck* H₂ map, by removing the contribution of the ambient gas that is not associated with cores along the line of sight.
4. The mean diameter, mass, and velocity widths of the starless cores are estimated to be $0.16 \pm 0.05 \text{ pc}$, $0.92 \pm 1.65 M_{\odot}$, and $0.32 \pm 0.14 \text{ km s}^{-1}$, respectively.
4. The CMF of the starless bound cores has a slope similar to the Salpeter IMF in the high-mass part (a power index of $\alpha = -2.24 \pm 0.16$ at $\gtrsim 0.44 M_{\odot}$). and has a peak at $0.3 M_{\odot}$.
5. The test of completeness indicates that this peak mass may be affected by the angular resolution of the map, and the actual peak mass, if exists, would be smaller than the observed value from our data.
6. The estimated mass of cores based on the dust observations is likely to be overestimated the actual core mass, presumably be a factor of ~ 3 .
7. If we adopt this correction factor for the CMF obtained by Nutter & Ward-Thompson (2007), the peak mass in the CMF tends to be comparable to the stellar IMF.

Acknowledgments

This work was carried out as one of the large projects of the Nobeyama Radio Observatory (NRO), which is a branch of the National Astronomical Observatory of Japan, National Institute of Natural Sciences. We thank the NRO staff for both operating the 45 m and helping us with the data reduction. Data analysis was carried out on the Multi-wavelength Data Analysis System operated by the Astronomy Data Center (ADC), National Astronomical Observatory of Japan. P.S. was partially supported by a Grant-in-Aid for Scientific Research (KAKENHI Number 18H01259) of Japan Society for the Promotion of Science (JSPS). This work was supported in part by The Graduate University for Advanced Studies, SOKENDAI. We thank the anonymous referee for

many useful comments that have improved the presentation.

References

- Alves, J., Lombardi, M., & Lada, C.J. 2007, *A&A*, 462, 1, L17
- Bally, J., Langer, W.D., Stark, A.A., & Wilson, R.W. 1987, *ApJL*, 312, L45
- Beaumont, C.N., Offner, S.S.R., Shetty, R., Glover, S.C.O., & Goodman, A.A. 2013, *ApJ*, 777, 2, 173
- Bergin, E.A., & Tafalla, M. 2007, *ARA&A*, 45, 1, 339
- Berry, D.S. 2015, *Astronomy and Computing*, 10, 22
- Bertoldi, F., & McKee, C.F. 1992, *ApJ*, 395, 140
- Bontemps, S., et al. 2001, *A&A*, 372, 173
- Burkhart, B., Lazarian, A., Goodman, A., & Rosolowsky, E. 2013, *ApJ*, 770, 2, 141
- Caselli, P., Walmsley, C.M., Tafalla, M., Dore, L., & Myers, P.C. 1999, *ApJL*, 523, 2, L165
- Cheng, Y., Tan, J.C., Liu, M., Kong, S., Lim, W., Andersen, M., & Da Rio, N. 2018, *ApJ*, 853, 2, 160
- Da Rio, N., Robberto, M., Hillenbrand, L.A., Henning, T., & Stassun, K.G. 2012, *ApJ*, 748, 1, 14
- Feddersen, J.R., et al. 2018, *ApJ*, 862, 2, 121
- Frerking, M.A., Langer, W.D., & Wilson, R.W. 1982, *ApJ*, 262, 590
- Fukui, Y., et al. 2018, *ApJ*, 859, 2, 166
- Furlan, E., et al. 2016, *ApJS*, 224, 1, 5
- Genzel, R., & Stutzki, J. 1989, *ARA&A*, 27, 41
- Goodman, A.A., Rosolowsky, E.W., Borkin, M.A., Foster, J.B., Halle, M., Kauffmann, J., & Pineda, J.E. 2009, *Nature*, 457, 7225, 63
- Gratier, P., et al. 2020, arXiv e-prints, arXiv:2008.13417
- Hacar, A., Alves, J., Tafalla, M., & Goicoechea, J.R. 2017, *A&A*, 602, L2
- Hillenbrand, L.A. 1997, *AJ*, 113, 1733
- Ikeda, N., & Kitamura, Y. 2009, *ApJL*, 705, 1, L95
- Ikeda, N., Sunada, K., & Kitamura, Y. 2007, *ApJ*, 665, 2, 1194
- Ishii, S., Nakamura, F., Shimajiri, Y., Kawabe, R., Tsukagoshi, T., Dobashi, K., & Shimoikura, T. 2019, *PASJ*, 71, S9
- Kong, S. 2019, *ApJ*, 873, 1, 31
- Kong, S., et al. 2018, *ApJS*, 236, 2, 25
- Könyves, V., et al. 2010, *A&A*, 518, L106
- Lada, C.J., Lada, E.A., Clemens, D.P., & Bally, J. 1994, *ApJ*, 429, 694
- Lin, S.J., et al. 2016, *ApJ*, 826, 2, 193

- Liu, M., Tan, J.C., Cheng, Y., & Kong, S. 2018, *ApJ*, 862, 2, 105
- Lombardi, M., Bouy, H., Alves, J., & Lada, C.J. 2014, *A&A*, 566, A45
- Machida, M.N., & Matsumoto, T. 2012, *MNRAS*, 421, 1, 588
- Maruta, H., Nakamura, F., Nishi, R., Ikeda, N., & Kitamura, Y. 2010, *ApJ*, 714, 1, 680
- Matzner, C.D., & McKee, C.F. 2000, *ApJ*, 545, 1, 364
- Menten, K.M., Reid, M.J., Forbrich, J., & Brunthaler, A. 2007, *A&A*, 474, 2, 515
- Minamidani, T., et al. 2016, in *Proc. SPIE*, vol. 9914 of Society of Photo-Optical Instrumentation Engineers (SPIE) Conference Series, 99141Z
- Motte, F., Andre, P., & Neri, R. 1998, *A&A*, 336, 150
- Motte, F., et al. 2018, *Nature Astronomy*, 2, 478
- Nakamura, F., et al. 2012, *ApJ*, 746, 1, 25
- Nakamura, F., et al. 2019, *PASJ*, 71, S3
- Nutter, D., & Ward-Thompson, D. 2007, *MNRAS*, 374, 4, 1413
- Padoan, P., Pan, L., Juvela, M., Haugbølle, T., & Nordlund, Å. 2020, *ApJ*, 900, 1, 82
- Palla, F., & Stahler, S.W. 1999, *ApJ*, 525, 2, 772
- Pety, J., et al. 2017, *A&A*, 599, A98
- Ripple, F., Heyer, M.H., Gutermuth, R., Snell, R.L., & Brunt, C.M. 2013, *MNRAS*, 431, 2, 1296
- Rosolowsky, E.W., Pineda, J.E., Kauffmann, J., & Goodman, A.A. 2008, *ApJ*, 679, 2, 1338
- Salpeter, E.E. 1955, *ApJ*, 121, 161
- Sanhueza, P., et al. 2019, *ApJ*, 886, 2, 102
- Savva, D., Little, L.T., Phillips, R.R., & Gibb, A.G. 2003, *MNRAS*, 343, 1, 259
- Shimajiri, Y., et al. 2011, *PASJ*, 63, 105
- Shimajiri, Y., et al. 2014, *A&A*, 564, A68
- Shimajiri, Y., et al. 2015, *ApJS*, 217, 1, 7
- Stutz, A.M., & Kainulainen, J. 2015, *A&A*, 577, L6
- Tanabe, Y., et al. 2019, *PASJ*, 71, S8
- Tatematsu, K., Ohashi, S., Sanhueza, P., Nguyen Luong, Q., Umemoto, T., & Mizuno, N. 2016, *PASJ*, 68, 2, 24
- Vázquez-Semadeni, E., Palau, A., Ballesteros-Paredes, J., Gómez, G.C., & Zamora-Avilés, M. 2019, *MNRAS*, 490, 3, 3061
- Williams, J.P., de Geus, E.J., & Blitz, L. 1994, *ApJ*, 428, 693

Appendix 1 H₂ column densities of leaf and trunk with different temperature

In equation 2, we derived core mass with C¹⁸O intensity ratio, $I_{C^{18}O,leaf}/I_{C^{18}O,trunk}$ (Figure 13), of leaves and trunks by assuming that leaves and trunks have the same temperature and fractional abundance of C¹⁸O to H₂. In the real situation, however, cores and ambient gas seem to have different temperature and fractional abundance i.e., ambient gas has a higher temperature and larger abundance ratio than cores. In this section, we investigate the influence of such differences on core mass estimation. To do so, we calculate the ratio of H₂ column density of leaf and trunk from the intensity ratio of leaves and trunks without the assumption that leaves and trunks have the same temperature and fractional abundance using a simple model. First, we fixed the intensity ratio of leaf and trunk and the temperature of leaf as 3:7 (see section 5.2) and 20 K. Second, we calculated C¹⁸O column density ratio of leaf and trunk, $N_{C^{18}O,leaf}/N_{C^{18}O,trunk}$, from the temperature of trunk is 20 K to 100 K. Finally, we converted the C¹⁸O column density ratio to H₂ column density ratio, $N_{H_2,leaf}/N_{H_2,trunk}$, with the ratio of fractional abundance ratio, $X_{C^{18}O,trunk}/X_{C^{18}O,leaf}$, from 1 to 5. Figure 14 (a) shows the relationship between H₂ column density ratio and the temperature of trunk. In figure 14 (b), we normalized H₂ column density ratio with intensity ratio. When trunks (ambient gas) have higher temperature compare to leaves (cores), H₂ column density ratio, $N_{H_2,leaf}/N_{H_2,trunk}$, is larger than intensity ratio and we underestimate the core masses. In contrast, when the abundance ratio of a trunk is larger than that of a leaf, H₂ column density ratio becomes larger. For example, when $T_{trunk}=40$ K ($=2T_{leaf}$) and $X_{C^{18}O,trunk}/X_{C^{18}O,leaf}=2$, H₂ column density ratio is similar to C¹⁸O intensity ratio. We expect both effects happen simultaneously in the real situation and we think we can derive H₂ column density ratio from C¹⁸O intensity ratio of a leaf and a trunk to calculate core mass with equation 2.

Appendix 2 Overlapping cores

As we mentioned in section 4.2.2, around 60% of identified cores overlap each other. In this section, we summarize the properties of overlapped cores such as the number of them, integrated C¹⁸O intensity, and H₂ column density. Figure 15 (a) shows a histogram of the number of overlapped cores, $N_{overlap}$. For more than 60% of overlapped cores, $N_{overlap}=1$ and several cores have $N_{overlap}$ of larger than 3. Figure 15 (b) represents the distributions of overlapped cores in $I_{C^{18}O}-N_{H_2,leaf}$ plane and there is no bias of the distribution. Then, we do not recognize any critical integrated intensity or column density which overlapping effect becomes severe.

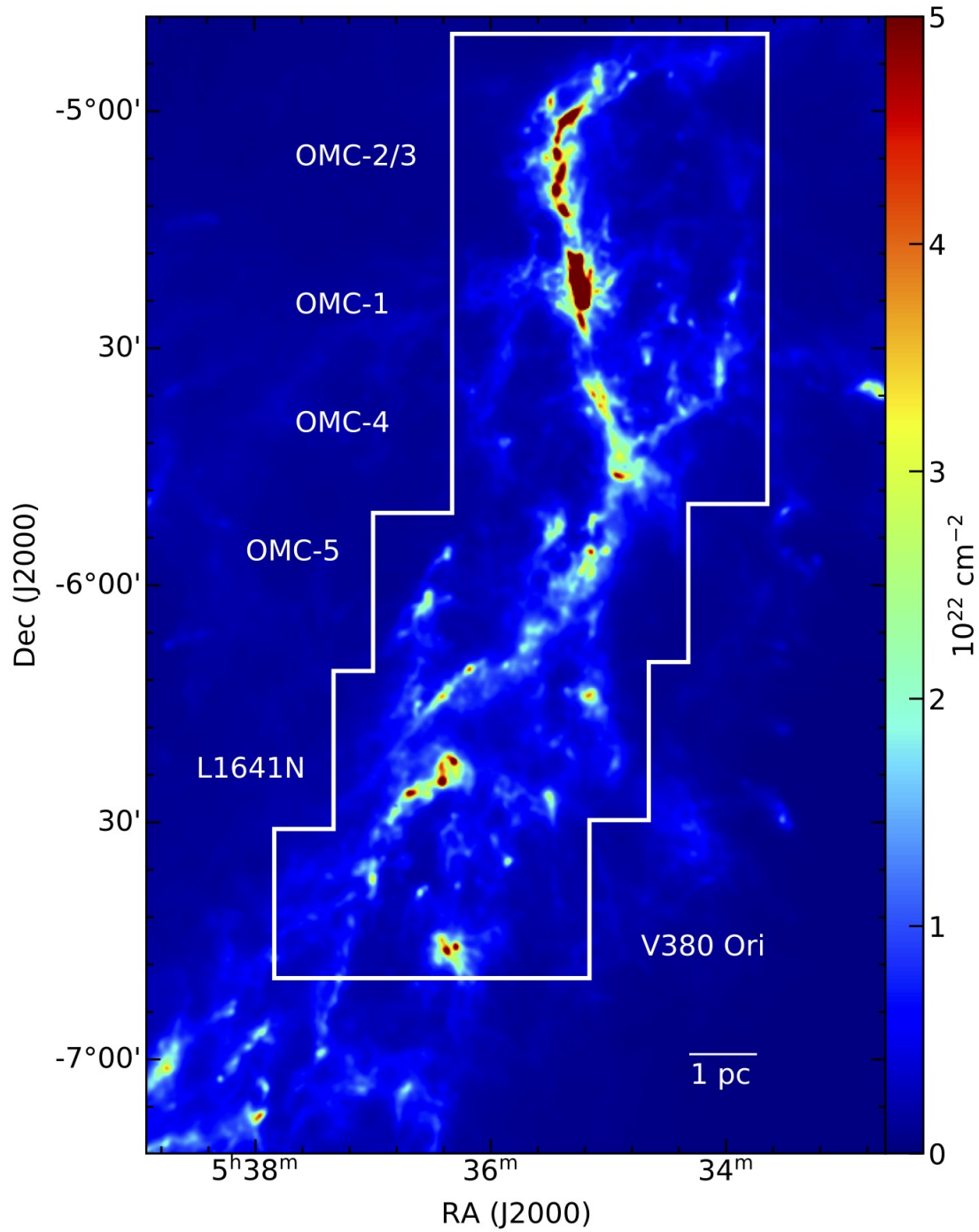


Fig. 1. The C^{18}O ($J=1-0$) observation area overlaid on the *Herschel-Planck* H_2 map (Lombardi et al. 2014). The observed area is indicated with the white solid line. Our map covers a wide area of 1×2 square degree which is from OMC-1/2/3/4 to L1641N, and V380 Ori.

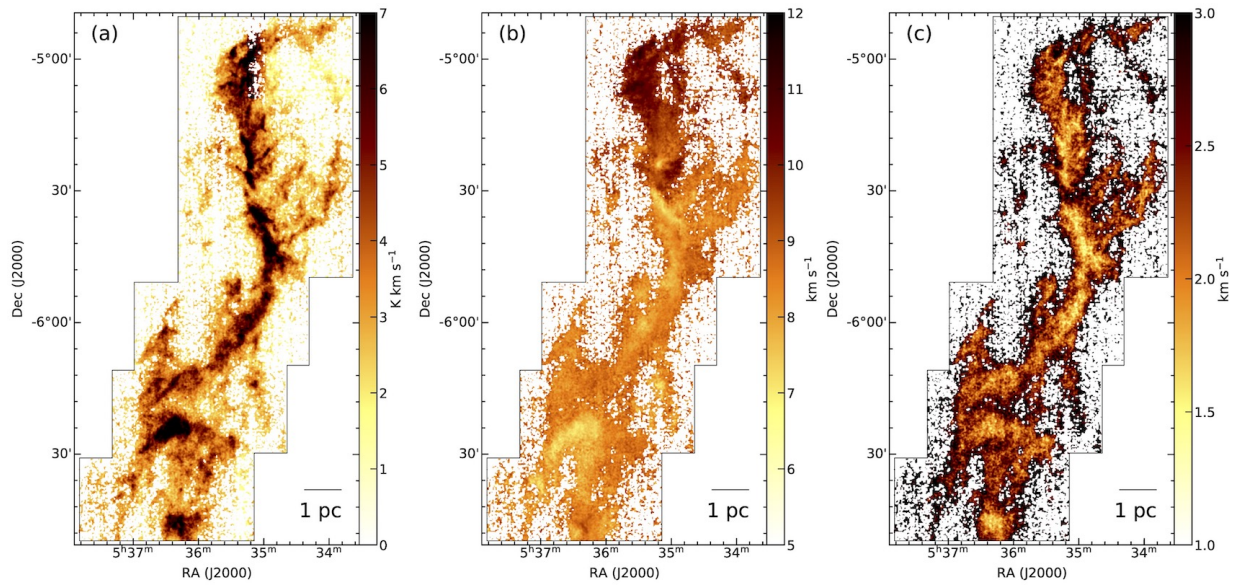


Fig. 2. (a) Integrated intensity map (moment-0 map) of the $C^{18}O$ ($J=1-0$) emission, (b) intensity weighted coordinate (moment-1 map) and (c) intensity weighted dispersion of the coordinate (moment-2 map), respectively. The integration was done in the velocity range from $\sim 3 km s^{-1}$ to $\sim 15 km s^{-1}$ for the pixels whose integrated intensity is larger than 15 local rams noise. We made these maps with the CASA software. The observed area is indicated with the black solid line in each panel.

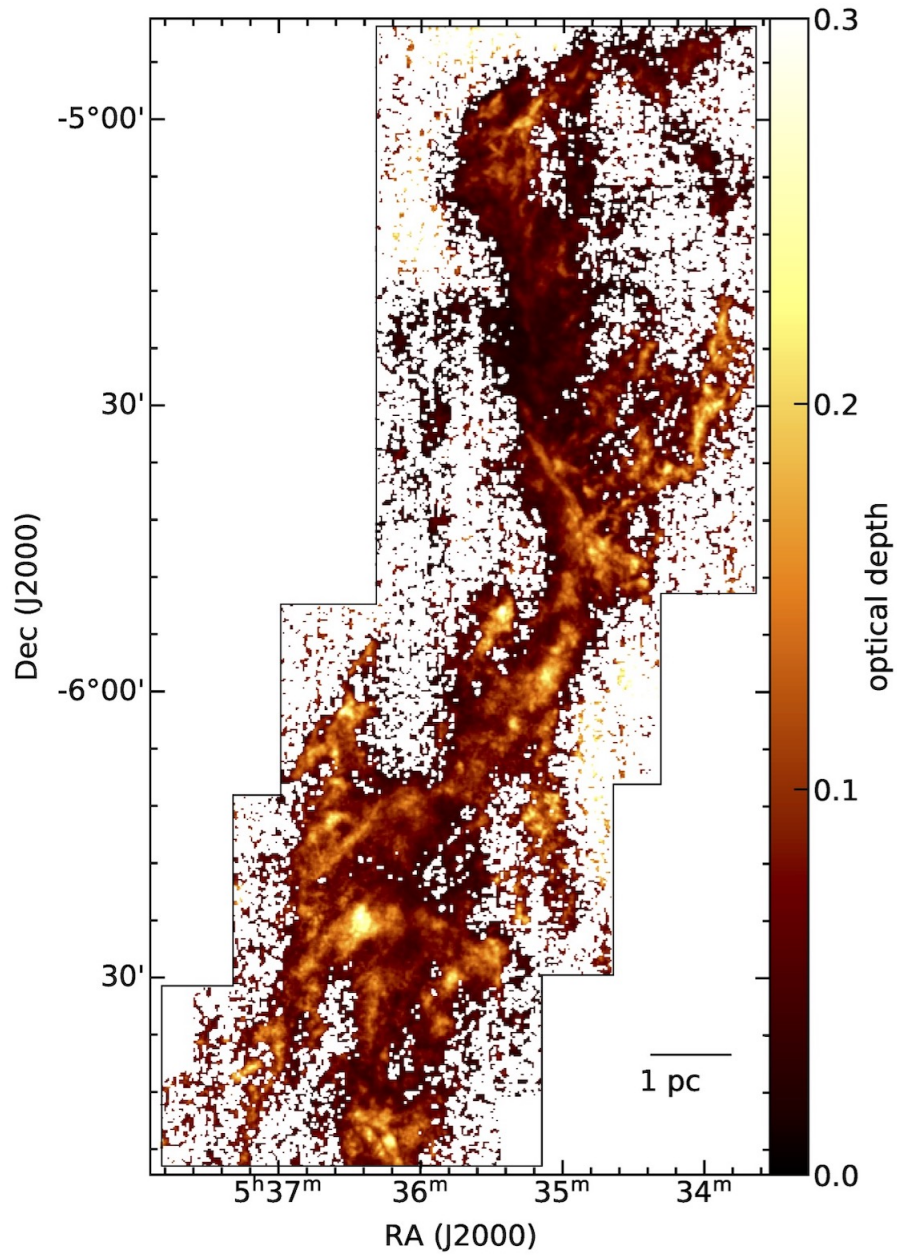


Fig. 3. The optical depth of the C^{18}O ($J = 1-0$) emission in Orion A. We calculated the optical depth for the same pixels of figure 2 by using the temperature derived from ^{12}CO ($J=1-0$) observations.

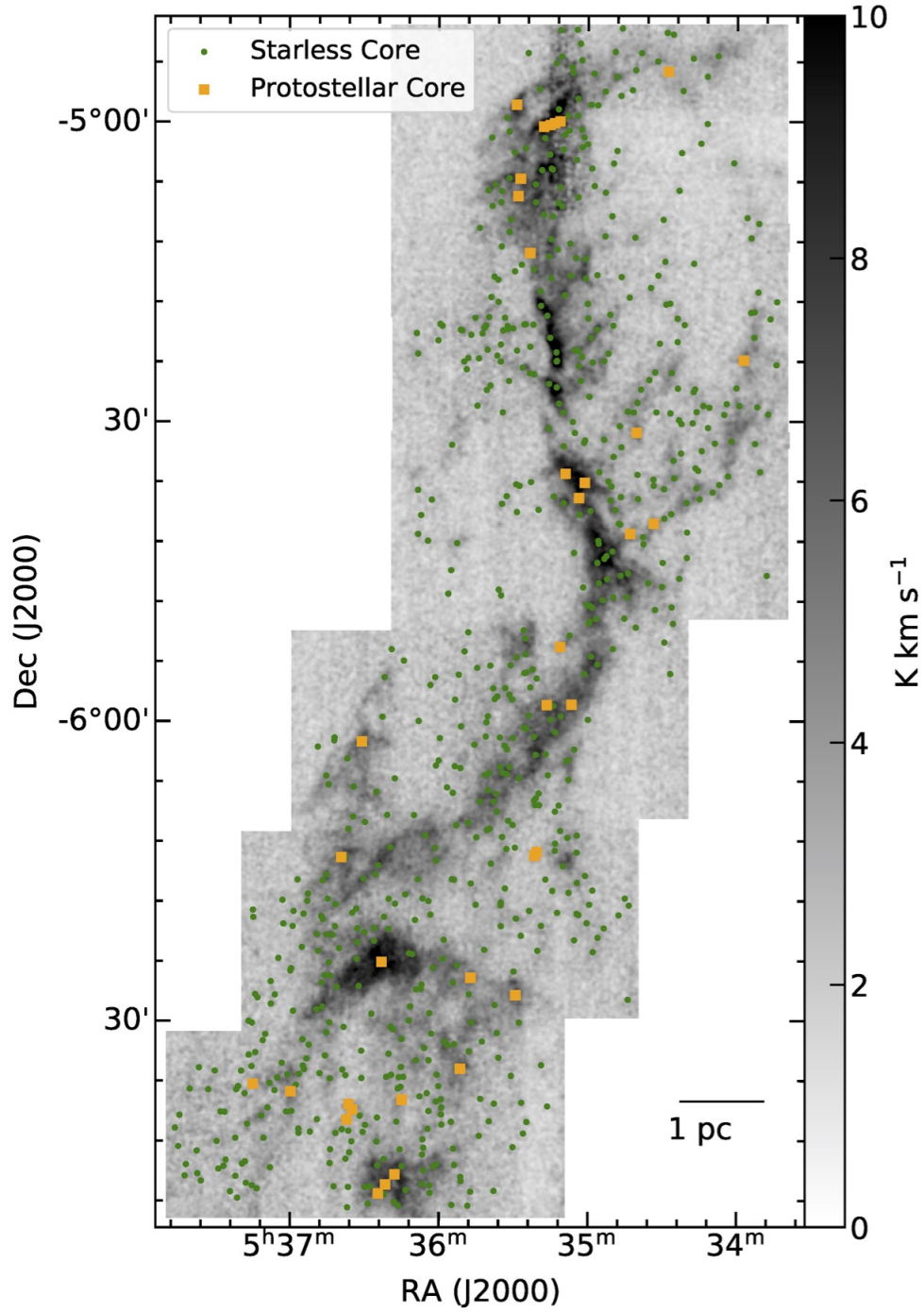


Fig. 4. The identified starless cores (green circles) and protostellar cores (orange squares) are plotted on the integrated intensity map of the $C^{18}O$ emission.

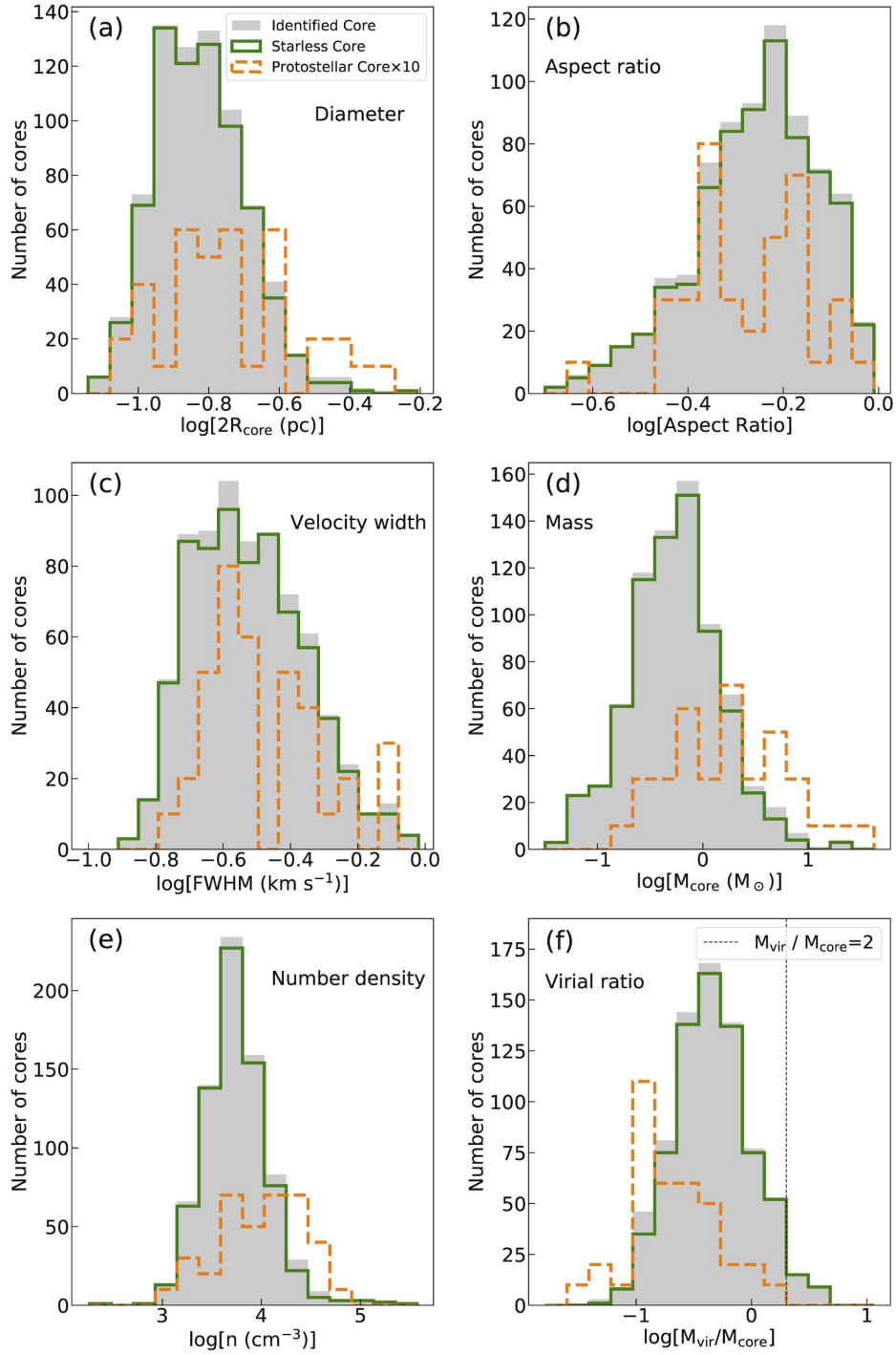


Fig. 5. The histograms of (a) the diameter (b) the aspect ratio, (c) the FWHM velocity width, (d) the core mass, (e) the number density and (f) the virial ratio of $C^{18}O$ cores calculated from $C^{18}O$ observation, respectively. The histogram for all identified cores is shown in grey. The green and orange histograms are for starless cores and protostellar cores. The vertical line in (d) shows $M_{\text{core}}/M_{\text{vir}} = 2$.

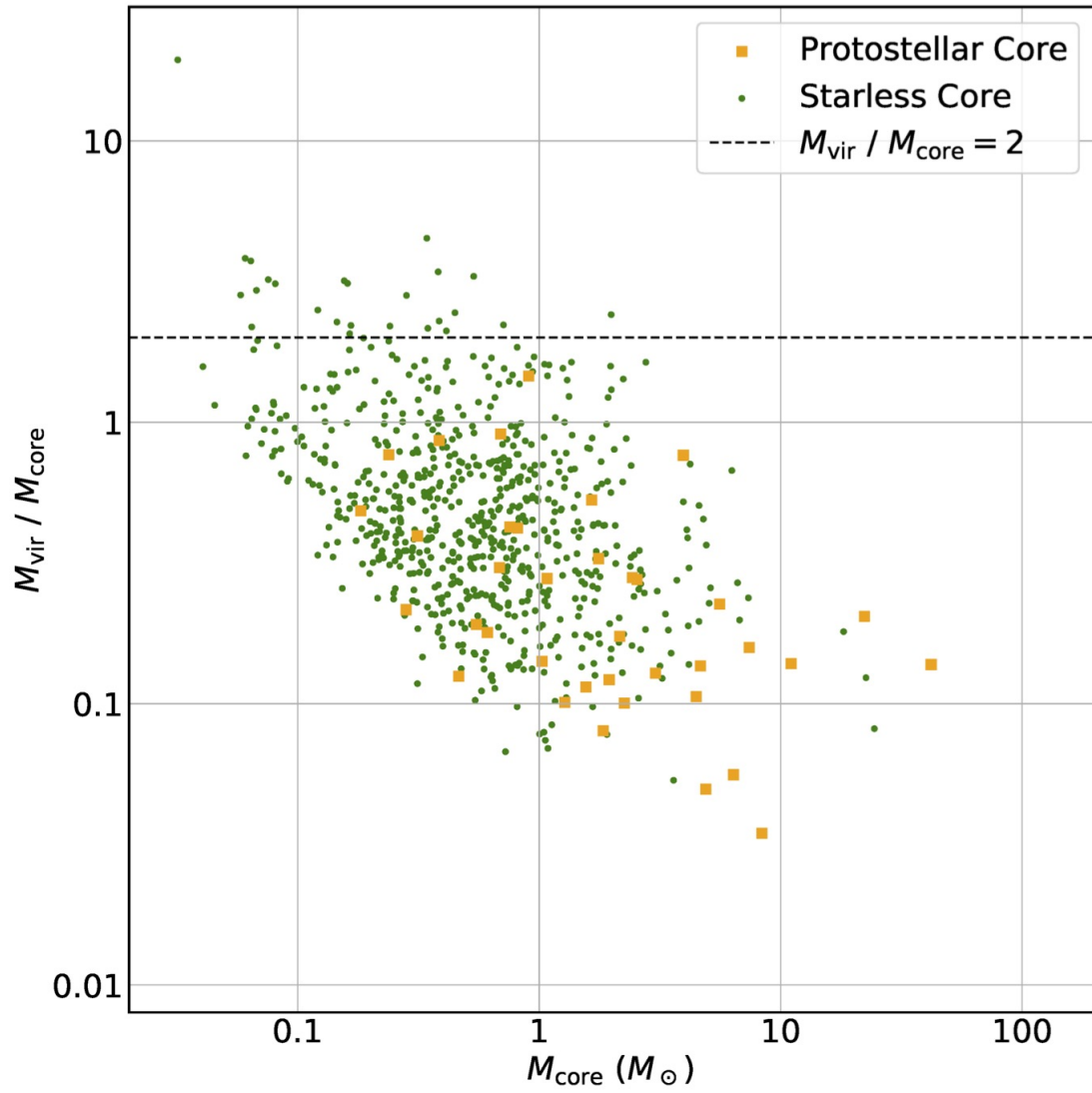


Fig. 6. Virial ratio ($M_{\text{core}}/M_{\text{vir}}$) – core mass relation. The horizontal dashed line shows $M_{\text{core}}/M_{\text{vir}}=2$. The starless cores and protostellar cores are shown as green dots and orange squares, respectively.

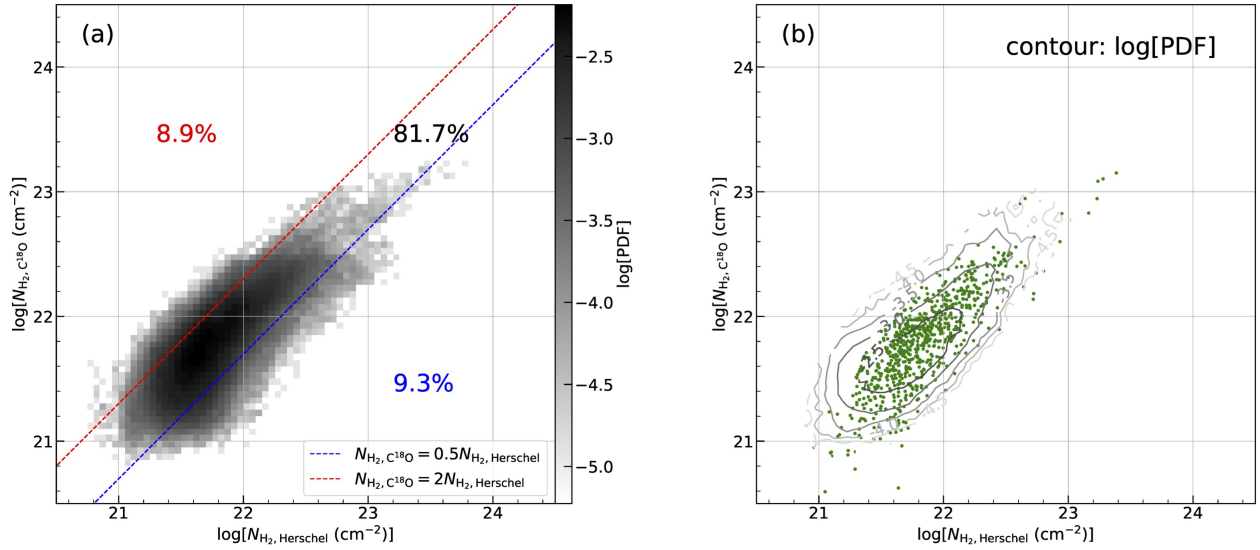


Fig. 7. Relationship between the H₂ column density derived directly from the C¹⁸O integrated intensity, $N_{\text{H}_2, \text{C}^{18}\text{O}}$, and the *Herschel-Planck* H₂ column density, $N_{\text{H}_2, \text{Herschel}}$ is shown as (a) two dimensional histogram of PDF and (b) contour. Here we calculated values of pixels whose integrated intensity is larger than 15 local rms noise in the projections of all identified trunks onto the sky plane. The blue and red dashed lines in (a) show $2N_{\text{H}_2, \text{C}^{18}\text{O}} = N_{\text{H}_2, \text{Herschel}}$ and $N_{\text{H}_2, \text{C}^{18}\text{O}} = 2N_{\text{H}_2, \text{Herschel}}$. $N_{\text{H}_2, \text{C}^{18}\text{O}}$ is the column density of H₂ calculated from the C¹⁸O ($J=1-0$) observations and mean abundance ratio of C¹⁸O. $N_{\text{H}_2, \text{Herschel}}$ is the column density of H₂ derived from *Herschel* observations. Each percentage represents the fraction of N in each range: $N_{\text{H}_2, \text{C}^{18}\text{O}} / N_{\text{H}_2, \text{Herschel}} > 2$ (red), $1/2 \leq N_{\text{H}_2, \text{C}^{18}\text{O}} / N_{\text{H}_2, \text{Herschel}} \leq 2$ (black) and $N_{\text{H}_2, \text{C}^{18}\text{O}} / N_{\text{H}_2, \text{Herschel}} < 1/2$ (blue). In (b), the contour is drawn from $\log[\text{PDF}] = -4.5$ to -2.5 every $\log[\text{PDF}] = 0.5$. The dots show all identified C¹⁸O cores. The mean values of $N_{\text{H}_2, \text{C}^{18}\text{O}}$ and $N_{\text{H}_2, \text{Herschel}}$ in the projections of cores onto the plane of the sky are used to plot cores onto the figure.

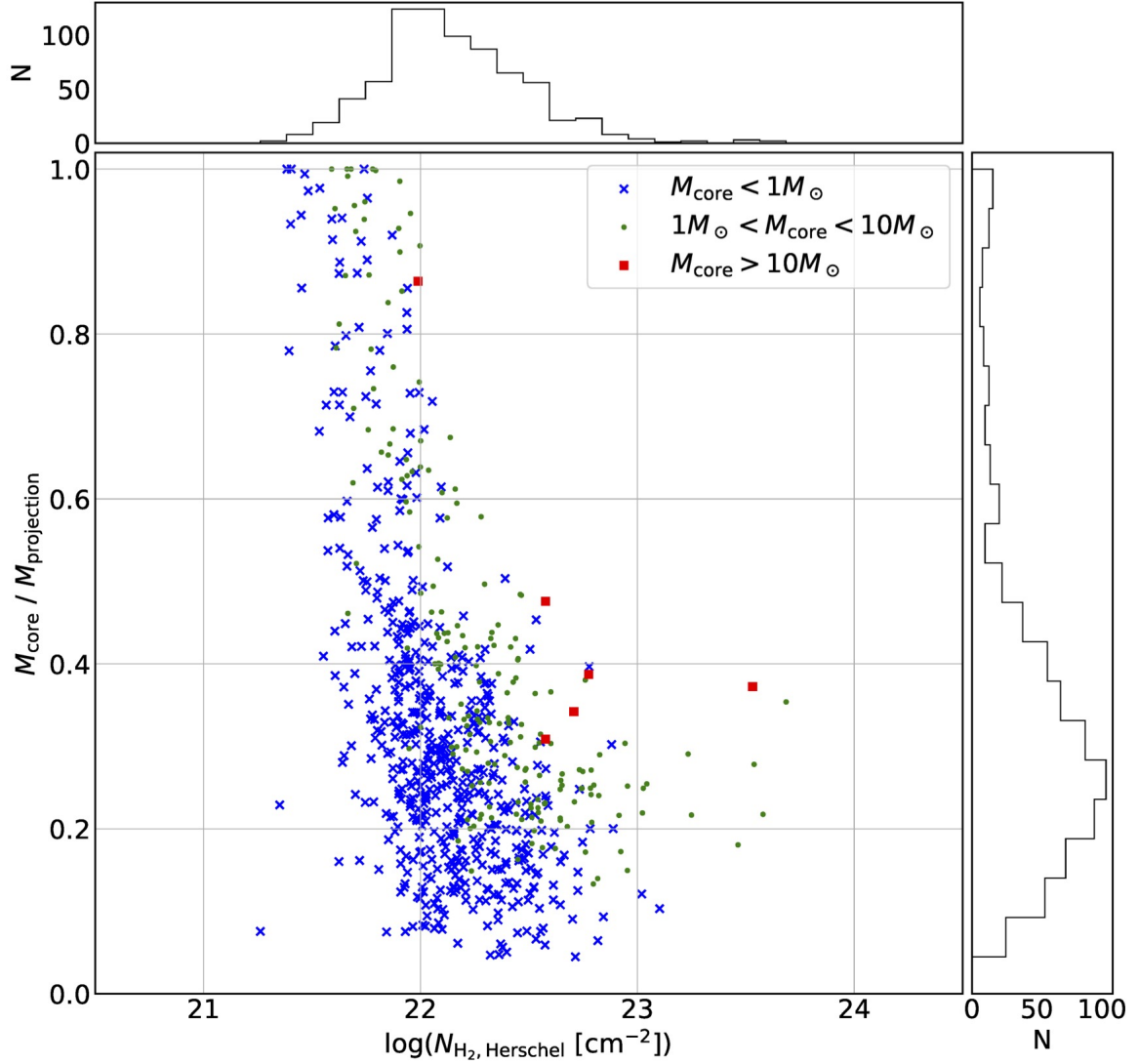


Fig. 8. Mass ratio $M_{\text{core}} / M_{\text{projection}} - N_{\text{H}_2, \text{Herschel}}$ relation. To calculate $M_{\text{projection}}$, all H_2 column density is assigned to cores. When multiple cores overlap along the line of sight, H_2 column density proportional to each intensity is distributed to each core. The mean value and standard deviation of mass ratio $M_{\text{core}} / M_{\text{projection}}$ are 0.35 ± 0.21 . The blue crosses, green circles and red squares show the cores whose masses are $M_{\text{core}} < 1M_{\odot}$, $1M_{\odot} < M_{\text{core}} < 10M_{\odot}$ and $M_{\text{core}} > 10M_{\odot}$, respectively.

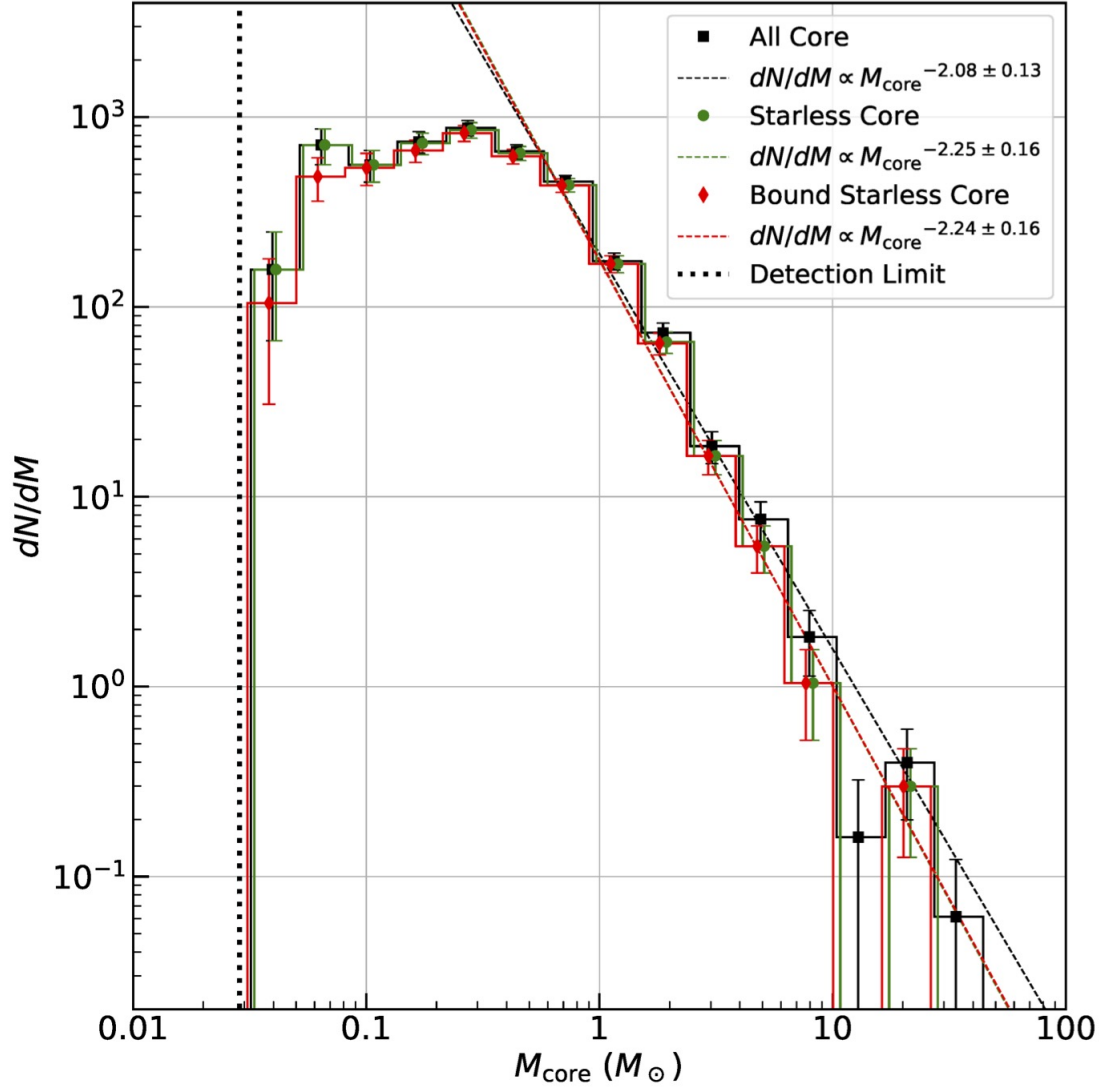


Fig. 9. CMFs for the identified cores (black line), starless cores (green line), and gravitationally bound starless cores (red line). The error bars show the statistical uncertainty calculated as the square root of the number of cores in each mass bin, \sqrt{N} . The dashed line shows the best-fit single power-law functions for each CMF between one mass bins above the turnover and the high-mass end. The dotted line shows the detection mass limit of $\sim 0.03M_{\odot}$.

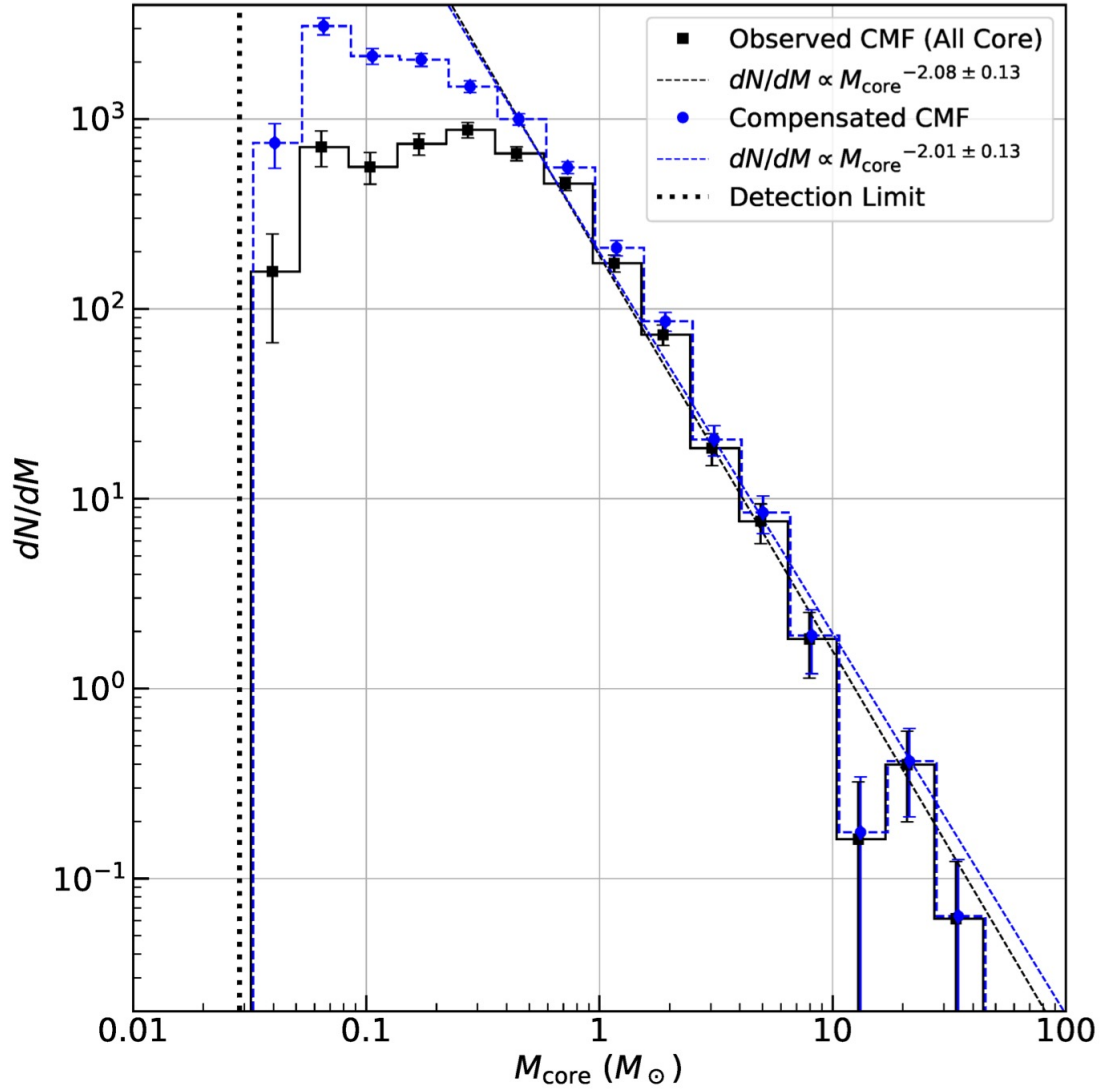


Fig. 10. Observed CMF (black line) and compensated CMF (blue line) for the identified cores. In compensated CMF, we derived the number of cores in each mass bin by dividing the observed number by detection probability.

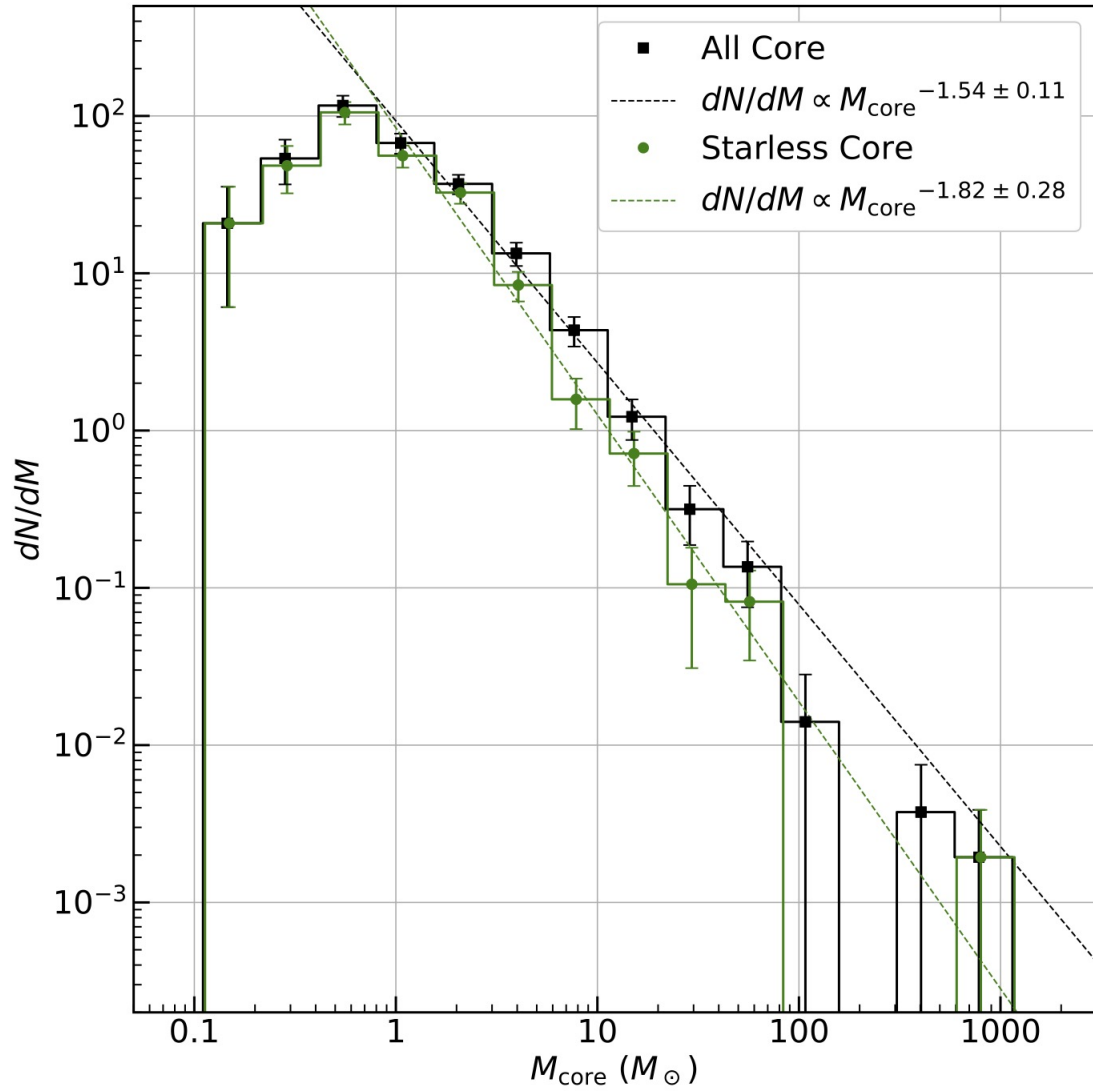


Fig. 11. CMFs of all dust cores and starless cores identified in (nutter07) in Orion A. The dashed line shows the best-fit single power-law functions for each CMF above the turnover as figure 9.

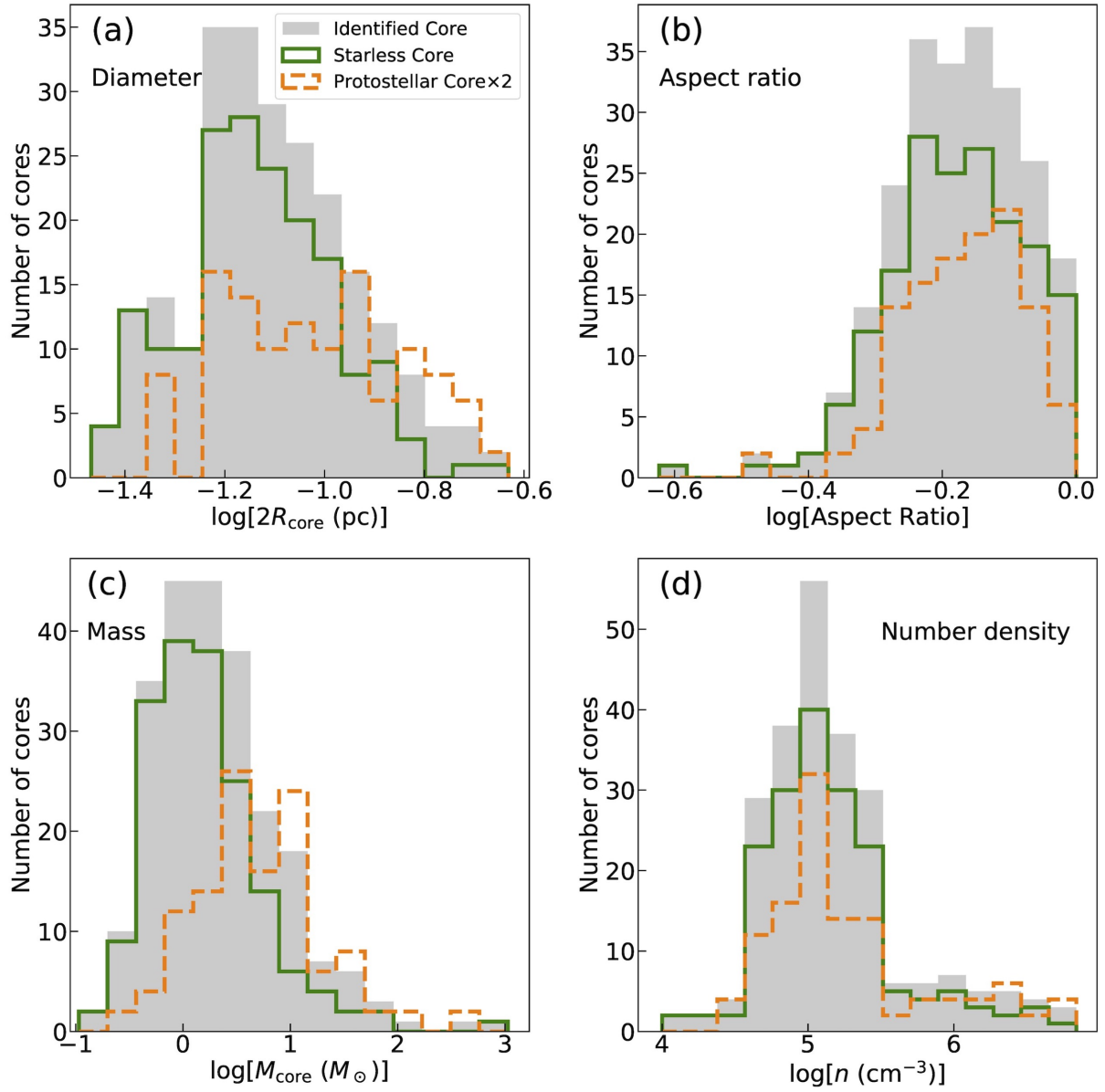


Fig. 12. The histograms of (a) the diameter (b) the aspect ratio, (c) the core mass, (d) the number density of dust cores, respectively. The histogram for the all dust cores is shown in grey. The green and orange histograms are for starless cores and protostellar cores.

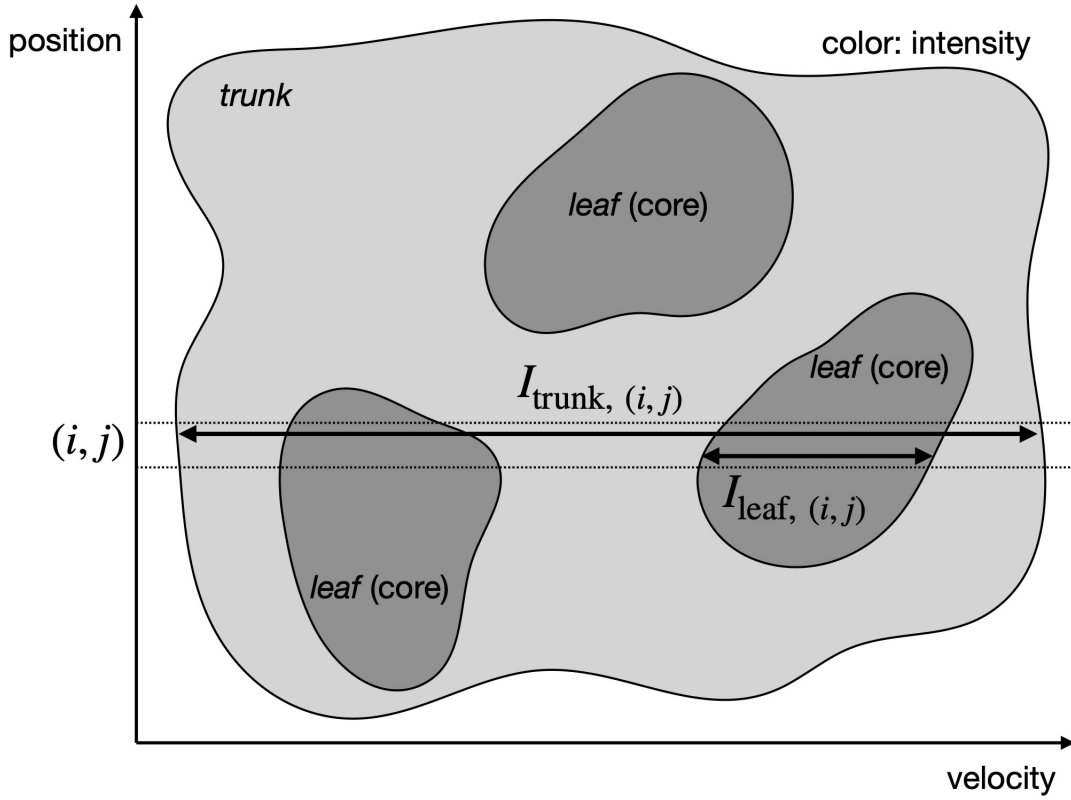


Fig. 13. Schematic representation of how to calculate the core masses using the *Herschel-Planck* H_2 column density and $C^{18}O$ intensity maps.

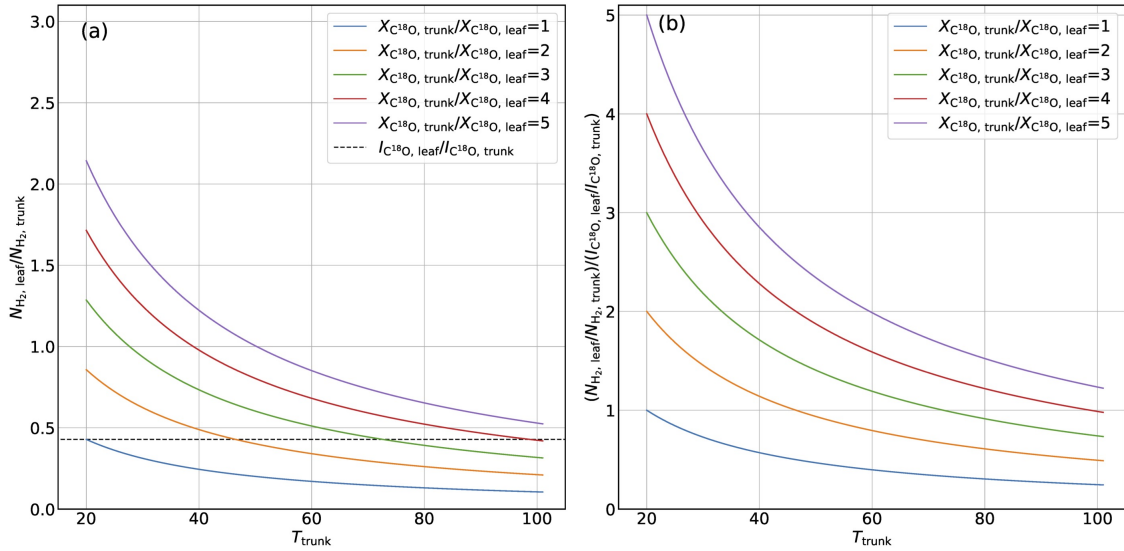


Fig. 14. (a) The relationship between H_2 column density ratio, $N_{H_2, leaf} / N_{H_2, trunk}$ and temperature of trunk with the abundance ratio, $X_{C^{18}O, trunk} / X_{C^{18}O, leaf}$, of form 1 to 5. Here we fix the temperature of leaf and integrated intensity ratio, $I_{C^{18}O, leaf} / I_{C^{18}O, trunk}$, as 20 K and 3/7 (from section 8), respectively. (b) The relationship between ratio of H_2 column density ratio to integrated intensity ratio and temperature of trunk.

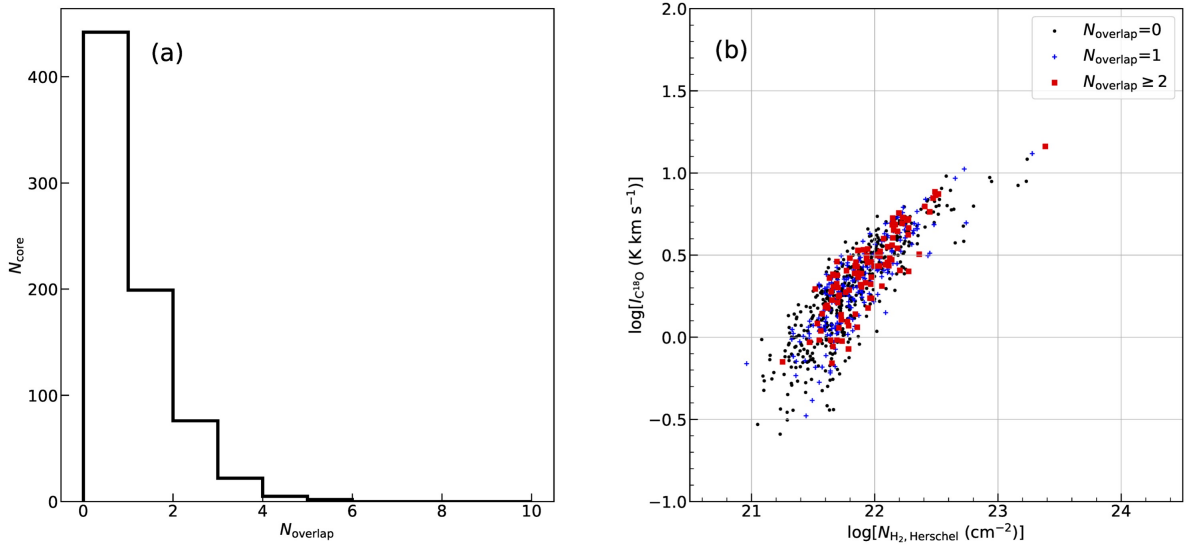


Fig. 15. (a) The histogram of the number of overlapped cores. (b) The distribution of overlapped cores in $I_{\text{C}18\text{O}} - N_{\text{H}_2, \text{leaf}}$ plane.

Table 1. The Results of Core Identification in Orion A

Core Category	Identification N
Identified Core	746
Starless Core	709
Protostellar Core	37

Table 2. The Summary of Core Properties in Orion A

Property	Category	Minimum	Maximum	Mean \pm Std.
Diameter (pc)	Identified Core	0.07	0.62	0.16 ± 0.06
	Starless Core	0.07	0.62	0.16 ± 0.05
	Protostellar Core	0.08	0.50	0.20 ± 0.10
Aspect Ratio	Identified Core	0.20	0.98	0.58 ± 0.16
	Starless Core	0.20	0.98	0.58 ± 0.16
	Protostellar Core	0.24	0.92	0.56 ± 0.16
FWHM (km s^{-1})	Identified Core	0.12	0.96	0.33 ± 0.14
	Starless Core	0.12	0.96	0.32 ± 0.14
	Protostellar Core	0.18	0.81	0.36 ± 0.16
Mass (M_{\odot})	Identified Core	0.03	42.00	1.08 ± 2.42
	Starless Core	0.03	24.45	0.92 ± 1.65
	Protostellar Core	0.18	42.00	4.12 ± 7.51
Number Density (10^4 cm^{-3})	Identified Core	0.02	37.36	0.87 ± 1.92
	Starless Core	0.02	37.36	0.84 ± 1.94
	Protostellar Core	0.12	6.53	1.54 ± 1.38
Virial Ratio	Identified Core	0.03	19.45	0.64 ± 0.89
	Starless Core	0.05	19.45	0.66 ± 0.91
	Protostellar Core	0.03	1.46	0.31 ± 0.30

Table 3: Properties of Identified Cores (1)

ID	RA (J2000)	Dec (J2000)	v_{LSR} (km s^{-1})	A (arcsec^2)	$2R_{\text{core}}$ (arcsec)	$2R_{\text{core}}$ (pc)	a_{major} (arcsec)	a_{minor} (arcsec)	PA (deg)	dV_{core} (km s^{-1})	YSO
1	5 33 44.7	-5 18 5	9.3	5738	85	0.17	21.8	19.3	-149	0.38	N
2	5 33 45.0	-5 24 24	8.2	2756	59	0.12	25.0	10.8	89	0.18	N
3	5 33 47.3	-5 19 48	8.3	2925	61	0.12	30.8	8.9	84	0.17	N
4	5 33 48.2	-5 29 20	7.9	5119	81	0.16	34.1	9.1	61	0.28	N
5	5 33 48.7	-5 45 29	7.7	2925	61	0.12	20.5	13.6	74	0.22	N
6	5 33 51.5	-5 35 7	8.0	8100	102	0.20	24.3	20.3	-175	0.34	N
7	5 33 51.9	-5 10 15	10.5	2756	59	0.12	16.2	11.1	80	0.25	N
8	5 33 52.2	-5 17 8	10.2	3263	64	0.13	24.3	12.5	-138	0.19	N
9	5 33 52.6	-5 28 36	8.4	2475	56	0.11	27.9	8.9	59	0.25	N
10	5 33 53.4	-5 32 17	8.1	5794	86	0.17	23.7	15.1	145	0.34	N
11	5 33 53.6	-5 19 6	9.1	2250	54	0.11	16.1	10.2	85	0.19	Y
12	5 33 53.8	-5 21 39	8.3	6581	92	0.18	39.4	10.7	87	0.30	N
13	5 33 54.9	-5 11 42	10.7	4838	78	0.16	22.0	11.4	56	0.77	N
14	5 33 55.1	-5 19 10	9.7	2250	54	0.11	17.8	10.1	46	0.27	N
15	5 33 56.5	-5 9 40	10.7	6694	92	0.19	44.4	13.8	59	0.37	N
16	5 33 58.0	-5 23 57	8.2	3769	69	0.14	23.4	10.1	88	0.22	N
17	5 33 59.9	-5 28 29	8.0	4444	75	0.15	20.6	12.6	117	0.29	N
18	5 34 1.0	-5 26 43	8.6	3488	67	0.13	19.7	11.1	72	0.22	N
19	5 34 1.9	-5 4 11	10.9	36563	216	0.43	53.6	40.1	117	0.72	N
20	5 34 3.0	-5 32 3	8.3	10294	114	0.23	61.3	15.8	71	0.38	N
21	5 34 4.3	-5 35 33	8.4	2419	55	0.11	22.2	9.1	99	0.22	N
22	5 34 4.9	-5 28 17	8.4	3038	62	0.12	14.7	12.4	-140	0.32	N
23	5 34 5.9	-5 29 23	8.2	2925	61	0.12	13.4	13.1	-168	0.34	N
24	5 34 7.8	-5 36 24	9.5	4556	76	0.15	29.4	14.5	-137	0.18	N
25	5 34 8.3	-4 53 28	9.4	11644	122	0.24	43.7	22.1	63	0.37	N
26	5 34 9.6	-5 32 15	8.1	2644	58	0.12	19.0	9.2	155	0.26	N
27	5 34 10.5	-5 37 9	8.2	6075	88	0.18	31.4	18.3	176	0.36	N
28	5 34 11.9	-5 28 39	9.1	8269	103	0.21	38.1	22.1	157	0.48	N
29	5 34 12.4	-5 30 41	9.2	5569	84	0.17	31.4	16.9	113	0.31	N
30	5 34 12.5	-4 55 31	10.3	3488	67	0.13	35.1	9.8	104	0.15	N
31	5 34 12.6	-5 0 15	10.5	8325	103	0.21	30.0	21.1	-149	0.45	N
32	5 34 14.3	-5 28 29	8.2	3825	70	0.14	19.0	12.3	164	0.28	N
33	5 34 15.0	-5 33 0	7.8	4669	77	0.15	21.1	16.5	162	0.29	N
34	5 34 15.1	-5 2 13	10.6	13950	133	0.27	64.4	20.0	-143	0.40	Y
35	5 34 15.8	-5 37 49	9.9	5513	84	0.17	28.0	16.5	134	0.17	N
36	5 34 16.4	-5 34 58	7.6	2475	56	0.11	14.9	10.7	-139	0.22	N
37	5 34 17.0	-5 29 6	8.9	2925	61	0.12	17.6	10.9	85	0.20	Y
38	5 34 17.1	-5 36 44	7.7	7706	99	0.20	25.3	21.0	-172	0.37	N
39	5 34 17.5	-5 34 43	8.1	1856	49	0.10	17.7	8.4	178	0.20	Y
40	5 34 17.6	-5 26 49	8.3	6356	90	0.18	40.4	14.5	128	0.35	N
41	5 34 18.0	-5 14 14	10.5	6075	88	0.18	29.8	15.4	172	0.31	N
42	5 34 18.2	-4 53 42	9.7	5569	84	0.17	20.2	19.4	-138	0.30	N
43	5 34 18.2	-5 27 6	8.9	2925	61	0.12	18.7	10.4	104	0.25	N
44	5 34 18.6	-5 30 13	8.5	2531	57	0.11	15.4	11.1	51	0.25	N
45	5 34 20.8	-5 41 9	10.1	5119	81	0.16	24.6	15.2	151	0.35	N
46	5 34 20.9	-5 43 42	9.5	10744	117	0.23	28.9	21.7	102	0.45	N
47	5 34 21.0	-5 38 11	8.1	10181	114	0.23	34.3	18.2	-176	0.83	N
48	5 34 21.8	-5 20 23	9.4	11700	122	0.24	31.2	22.3	108	0.52	N
49	5 34 22.3	-4 56 57	9.7	7425	97	0.20	36.8	14.9	133	0.31	N

Table 3: Continued

ID	RA (J2000)	Dec (J2000)	v_{LSR} (km s ⁻¹)	A (arcsec ²)	$2R_{\text{core}}$ (arcsec)	$2R_{\text{core}}$ (pc)	a_{major} (arcsec)	a_{minor} (arcsec)	PA (deg)	dV_{core} (km s ⁻¹)	YSO
50	5 34 23.0	-5 3 9	9.6	9675	111	0.22	32.7	19.7	-154	0.26	N
51	5 34 23.1	-5 30 18	9.6	7369	97	0.19	47.8	17.1	74	0.27	Y
52	5 34 23.4	-5 33 15	9.8	1688	46	0.09	11.5	8.7	137	0.15	N
53	5 34 24.0	-5 6 56	10.2	7650	99	0.20	24.0	21.4	92	0.49	N
54	5 34 24.0	-5 45 47	9.1	2925	61	0.12	13.7	11.7	68	0.35	N
55	5 34 24.2	-5 29 55	8.8	7875	100	0.20	34.9	15.4	77	0.33	N
56	5 34 24.6	-5 26 45	8.4	1069	37	0.07	8.7	6.7	-138	0.36	Y
57	5 34 24.7	-5 19 45	8.3	7819	100	0.20	28.7	16.6	121	0.42	N
58	5 34 24.7	-5 22 5	9.1	4050	72	0.14	26.2	13.9	56	0.22	N
59	5 34 26.1	-5 35 44	7.7	2869	60	0.12	17.8	10.1	80	0.33	N
60	5 34 26.3	-4 51 18	12.3	4669	77	0.15	23.4	16.9	138	0.19	Y
61	5 34 26.4	-5 33 58	7.9	2588	57	0.12	15.3	10.1	108	0.19	N
62	5 34 26.6	-5 50 17	9.7	4894	79	0.16	18.4	15.8	111	0.28	N
63	5 34 27.1	-5 25 11	8.1	7819	100	0.20	42.6	11.8	76	0.59	N
64	5 34 27.1	-5 48 39	9.2	3263	64	0.13	17.4	11.7	162	0.22	Y
65	5 34 27.2	-5 39 19	8.0	2588	57	0.12	16.0	11.2	-150	0.42	N
66	5 34 27.6	-5 29 14	9.4	2869	60	0.12	14.5	12.8	178	0.18	N
67	5 34 27.6	-5 55 19	8.0	8550	104	0.21	34.1	15.3	96	0.27	N
68	5 34 27.7	-5 18 14	8.3	4838	78	0.16	20.0	14.7	164	0.26	N
69	5 34 28.2	-4 55 0	9.9	2081	51	0.10	15.0	10.2	106	0.18	N
70	5 34 28.8	-4 51 8	9.8	2419	55	0.11	24.3	11.1	92	0.14	N
71	5 34 29.3	-5 18 20	10.5	7875	100	0.20	26.4	20.9	-146	0.67	N
72	5 34 29.7	-5 14 3	10.9	6300	90	0.18	22.0	16.9	116	0.68	N
73	5 34 30.0	-5 39 45	10.0	2869	60	0.12	22.9	10.0	-139	0.34	N
74	5 34 30.1	-5 52 9	10.3	10181	114	0.23	46.1	22.0	-172	0.29	N
75	5 34 30.2	-5 36 49	7.7	4950	79	0.16	26.9	13.0	66	0.26	N
76	5 34 30.4	-5 9 51	11.4	6244	89	0.18	30.6	24.9	115	0.30	N
77	5 34 30.7	-5 44 11	8.2	2194	53	0.11	16.4	10.7	158	0.18	N
78	5 34 31.0	-5 46 36	8.9	5344	82	0.17	24.3	15.2	90	0.21	N
79	5 34 31.9	-5 22 15	7.9	23738	174	0.35	40.9	33.2	-177	0.42	N
80	5 34 32.5	-5 15 26	10.8	13950	133	0.27	54.9	27.1	82	0.40	N
81	5 34 32.6	-4 53 60	10.7	7763	99	0.20	29.5	14.9	-145	0.63	N
82	5 34 33.2	-5 29 7	9.9	5906	87	0.17	28.5	16.0	-173	0.48	N
83	5 34 33.7	-5 25 7	9.3	9281	109	0.22	34.6	14.4	49	0.54	Y
84	5 34 33.8	-5 48 54	9.1	3263	64	0.13	17.8	13.9	-177	0.19	N
85	5 34 34.3	-5 36 28	9.8	9844	112	0.22	43.3	17.2	152	0.50	N
86	5 34 34.3	-5 40 16	7.8	4669	77	0.15	23.6	11.9	-141	0.44	N
87	5 34 34.4	-5 35 51	7.9	2531	57	0.11	19.0	10.6	80	0.21	N
88	5 34 35.4	-5 16 40	10.0	11419	121	0.24	54.7	15.7	76	0.56	N
89	5 34 36.1	-5 25 53	8.2	2700	59	0.12	14.8	14.1	86	0.27	N
90	5 34 36.5	-5 46 13	8.4	3769	69	0.14	33.8	9.8	156	0.24	N
91	5 34 38.4	-5 42 19	9.4	2025	51	0.10	17.5	8.0	62	0.26	N
92	5 34 38.6	-5 41 37	8.1	3713	69	0.14	20.1	17.7	144	0.27	N
93	5 34 39.0	-4 53 9	11.3	10125	114	0.23	33.3	21.8	-151	0.44	N
94	5 34 39.5	-5 26 51	8.6	5231	82	0.16	32.8	16.1	-143	0.44	N
95	5 34 40.7	-5 37 48	8.1	7763	99	0.20	23.1	18.3	68	0.59	N
96	5 34 40.8	-5 35 23	8.0	4331	74	0.15	27.0	12.8	-158	0.25	N
97	5 34 40.9	-5 28 10	7.9	2475	56	0.11	17.4	9.2	176	0.22	N
98	5 34 41.2	-5 31 11	7.2	11700	122	0.24	38.8	19.3	77	0.81	N

Table 3: Continued

ID	RA (J2000)	Dec (J2000)	v_{LSR} (km s ⁻¹)	A (arcsec ²)	$2R_{\text{core}}$ (arcsec)	$2R_{\text{core}}$ (pc)	a_{major} (arcsec)	a_{minor} (arcsec)	PA (deg)	dV_{core} (km s ⁻¹)	YSO
99	5 34 41.4	-4 54 51	11.0	5738	85	0.17	26.1	13.6	-158	0.44	N
100	5 34 41.5	-5 50 40	9.9	6413	90	0.18	26.3	20.6	-162	0.40	N
101	5 34 41.7	-5 11 37	11.0	15919	142	0.29	41.8	25.1	-151	0.60	N
102	5 34 42.3	-5 29 8	9.4	2531	57	0.11	18.9	11.0	-177	0.34	N
103	5 34 42.8	-4 56 52	8.8	4219	73	0.15	23.2	15.3	68	0.32	N
104	5 34 43.8	-5 41 18	7.6	1406	42	0.08	14.2	6.6	68	0.19	N
105	5 34 44.0	-5 17 38	11.2	2700	59	0.12	15.8	12.6	95	0.23	N
106	5 34 44.3	-6 18 30	12.3	3206	64	0.13	20.2	12.7	143	0.21	N
107	5 34 44.6	-5 45 15	7.7	1800	48	0.10	13.0	8.2	155	0.24	N
108	5 34 44.7	-5 29 4	8.2	6075	88	0.18	26.0	19.3	167	0.25	N
109	5 34 44.7	-6 27 55	8.2	1969	50	0.10	14.4	8.9	122	0.22	N
110	5 34 45.2	-5 47 37	9.4	4331	74	0.15	21.3	12.2	50	0.25	N
111	5 34 45.9	-6 17 48	7.6	2813	60	0.12	19.9	10.5	-135	0.36	N
112	5 34 46.1	-5 49 46	7.3	9394	109	0.22	30.3	18.7	54	0.63	N
113	5 34 46.8	-4 50 41	7.3	2644	58	0.12	19.4	13.2	-141	0.24	N
114	5 34 47.2	-5 15 34	9.8	9169	108	0.22	31.1	17.6	128	0.62	N
115	5 34 47.3	-4 57 26	11.6	1575	45	0.09	12.0	8.0	-138	0.18	N
116	5 34 47.3	-5 32 37	7.5	2419	55	0.11	17.5	9.8	149	0.17	Y
117	5 34 47.5	-5 37 36	7.2	1744	47	0.09	12.5	8.7	-170	0.26	N
118	5 34 47.6	-5 45 29	9.1	4500	76	0.15	28.6	11.7	143	0.31	N
119	5 34 47.8	-5 40 21	6.5	5681	85	0.17	23.2	17.0	-180	0.25	N
120	5 34 48.0	-5 30 30	8.5	5906	87	0.17	29.3	12.6	97	0.44	N
121	5 34 48.3	-5 40 16	10.0	2475	56	0.11	12.9	11.2	81	0.27	N
122	5 34 48.4	-6 19 28	7.4	4219	73	0.15	30.5	12.5	101	0.22	N
123	5 34 48.9	-4 55 33	10.6	5175	81	0.16	20.6	14.4	-176	0.50	N
124	5 34 48.9	-5 2 57	11.2	13894	133	0.27	45.3	24.0	-165	0.48	Y
125	5 34 49.6	-4 53 2	11.0	5175	81	0.16	35.7	10.3	55	0.40	N
126	5 34 49.8	-5 38 54	7.7	11700	122	0.24	30.1	24.7	162	0.67	N
127	5 34 50.3	-5 4 13	10.4	8606	105	0.21	27.9	18.1	-158	0.45	N
128	5 34 50.4	-5 33 34	7.0	5344	82	0.17	38.4	10.5	-141	0.45	N
129	5 34 50.5	-5 47 40	8.5	2306	54	0.11	14.6	9.7	102	0.21	N
130	5 34 50.6	-5 20 27	10.6	18563	154	0.31	58.3	26.8	74	0.91	N
131	5 34 50.8	-5 52 49	9.2	6638	92	0.18	24.2	20.0	150	0.42	N
132	5 34 50.9	-5 43 3	8.5	2138	52	0.10	13.4	9.0	111	0.49	N
133	5 34 51.0	-5 9 29	11.2	11138	119	0.24	41.6	17.0	160	0.31	N
134	5 34 51.3	-5 36 34	7.4	2306	54	0.11	14.0	9.0	-138	0.30	N
135	5 34 51.7	-5 37 56	6.7	1181	39	0.08	9.7	7.1	129	0.28	N
136	5 34 51.8	-5 19 21	9.1	1800	48	0.10	13.3	7.9	55	0.33	N
137	5 34 52.5	-5 23 14	10.3	5738	85	0.17	45.2	12.5	53	0.30	N
138	5 34 52.6	-5 36 3	10.2	7200	96	0.19	35.8	14.5	153	0.34	Y
139	5 34 53.1	-5 45 49	8.2	3094	63	0.13	39.5	8.4	97	0.24	N
140	5 34 53.3	-5 43 31	7.8	9056	107	0.22	42.6	15.5	53	0.44	N
141	5 34 53.6	-4 56 60	10.9	4219	73	0.15	27.2	8.9	56	0.33	N
142	5 34 53.6	-5 7 7	11.3	6806	93	0.19	24.0	16.9	121	0.46	N
143	5 34 53.7	-5 11 30	10.7	4725	78	0.16	30.0	15.9	165	0.25	N
144	5 34 54.2	-5 23 60	11.4	4275	74	0.15	31.8	9.4	70	0.48	N
145	5 34 54.2	-5 31 52	7.7	6131	88	0.18	19.4	18.2	75	0.58	N
146	5 34 54.2	-5 43 47	9.0	1688	46	0.09	17.6	7.1	135	0.26	N
147	5 34 54.4	-6 20 47	7.5	6863	93	0.19	22.5	19.6	-152	0.35	N

Table 3: Continued

ID	RA (J2000)	Dec (J2000)	v_{LSR} (km s ⁻¹)	A (arcsec ²)	$2R_{\text{core}}$ (arcsec)	$2R_{\text{core}}$ (pc)	a_{major} (arcsec)	a_{minor} (arcsec)	PA (deg)	dV_{core} (km s ⁻¹)	YSO
148	5 34 54.9	-5 47 55	8.7	4275	74	0.15	31.9	10.3	103	0.37	N
149	5 34 56.2	-5 35 7	8.9	3938	71	0.14	21.2	15.4	122	0.44	N
150	5 34 56.3	-5 46 14	7.5	1125	38	0.08	9.0	7.8	85	0.20	N
151	5 34 56.4	-5 42 16	8.9	6919	94	0.19	31.9	15.4	103	0.43	N
152	5 34 56.6	-4 58 23	12.1	4275	74	0.15	22.6	14.5	-138	0.21	N
153	5 34 56.6	-5 41 59	7.3	9619	111	0.22	37.2	17.6	99	0.26	N
154	5 34 56.9	-5 15 22	7.9	3375	66	0.13	19.7	16.5	148	0.45	N
155	5 34 56.9	-6 21 43	6.5	2813	60	0.12	23.0	8.6	73	0.15	N
156	5 34 57.0	-5 20 51	8.4	1350	41	0.08	12.3	6.6	61	0.25	N
157	5 34 57.0	-5 44 11	7.0	6188	89	0.18	30.3	21.2	-167	0.31	N
158	5 34 57.0	-5 54 22	8.4	2813	60	0.12	18.6	10.5	174	0.30	N
159	5 34 57.7	-5 49 49	8.2	3319	65	0.13	19.4	12.0	121	0.27	N
160	5 34 58.1	-4 55 12	11.1	7200	96	0.19	41.9	18.4	-178	0.25	N
161	5 34 58.1	-5 6 28	11.0	3206	64	0.13	17.8	10.8	120	0.34	N
162	5 34 58.8	-5 24 8	11.2	3038	62	0.12	20.6	11.2	120	0.16	N
163	5 34 58.8	-6 23 9	6.5	3206	64	0.13	25.8	11.9	63	0.30	N
164	5 34 59.0	-5 48 40	7.2	7650	99	0.20	33.1	14.4	91	0.32	N
165	5 34 59.0	-6 16 59	6.4	3150	63	0.13	20.8	9.9	125	0.22	N
166	5 34 59.1	-5 4 42	11.3	12881	128	0.26	51.8	22.0	118	0.43	N
167	5 34 59.3	-4 58 19	10.9	3825	70	0.14	19.9	11.4	-166	0.31	N
168	5 34 59.4	-5 21 39	8.5	1069	37	0.07	8.7	6.7	46	0.61	N
169	5 34 59.5	-5 53 34	7.5	3488	67	0.13	17.4	12.5	171	0.33	N
170	5 34 59.8	-5 38 59	9.0	2925	61	0.12	21.4	9.0	134	0.20	N
171	5 34 59.8	-5 48 32	9.5	3713	69	0.14	22.8	14.0	-173	0.16	N
172	5 35 0.2	-5 27 34	9.2	3150	63	0.13	16.5	10.8	161	0.46	N
173	5 35 0.2	-5 50 4	6.9	2869	60	0.12	17.9	10.7	129	0.18	N
174	5 35 0.3	-6 18 25	6.5	5231	82	0.16	24.5	13.1	156	0.32	N
175	5 35 0.4	-5 50 16	8.7	2756	59	0.12	26.7	8.6	75	0.23	N
176	5 35 0.7	-5 19 44	7.8	5006	80	0.16	17.6	16.0	73	0.76	N
177	5 35 0.8	-5 2 17	12.8	4219	73	0.15	23.0	11.6	113	0.23	N
178	5 35 0.8	-5 18 16	8.7	9338	109	0.22	22.8	22.2	178	0.75	N
179	5 35 0.8	-5 59 54	9.9	1519	44	0.09	11.5	7.4	-137	0.17	N
180	5 35 1.3	-5 48 23	8.3	1800	48	0.10	19.5	7.1	135	0.20	N
181	5 35 1.3	-6 20 15	8.4	3713	69	0.14	27.6	13.4	173	0.34	N
182	5 35 1.6	-5 15 43	9.3	4669	77	0.15	25.3	11.6	111	0.55	N
183	5 35 1.7	-5 13 44	9.9	4163	73	0.15	23.9	9.6	71	0.58	N
184	5 35 1.9	-5 31 56	10.3	26381	183	0.37	67.2	29.4	64	0.58	N
185	5 35 1.9	-6 15 32	6.0	3544	67	0.13	16.0	11.8	174	0.44	N
186	5 35 2.0	-5 36 10	6.9	37350	218	0.44	67.3	36.4	114	0.74	N
187	5 35 2.2	-5 1 35	11.4	9956	113	0.23	28.4	23.0	-140	0.36	N
188	5 35 2.2	-5 55 19	8.2	8888	106	0.21	43.0	15.0	55	0.50	N
189	5 35 2.3	-5 32 10	8.3	2250	54	0.11	18.9	8.4	115	0.24	N
190	5 35 2.7	-5 46 39	10.0	17663	150	0.30	61.2	20.5	103	0.54	N
191	5 35 2.9	-5 2 35	12.2	6075	88	0.18	29.9	18.5	132	0.36	N
192	5 35 3.1	-4 53 52	6.0	1856	49	0.10	14.1	10.5	-152	0.22	N
193	5 35 3.1	-5 0 48	12.2	8325	103	0.21	28.5	17.4	162	0.36	N
194	5 35 3.2	-5 23 36	10.4	2250	54	0.11	15.7	8.6	-140	0.41	N
195	5 35 3.6	-4 52 13	12.5	4331	74	0.15	25.0	17.5	99	0.22	Y
196	5 35 3.6	-5 25 58	11.6	11644	122	0.24	40.4	20.8	-149	0.82	N

Table 3: Continued

ID	RA (J2000)	Dec (J2000)	v_{LSR} (km s ⁻¹)	A (arcsec ²)	$2R_{\text{core}}$ (arcsec)	$2R_{\text{core}}$ (pc)	a_{major} (arcsec)	a_{minor} (arcsec)	PA (deg)	dV_{core} (km s ⁻¹)	YSO
197	5 35 4.2	-5 39 22	7.7	4163	73	0.15	20.5	13.0	142	0.30	N
198	5 35 4.3	-5 24 29	8.7	7200	96	0.19	39.4	10.8	149	0.93	N
199	5 35 4.4	-5 37 41	8.6	2194	53	0.11	21.3	7.6	127	0.27	N
200	5 35 4.6	-4 57 43	11.4	2813	60	0.12	16.9	10.5	-146	0.27	N
201	5 35 4.6	-5 7 36	10.8	4725	78	0.16	25.4	13.0	88	0.30	N
202	5 35 4.6	-5 22 59	8.6	3938	71	0.14	16.3	13.8	-135	0.62	N
203	5 35 4.6	-6 19 27	9.1	8550	104	0.21	29.8	21.2	135	0.57	N
204	5 35 4.7	-4 59 25	10.6	4669	77	0.15	28.3	18.4	-146	0.41	N
205	5 35 4.8	-4 50 49	7.8	3319	65	0.13	18.5	12.7	63	0.31	N
206	5 35 5.2	-5 3 50	11.6	5681	85	0.17	24.8	20.1	-147	0.20	N
207	5 35 5.2	-6 11 29	8.0	8213	102	0.21	29.3	19.6	110	0.28	N
208	5 35 5.2	-6 16 13	6.2	3038	62	0.12	14.3	13.1	126	0.26	N
209	5 35 5.3	-6 13 12	8.4	5175	81	0.16	32.0	18.6	-151	0.16	N
210	5 35 5.4	-6 19 19	6.1	4331	74	0.15	20.9	12.1	79	0.35	N
211	5 35 5.5	-5 13 40	9.4	2475	56	0.11	16.2	8.8	70	0.28	N
212	5 35 6.0	-5 31 11	12.3	9338	109	0.22	26.2	22.5	-171	0.51	N
213	5 35 6.1	-5 22 52	6.9	2081	51	0.10	13.4	8.2	-147	0.52	N
214	5 35 6.3	-5 43 12	8.3	2869	60	0.12	19.1	10.1	81	0.18	N
215	5 35 6.3	-6 2 53	9.1	7819	100	0.20	27.0	18.9	66	0.36	N
216	5 35 6.3	-6 21 58	8.6	11025	118	0.24	41.8	23.8	110	0.50	N
217	5 35 6.6	-4 55 8	13.2	3263	64	0.13	20.1	11.8	88	0.21	N
218	5 35 6.9	-4 54 34	5.7	2419	55	0.11	19.5	8.2	67	0.34	N
219	5 35 6.9	-5 30 5	9.1	4444	75	0.15	19.5	13.1	-163	0.50	N
220	5 35 7.4	-5 58 22	8.3	26663	184	0.37	60.0	27.6	70	0.47	N
221	5 35 7.6	-5 15 27	9.6	10688	117	0.23	34.3	22.5	-171	0.46	N
222	5 35 7.9	-5 12 14	8.1	7763	99	0.20	27.5	15.4	93	0.54	N
223	5 35 8.1	-5 0 55	11.3	1463	43	0.09	14.1	7.4	51	0.19	N
224	5 35 8.1	-5 51 28	6.7	2700	59	0.12	14.7	12.7	64	0.26	N
225	5 35 8.6	-4 59 25	10.3	3319	65	0.13	25.8	10.4	170	0.23	N
226	5 35 8.6	-6 5 55	7.5	4219	73	0.15	17.9	13.3	64	0.39	N
227	5 35 8.6	-6 17 13	6.4	5794	86	0.17	32.8	13.7	66	0.40	N
228	5 35 8.7	-6 3 56	9.6	6075	88	0.18	24.5	15.2	122	0.36	N
229	5 35 9.0	-6 11 43	7.4	4556	76	0.15	31.7	12.7	-156	0.40	N
230	5 35 9.3	-6 4 1	8.2	9956	113	0.23	27.5	19.6	63	0.63	Y
231	5 35 9.7	-5 35 15	8.0	10575	116	0.23	51.4	12.6	123	0.52	N
232	5 35 10.0	-5 1 20	5.6	2475	56	0.11	16.1	10.8	155	0.20	N
233	5 35 10.0	-5 17 24	9.2	7425	97	0.20	24.6	17.1	83	0.45	Y
234	5 35 10.4	-5 38 13	7.4	6244	89	0.18	21.9	14.6	78	0.77	N
235	5 35 10.5	-5 2 47	11.9	2194	53	0.11	27.6	7.5	-174	0.31	N
236	5 35 10.5	-5 32 31	5.8	3938	71	0.14	18.0	13.1	74	0.45	N
237	5 35 10.7	-5 29 8	11.1	3150	63	0.13	15.4	11.2	134	0.45	N
238	5 35 10.9	-6 14 34	5.8	28631	191	0.38	43.7	35.3	80	0.67	N
239	5 35 11.1	-5 8 29	10.9	4500	76	0.15	21.2	14.5	120	0.44	N
240	5 35 11.2	-4 53 30	11.0	3769	69	0.14	27.1	12.2	-148	0.16	N
241	5 35 11.4	-4 50 51	7.7	6300	90	0.18	33.9	15.2	-160	0.43	N
242	5 35 11.7	-5 6 35	11.2	2644	58	0.12	23.4	8.7	91	0.27	N
243	5 35 11.7	-5 59 34	9.3	3094	63	0.13	17.2	12.1	121	0.25	N
244	5 35 11.9	-4 59 59	6.4	4781	78	0.16	23.9	16.4	-144	0.25	Y
245	5 35 11.9	-5 52 37	7.9	9281	109	0.22	37.1	15.3	-151	0.41	N

Table 3: Continued

ID	RA (J2000)	Dec (J2000)	v_{LSR} (km s ⁻¹)	A (arcsec ²)	$2R_{\text{core}}$ (arcsec)	$2R_{\text{core}}$ (pc)	a_{major} (arcsec)	a_{minor} (arcsec)	PA (deg)	dV_{core} (km s ⁻¹)	YSO
246	5 35 11.9	-6 11 1	7.0	3150	63	0.13	25.0	11.9	137	0.31	N
247	5 35 12.4	-5 28 15	10.0	2925	61	0.12	19.5	11.5	123	0.38	N
248	5 35 12.5	-4 58 47	10.9	4838	78	0.16	31.7	10.7	57	0.51	N
249	5 35 12.6	-6 8 29	6.9	5456	83	0.17	28.1	16.5	88	0.24	N
250	5 35 12.7	-5 8 7	13.3	6525	91	0.18	29.2	21.1	98	0.31	N
251	5 35 12.9	-5 12 49	8.7	5231	82	0.16	19.5	11.8	94	0.71	N
252	5 35 13.2	-5 23 58	7.1	1913	49	0.10	16.6	6.7	102	0.46	Y
253	5 35 13.2	-6 19 13	6.6	5175	81	0.16	27.1	13.4	115	0.26	N
254	5 35 13.3	-4 54 10	7.8	1463	43	0.09	14.5	6.7	159	0.20	N
255	5 35 13.3	-5 26 37	8.7	2194	53	0.11	14.6	8.9	119	0.62	N
256	5 35 13.4	-5 23 7	8.4	2138	52	0.10	14.1	7.9	95	0.82	N
257	5 35 13.4	-5 24 2	6.1	1013	36	0.07	8.8	5.9	93	0.76	N
258	5 35 13.9	-6 1 9	9.5	7875	100	0.20	29.7	15.4	80	0.23	N
259	5 35 14.0	-5 0 10	8.8	6019	88	0.18	28.4	19.7	130	0.32	N
260	5 35 14.0	-6 9 5	9.0	5681	85	0.17	32.6	12.5	163	0.24	N
261	5 35 14.0	-6 12 18	8.7	2081	51	0.10	18.4	8.4	143	0.19	N
262	5 35 14.1	-6 13 0	6.9	6638	92	0.18	24.5	19.7	-160	0.21	N
263	5 35 14.5	-5 37 33	8.7	4669	77	0.15	24.5	13.0	112	0.55	N
264	5 35 14.7	-5 58 30	7.6	2644	58	0.12	16.0	10.4	-145	0.24	N
265	5 35 14.9	-5 4 48	11.0	2981	62	0.12	20.2	10.9	56	0.32	N
266	5 35 14.9	-5 9 30	9.5	2644	58	0.12	17.8	9.8	116	0.37	Y
267	5 35 15.1	-6 17 1	6.8	8044	101	0.20	31.3	19.9	86	0.41	N
268	5 35 15.4	-5 4 43	10.5	3431	66	0.13	17.2	13.5	94	0.37	N
269	5 35 15.5	-5 11 47	10.7	5288	82	0.16	27.2	11.7	77	0.50	N
270	5 35 15.5	-5 15 41	10.3	6131	88	0.18	38.5	10.7	95	0.39	N
271	5 35 15.8	-5 0 21	10.4	2194	53	0.11	13.4	9.4	175	0.39	N
272	5 35 15.8	-5 59 52	7.9	7763	99	0.20	33.0	17.7	136	0.33	N
273	5 35 15.9	-5 3 18	10.4	3206	64	0.13	29.3	10.2	110	0.29	N
274	5 35 16.0	-5 21 39	10.0	5231	82	0.16	30.3	10.2	101	0.80	N
275	5 35 16.4	-5 13 31	10.5	3150	63	0.13	24.7	8.2	71	0.33	N
276	5 35 16.4	-5 26 16	9.8	2250	54	0.11	17.8	7.3	123	0.53	N
277	5 35 16.5	-5 30 44	6.1	12150	124	0.25	37.0	16.4	113	0.62	N
278	5 35 16.9	-6 5 27	7.1	9225	108	0.22	34.3	21.5	92	0.31	N
279	5 35 17.1	-5 19 26	9.3	1856	49	0.10	14.5	7.5	133	0.32	N
280	5 35 17.2	-6 38 36	8.5	7763	99	0.20	36.5	23.4	136	0.22	N
281	5 35 17.3	-5 58 25	10.1	11475	121	0.24	40.7	23.7	62	0.26	N
282	5 35 17.8	-6 3 21	9.4	4444	75	0.15	19.2	15.9	129	0.22	N
283	5 35 17.9	-6 15 54	6.2	2363	55	0.11	18.3	9.2	100	0.29	N
284	5 35 18.0	-5 1 39	10.5	1519	44	0.09	12.8	6.6	87	0.28	N
285	5 35 18.3	-5 9 19	11.0	4781	78	0.16	29.2	12.5	86	0.32	N
286	5 35 18.4	-5 0 31	11.1	5175	81	0.16	30.2	13.0	-164	0.31	N
287	5 35 19.2	-5 4 52	9.3	1800	48	0.10	14.8	7.3	55	0.34	N
288	5 35 19.6	-5 18 27	9.5	1575	45	0.09	12.7	6.8	113	0.48	N
289	5 35 19.6	-6 20 31	6.7	15863	142	0.29	42.2	26.1	71	0.31	N
290	5 35 19.6	-6 34 28	8.9	13050	129	0.26	37.2	23.8	95	0.29	N
291	5 35 19.8	-5 16 59	11.1	2081	51	0.10	16.6	9.1	145	0.20	N
292	5 35 20.0	-4 56 45	12.1	3150	63	0.13	22.1	9.4	-162	0.46	N
293	5 35 20.4	-6 8 27	8.8	6188	89	0.18	35.8	17.4	168	0.35	N
294	5 35 20.6	-5 38 52	9.3	4050	72	0.14	30.6	13.0	117	0.37	Y

Table 3: Continued

ID	RA (J2000)	Dec (J2000)	v_{LSR} (km s ⁻¹)	A (arcsec ²)	$2R_{\text{core}}$ (arcsec)	$2R_{\text{core}}$ (pc)	a_{major} (arcsec)	a_{minor} (arcsec)	PA (deg)	dV_{core} (km s ⁻¹)	YSO
295	5 35 20.6	-6 7 16	8.5	3544	67	0.13	28.4	12.0	124	0.17	N
296	5 35 21.1	-6 23 1	8.9	9900	112	0.23	70.8	24.6	95	0.33	N
297	5 35 21.4	-5 55 46	8.0	1406	42	0.08	13.6	7.4	102	0.23	N
298	5 35 21.5	-6 13 8	5.4	1406	42	0.08	11.7	7.0	169	0.26	N
299	5 35 21.7	-5 6 17	10.9	6525	91	0.18	24.2	16.8	95	0.45	N
300	5 35 21.7	-5 8 5	10.9	4106	72	0.15	28.1	9.0	68	0.49	N
301	5 35 21.8	-6 3 24	8.2	12094	124	0.25	35.3	20.4	89	0.60	N
302	5 35 21.8	-6 7 45	9.8	3825	70	0.14	23.2	13.5	60	0.33	N
303	5 35 22.0	-6 8 27	7.6	4219	73	0.15	24.5	16.1	46	0.32	N
304	5 35 22.3	-6 13 30	6.0	3319	65	0.13	26.5	10.9	162	0.37	N
305	5 35 22.4	-6 7 58	10.3	1688	46	0.09	24.9	6.1	79	0.26	N
306	5 35 22.5	-5 14 48	10.5	4669	77	0.15	23.8	13.8	98	0.36	N
307	5 35 22.5	-5 25 19	10.4	1856	49	0.10	13.3	7.5	149	0.40	N
308	5 35 22.5	-6 1 36	4.8	2194	53	0.11	18.2	8.6	135	0.15	N
309	5 35 22.7	-5 20 20	11.4	2419	55	0.11	17.5	8.8	57	0.28	N
310	5 35 23.0	-5 54 51	8.8	3038	62	0.12	14.8	11.5	101	0.26	N
311	5 35 23.7	-5 36 6	9.1	3825	70	0.14	19.0	14.1	116	0.36	N
312	5 35 23.9	-5 56 39	7.8	3263	64	0.13	19.6	12.0	-148	0.24	N
313	5 35 24.0	-5 13 9	10.6	3713	69	0.14	20.9	14.1	128	0.24	N
314	5 35 24.0	-5 22 33	10.5	4669	77	0.15	27.7	15.0	-162	0.33	N
315	5 35 24.1	-5 25 13	8.0	3656	68	0.14	26.6	13.8	-144	0.19	N
316	5 35 24.4	-6 19 2	6.2	2475	56	0.11	15.2	10.4	-165	0.32	N
317	5 35 24.5	-5 59 28	7.3	6694	92	0.19	30.1	14.5	148	0.36	Y
318	5 35 24.6	-4 53 9	11.3	2700	59	0.12	20.5	9.4	-157	0.19	N
319	5 35 25.5	-5 55 10	9.4	1969	50	0.10	14.2	9.8	142	0.24	N
320	5 35 25.5	-6 40 9	8.1	7256	96	0.19	27.9	13.2	126	0.40	N
321	5 35 25.6	-6 0 47	5.4	18956	155	0.31	42.6	27.4	108	0.41	N
322	5 35 25.7	-5 2 40	11.1	1463	43	0.09	15.3	7.3	78	0.28	N
323	5 35 25.8	-5 20 18	6.3	2419	55	0.11	16.6	8.2	-160	0.48	N
324	5 35 25.9	-5 51 45	7.8	18563	154	0.31	44.6	25.8	62	0.55	N
325	5 35 25.9	-5 53 21	7.2	2250	54	0.11	22.3	8.3	-159	0.21	N
326	5 35 26.3	-5 20 19	7.0	1519	44	0.09	10.4	8.8	-167	0.20	N
327	5 35 26.3	-5 55 13	6.2	7481	98	0.20	27.7	15.8	120	0.45	N
328	5 35 26.5	-6 0 41	6.6	12938	128	0.26	38.9	24.1	147	0.38	N
329	5 35 26.6	-5 50 55	7.1	2644	58	0.12	18.5	11.0	178	0.21	N
330	5 35 26.9	-6 41 19	8.2	5175	81	0.16	20.9	15.9	129	0.29	N
331	5 35 27.0	-5 24 39	10.3	6694	92	0.19	34.9	12.8	168	0.86	N
332	5 35 27.4	-5 14 20	11.7	4669	77	0.15	32.1	20.3	150	0.17	N
333	5 35 27.6	-6 38 14	8.4	2869	60	0.12	18.8	10.4	111	0.22	N
334	5 35 27.8	-5 5 43	11.4	4725	78	0.16	25.8	13.8	130	0.29	N
335	5 35 27.8	-6 21 31	6.6	2531	57	0.11	19.6	12.1	96	0.19	N
336	5 35 28.3	-5 36 29	9.3	2588	57	0.12	19.4	9.4	61	0.24	N
337	5 35 28.5	-6 5 44	8.4	4106	72	0.15	23.9	11.5	167	0.38	N
338	5 35 28.6	-6 30 12	8.8	3319	65	0.13	20.6	10.9	92	0.20	N
339	5 35 28.7	-5 7 29	11.4	3544	67	0.13	20.8	12.7	151	0.26	N
340	5 35 29.3	-4 58 20	11.7	6919	94	0.19	31.6	14.0	67	0.59	N
341	5 35 29.3	-5 22 57	8.9	4388	75	0.15	25.9	13.2	56	0.20	N
342	5 35 29.3	-5 39 6	9.9	6975	94	0.19	35.4	18.3	147	0.18	N
343	5 35 29.5	-5 53 39	6.5	2588	57	0.12	13.2	11.8	121	0.19	N

Table 3: Continued

ID	RA (J2000)	Dec (J2000)	v_{LSR} (km s ⁻¹)	A (arcsec ²)	$2R_{\text{core}}$ (arcsec)	$2R_{\text{core}}$ (pc)	a_{major} (arcsec)	a_{minor} (arcsec)	PA (deg)	dV_{core} (km s ⁻¹)	YSO
344	5 35 29.6	-5 36 20	9.8	4331	74	0.15	27.5	16.4	163	0.23	N
345	5 35 29.8	-6 19 48	6.6	5738	85	0.17	31.0	14.1	175	0.29	N
346	5 35 29.9	-6 27 27	8.6	5681	85	0.17	26.8	22.9	65	0.26	N
347	5 35 30.1	-5 3 6	10.5	1406	42	0.08	17.3	5.1	135	0.28	N
348	5 35 30.1	-5 14 60	10.1	4556	76	0.15	34.1	14.5	116	0.23	Y
349	5 35 30.2	-6 12 42	8.0	3150	63	0.13	29.2	14.0	101	0.18	N
350	5 35 30.7	-6 25 6	5.8	7369	97	0.19	25.9	16.6	-170	0.34	N
351	5 35 30.8	-5 20 43	7.0	6806	93	0.19	34.7	15.0	-157	0.79	N
352	5 35 31.0	-6 1 43	7.6	9000	107	0.21	24.5	23.7	-137	0.37	N
353	5 35 31.1	-6 10 26	8.8	2250	54	0.11	20.8	7.7	134	0.33	N
354	5 35 31.1	-6 42 40	8.4	3375	66	0.13	22.3	14.0	109	0.30	N
355	5 35 31.2	-5 57 52	7.8	7819	100	0.20	25.7	18.3	145	0.40	N
356	5 35 31.7	-5 9 48	11.1	5063	80	0.16	28.0	14.6	115	0.38	N
357	5 35 31.8	-6 35 33	7.7	4163	73	0.15	18.8	14.9	157	0.25	N
358	5 35 31.9	-5 54 26	7.8	3994	71	0.14	27.1	10.9	90	0.17	N
359	5 35 32.3	-5 0 60	12.9	3994	71	0.14	22.4	10.7	74	0.69	N
360	5 35 32.3	-5 5 40	11.9	2025	51	0.10	16.1	8.8	156	0.44	N
361	5 35 32.3	-5 11 2	10.7	5231	82	0.16	34.2	12.2	144	0.28	N
362	5 35 32.4	-5 57 23	9.3	7875	100	0.20	35.5	17.2	100	0.25	N
363	5 35 32.4	-6 4 37	7.2	2925	61	0.12	17.6	13.5	-170	0.26	N
364	5 35 32.5	-5 25 58	11.6	2700	59	0.12	19.7	11.2	56	0.21	N
365	5 35 32.9	-6 10 0	6.4	2756	59	0.12	20.2	11.9	102	0.20	N
366	5 35 33.0	-5 20 47	7.8	6581	92	0.18	30.6	13.3	56	0.69	N
367	5 35 33.1	-5 20 29	9.0	5681	85	0.17	46.8	12.8	109	0.33	N
368	5 35 33.2	-4 59 37	11.7	2250	54	0.11	21.5	7.5	176	0.23	N
369	5 35 33.4	-5 37 30	10.0	5513	84	0.17	22.3	18.0	141	0.43	N
370	5 35 33.4	-6 2 50	7.8	3544	67	0.13	23.9	11.4	129	0.16	N
371	5 35 33.4	-6 5 20	12.6	1238	40	0.08	11.4	6.5	-173	0.20	N
372	5 35 33.6	-6 12 49	5.8	4275	74	0.15	24.1	10.9	92	0.18	N
373	5 35 34.0	-5 56 43	7.2	2419	55	0.11	16.0	12.3	55	0.25	N
374	5 35 34.1	-5 19 39	6.8	3600	68	0.14	20.1	12.6	165	0.23	N
375	5 35 34.2	-6 16 46	8.4	4669	77	0.15	30.4	13.2	65	0.16	Y
376	5 35 34.3	-6 2 29	8.9	2025	51	0.10	14.7	10.0	153	0.17	N
377	5 35 34.8	-5 20 55	5.7	4838	78	0.16	34.4	16.1	65	0.24	N
378	5 35 35.0	-5 29 7	6.9	3994	71	0.14	30.4	17.6	136	0.20	N
379	5 35 35.0	-6 5 13	6.8	2475	56	0.11	19.2	8.9	-179	0.24	N
380	5 35 35.3	-5 6 57	12.4	3488	67	0.13	20.0	12.3	-170	0.32	N
381	5 35 35.3	-5 38 17	10.2	4388	75	0.15	25.0	16.0	144	0.25	N
382	5 35 35.3	-6 11 38	8.5	4725	78	0.16	19.2	18.3	91	0.16	N
383	5 35 35.4	-5 12 30	12.2	3656	68	0.14	23.7	12.8	88	0.24	N
384	5 35 35.6	-5 8 4	11.3	3488	67	0.13	16.6	13.7	136	0.59	N
385	5 35 35.7	-5 47 26	5.0	2250	54	0.11	16.8	9.1	92	0.21	N
386	5 35 35.8	-5 22 20	5.8	3206	64	0.13	22.5	12.9	-178	0.32	N
387	5 35 35.8	-5 24 1	11.2	2756	59	0.12	17.6	10.1	152	0.44	N
388	5 35 35.8	-6 20 33	9.0	2813	60	0.12	16.2	14.9	57	0.20	N
389	5 35 35.9	-6 18 11	6.5	4781	78	0.16	20.1	13.7	77	0.25	N
390	5 35 35.9	-6 18 28	8.6	4500	76	0.15	29.9	18.5	95	0.20	N
391	5 35 36.1	-6 4 36	8.0	5681	85	0.17	22.8	18.6	121	0.33	N
392	5 35 36.2	-6 1 40	6.8	11194	119	0.24	30.4	27.8	69	0.30	N

Table 3: Continued

ID	RA (J2000)	Dec (J2000)	v_{LSR} (km s ⁻¹)	A (arcsec ²)	$2R_{\text{core}}$ (arcsec)	$2R_{\text{core}}$ (pc)	a_{major} (arcsec)	a_{minor} (arcsec)	PA (deg)	dV_{core} (km s ⁻¹)	YSO
393	5 35 36.6	-5 46 52	8.2	2138	52	0.10	15.8	11.5	142	0.17	N
394	5 35 36.7	-5 18 3	8.5	3150	63	0.13	19.6	13.8	150	0.21	N
395	5 35 36.8	-5 15 50	9.6	2025	51	0.10	13.7	8.4	-174	0.49	N
396	5 35 36.8	-6 33 43	7.7	4950	79	0.16	32.6	18.1	59	0.26	N
397	5 35 37.2	-5 23 26	12.0	2756	59	0.12	31.3	12.3	-176	0.21	N
398	5 35 37.2	-5 57 33	7.9	2700	59	0.12	18.8	9.2	149	0.30	N
399	5 35 37.4	-6 9 5	9.4	5344	82	0.17	32.2	14.4	54	0.25	N
400	5 35 37.5	-6 31 15	7.8	1688	46	0.09	12.4	10.7	94	0.23	N
401	5 35 37.8	-6 7 18	8.0	4500	76	0.15	23.5	17.2	141	0.30	N
402	5 35 37.9	-5 6 19	11.7	2475	56	0.11	17.6	9.0	-175	0.39	N
403	5 35 38.3	-5 15 31	10.9	4894	79	0.16	28.2	12.5	99	0.28	N
404	5 35 38.3	-5 57 49	9.4	7369	97	0.19	33.3	16.2	50	0.33	N
405	5 35 38.4	-6 28 27	8.8	5794	86	0.17	31.3	19.7	137	0.28	N
406	5 35 38.6	-6 38 19	8.6	8100	102	0.20	46.9	24.6	91	0.20	N
407	5 35 38.7	-6 8 6	8.4	5400	83	0.17	26.4	16.7	75	0.26	N
408	5 35 38.8	-5 56 45	8.2	1913	49	0.10	12.1	11.3	59	0.18	N
409	5 35 38.8	-6 47 3	6.9	6975	94	0.19	34.4	17.5	114	0.35	N
410	5 35 39.1	-5 8 27	10.9	2138	52	0.10	15.0	8.7	137	0.37	N
411	5 35 39.3	-5 1 36	11.6	5288	82	0.16	32.9	12.4	-137	0.29	N
412	5 35 39.6	-5 17 34	9.2	3994	71	0.14	33.0	13.5	-174	0.24	N
413	5 35 39.8	-6 14 17	8.9	2531	57	0.11	13.6	11.8	-160	0.24	N
414	5 35 40.0	-5 26 26	8.0	4500	76	0.15	27.0	19.0	76	0.34	N
415	5 35 40.0	-5 54 28	8.2	5063	80	0.16	31.4	12.4	66	0.31	N
416	5 35 40.3	-6 10 47	6.8	5119	81	0.16	28.8	12.6	-155	0.32	N
417	5 35 40.5	-5 19 35	8.9	1913	49	0.10	15.1	9.2	-141	0.46	N
418	5 35 40.6	-6 5 13	9.2	11081	119	0.24	38.8	20.2	94	0.42	N
419	5 35 40.7	-5 6 52	12.4	1688	46	0.09	13.4	8.2	-167	0.21	Y
420	5 35 40.7	-6 40 5	7.6	3150	63	0.13	19.1	10.9	166	0.20	N
421	5 35 41.0	-5 59 32	9.6	2419	55	0.11	16.0	10.9	45	0.18	N
422	5 35 41.0	-6 6 57	9.0	5681	85	0.17	27.6	15.7	132	0.29	N
423	5 35 41.1	-5 22 51	5.7	3994	71	0.14	21.1	11.3	67	0.50	N
424	5 35 41.3	-6 10 55	8.8	4781	78	0.16	19.0	16.4	56	0.30	N
425	5 35 41.4	-5 26 53	9.1	7031	95	0.19	41.2	15.0	121	0.31	N
426	5 35 41.6	-6 0 8	8.4	4725	78	0.16	24.1	11.6	-142	0.21	N
427	5 35 41.7	-5 20 25	7.0	2419	55	0.11	16.5	11.4	50	0.21	N
428	5 35 41.9	-6 1 34	9.3	3769	69	0.14	27.0	12.6	54	0.26	N
429	5 35 42.2	-6 5 26	6.7	6244	89	0.18	26.1	20.3	46	0.27	N
430	5 35 42.3	-5 20 38	8.2	5681	85	0.17	23.8	13.2	-137	0.63	Y
431	5 35 42.5	-6 22 55	8.3	9113	108	0.22	44.0	20.5	74	0.26	N
432	5 35 43.2	-5 21 13	13.3	3150	63	0.13	30.2	9.0	96	0.17	N
433	5 35 43.5	-6 32 6	7.5	4500	76	0.15	22.2	17.1	133	0.36	N
434	5 35 44.1	-5 10 39	10.4	2869	60	0.12	24.8	9.8	-148	0.23	N
435	5 35 44.1	-6 37 50	7.4	2138	52	0.10	15.6	7.8	168	0.22	N
436	5 35 44.3	-6 8 5	7.9	6975	94	0.19	26.7	14.8	86	0.45	N
437	5 35 44.6	-5 23 42	11.1	4444	75	0.15	27.0	18.9	-175	0.15	N
438	5 35 44.7	-6 41 32	7.9	4613	77	0.15	18.1	14.9	150	0.51	N
439	5 35 45.2	-5 28 27	9.2	3544	67	0.13	25.2	11.2	156	0.19	N
440	5 35 45.3	-5 54 42	8.2	7594	98	0.20	46.8	17.4	112	0.24	N
441	5 35 45.7	-6 11 40	7.0	2700	59	0.12	13.9	12.1	-149	0.31	N

Table 3: Continued

ID	RA (J2000)	Dec (J2000)	v_{LSR} (km s ⁻¹)	A (arcsec ²)	$2R_{\text{core}}$ (arcsec)	$2R_{\text{core}}$ (pc)	a_{major} (arcsec)	a_{minor} (arcsec)	PA (deg)	dV_{core} (km s ⁻¹)	YSO
442	5 35 45.9	-6 18 25	8.6	3375	66	0.13	18.6	12.5	88	0.39	N
443	5 35 46.0	-5 19 39	9.5	6300	90	0.18	20.1	17.5	65	0.54	N
444	5 35 46.5	-6 2 23	8.5	5794	86	0.17	24.2	16.7	92	0.24	N
445	5 35 47.7	-5 21 21	8.6	2138	52	0.10	15.8	8.5	161	0.32	N
446	5 35 47.7	-6 30 10	8.4	23681	174	0.35	49.6	28.0	64	0.45	N
447	5 35 47.9	-6 16 17	8.5	8719	105	0.21	39.5	18.6	117	0.26	N
448	5 35 48.1	-6 25 43	6.0	19575	158	0.32	38.3	27.1	-146	0.38	N
449	5 35 48.2	-6 47 8	8.7	3150	63	0.13	36.3	8.7	83	0.14	N
450	5 35 48.7	-6 27 22	8.7	3150	63	0.13	16.3	13.6	140	0.23	N
451	5 35 48.7	-6 33 5	8.3	2531	57	0.11	20.2	11.8	52	0.21	N
452	5 35 48.8	-5 23 40	11.5	2756	59	0.12	18.3	13.9	-164	0.23	N
453	5 35 48.9	-5 51 8	9.5	3263	64	0.13	17.0	15.7	119	0.22	N
454	5 35 49.1	-6 10 11	8.4	6188	89	0.18	21.4	17.9	108	0.41	N
455	5 35 49.4	-6 48 32	7.9	4613	77	0.15	24.2	14.9	87	0.26	N
456	5 35 49.5	-5 24 48	5.2	2925	61	0.12	29.4	10.6	96	0.19	N
457	5 35 50.4	-5 53 3	8.4	3094	63	0.13	26.4	10.9	164	0.25	N
458	5 35 50.5	-5 24 1	11.9	3769	69	0.14	26.0	11.6	81	0.25	N
459	5 35 51.4	-5 20 54	9.4	5625	85	0.17	27.2	12.9	-148	0.45	N
460	5 35 51.9	-5 20 51	10.6	7931	100	0.20	29.6	18.4	87	0.55	N
461	5 35 51.9	-6 0 33	8.3	4613	77	0.15	18.1	15.9	83	0.34	N
462	5 35 52.1	-6 46 4	6.5	4444	75	0.15	23.9	14.3	134	0.22	N
463	5 35 52.2	-6 4 43	8.6	2363	55	0.11	27.7	7.2	89	0.15	N
464	5 35 52.2	-6 45 39	7.0	1913	49	0.10	19.7	8.3	122	0.18	N
465	5 35 52.3	-6 34 49	8.9	19069	156	0.31	39.2	31.7	74	0.28	N
466	5 35 52.8	-5 55 23	8.6	4275	74	0.15	22.7	16.1	155	0.46	N
467	5 35 53.4	-5 42 12	8.0	19406	157	0.32	36.5	31.0	-141	0.55	N
468	5 35 53.5	-6 24 29	8.9	6413	90	0.18	24.1	16.6	180	0.32	N
469	5 35 53.5	-6 34 45	7.7	8156	102	0.20	42.4	16.2	56	0.28	N
470	5 35 53.9	-6 10 27	8.3	4275	74	0.15	27.3	12.2	-135	0.39	N
471	5 35 54.2	-5 57 53	8.0	3713	69	0.14	18.9	14.3	168	0.24	N
472	5 35 54.4	-6 4 32	10.5	4275	74	0.15	23.8	20.2	-166	0.28	N
473	5 35 54.7	-6 15 54	8.7	3938	71	0.14	20.2	15.2	62	0.33	N
474	5 35 54.7	-6 32 22	6.3	2700	59	0.12	18.9	13.5	86	0.33	N
475	5 35 54.7	-6 44 27	8.5	13163	129	0.26	50.5	21.6	80	0.31	N
476	5 35 55.1	-6 26 12	8.8	5288	82	0.16	31.6	14.8	-179	0.41	N
477	5 35 55.1	-6 42 49	13.4	2700	59	0.12	20.6	9.9	-138	0.25	Y
478	5 35 55.2	-6 7 12	8.1	4331	74	0.15	25.2	15.0	88	0.48	N
479	5 35 55.4	-5 32 22	7.4	74475	308	0.62	99.1	43.2	65	0.49	Y
480	5 35 55.6	-6 15 51	7.4	2306	54	0.11	18.7	9.7	60	0.19	N
481	5 35 55.8	-5 44 55	7.8	4106	72	0.15	40.2	14.9	176	0.17	Y
482	5 35 55.8	-6 48 27	8.7	5006	80	0.16	44.6	10.0	50	0.40	N
483	5 35 56.0	-6 40 8	7.3	5119	81	0.16	33.0	19.2	136	0.18	N
484	5 35 57.0	-5 47 16	8.0	4725	78	0.16	29.2	18.0	-152	0.38	N
485	5 35 57.5	-6 6 39	9.0	8213	102	0.21	37.6	23.2	56	0.40	N
486	5 35 57.5	-6 32 28	8.3	11475	121	0.24	36.9	18.7	87	0.40	N
487	5 35 58.6	-6 32 4	9.1	4500	76	0.15	18.9	14.7	126	0.23	N
488	5 35 58.8	-6 21 55	7.5	10238	114	0.23	44.1	19.1	117	0.33	N
489	5 35 59.3	-5 20 27	11.1	1519	44	0.09	14.1	9.2	175	0.21	N
490	5 35 59.3	-6 23 50	8.6	2250	54	0.11	13.8	11.2	-164	0.21	N

Table 3: Continued

ID	RA (J2000)	Dec (J2000)	v_{LSR} (km s ⁻¹)	A (arcsec ²)	$2R_{\text{core}}$ (arcsec)	$2R_{\text{core}}$ (pc)	a_{major} (arcsec)	a_{minor} (arcsec)	PA (deg)	dV_{core} (km s ⁻¹)	YSO
491	5 35 59.8	-6 40 24	6.3	3600	68	0.14	24.2	12.1	-164	0.38	N
492	5 35 59.9	-6 38 42	8.6	7763	99	0.20	34.9	14.9	-143	0.23	N
493	5 35 60.0	-6 39 24	7.7	4163	73	0.15	30.9	11.1	87	0.17	N
494	5 36 0.1	-5 20 16	10.7	6356	90	0.18	34.3	19.5	61	0.30	N
495	5 36 0.1	-6 37 53	6.9	3938	71	0.14	29.7	10.2	-172	0.26	N
496	5 36 0.4	-6 1 44	8.8	2869	60	0.12	21.3	14.0	135	0.20	Y
497	5 36 0.9	-5 21 54	12.2	6356	90	0.18	27.7	16.7	78	0.37	N
498	5 36 0.9	-6 3 58	6.2	2363	55	0.11	16.4	9.8	-166	0.19	N
499	5 36 1.1	-6 36 34	8.6	2306	54	0.11	19.2	9.9	139	0.21	N
500	5 36 1.7	-6 35 25	7.5	8381	103	0.21	28.3	23.2	108	0.34	N
501	5 36 1.9	-6 13 59	8.7	6356	90	0.18	25.0	14.7	45	0.46	N
502	5 36 1.9	-6 44 23	7.0	4613	77	0.15	24.9	14.8	74	0.24	N
503	5 36 2.0	-6 4 28	11.4	4613	77	0.15	31.7	17.4	173	0.23	N
504	5 36 2.0	-6 38 7	7.7	2813	60	0.12	20.9	10.1	-164	0.37	N
505	5 36 2.2	-5 55 37	7.8	3994	71	0.14	29.2	12.5	96	0.37	N
506	5 36 2.3	-6 12 41	9.0	1969	50	0.10	15.1	8.5	97	0.31	N
507	5 36 3.1	-6 44 38	8.5	2025	51	0.10	20.5	8.7	149	0.20	N
508	5 36 3.2	-6 24 43	7.3	3544	67	0.13	18.8	11.7	-175	0.38	N
509	5 36 3.6	-5 37 51	7.5	13331	130	0.26	46.2	23.8	173	0.96	N
510	5 36 3.9	-6 31 19	7.6	5906	87	0.17	45.3	16.1	148	0.17	N
511	5 36 4.2	-5 56 25	7.5	11869	123	0.25	39.0	26.0	127	0.54	N
512	5 36 4.2	-6 19 23	9.5	3544	67	0.13	20.4	12.3	86	0.21	N
513	5 36 4.6	-6 47 15	9.6	2475	56	0.11	27.2	10.0	77	0.18	N
514	5 36 4.7	-6 29 16	8.3	6019	88	0.18	44.3	12.2	50	0.26	N
515	5 36 4.8	-6 46 30	6.8	12206	125	0.25	38.2	22.2	74	0.19	N
516	5 36 5.0	-6 18 2	8.8	6131	88	0.18	33.0	19.7	67	0.38	N
517	5 36 5.0	-6 33 58	9.0	4444	75	0.15	20.7	15.5	133	0.23	N
518	5 36 5.0	-6 39 3	7.5	2756	59	0.12	20.0	9.7	67	0.24	N
519	5 36 5.1	-5 41 58	8.2	3994	71	0.14	20.3	12.8	-160	0.24	N
520	5 36 5.4	-6 40 50	8.4	8550	104	0.21	25.5	18.4	48	0.33	N
521	5 36 5.7	-6 37 16	6.9	3488	67	0.13	17.9	14.2	77	0.19	N
522	5 36 6.3	-6 11 27	8.8	17044	147	0.30	40.8	30.5	-147	0.53	N
523	5 36 6.7	-6 32 44	9.7	6525	91	0.18	28.3	16.9	54	0.39	N
524	5 36 7.1	-6 42 44	6.8	2869	60	0.12	19.3	10.9	145	0.22	N
525	5 36 7.1	-6 44 59	9.0	2194	53	0.11	14.4	10.7	97	0.18	N
526	5 36 7.4	-6 17 45	7.1	5231	82	0.16	28.5	15.4	83	0.26	N
527	5 36 7.5	-6 41 53	7.2	3375	66	0.13	15.5	14.1	75	0.42	N
528	5 36 7.6	-6 43 24	11.8	2475	56	0.11	26.8	9.1	68	0.16	N
529	5 36 7.8	-6 26 23	8.3	2588	57	0.12	21.5	9.1	118	0.33	N
530	5 36 7.8	-6 46 22	8.6	3881	70	0.14	22.3	12.3	162	0.23	N
531	5 36 7.9	-5 39 24	8.1	7875	100	0.20	41.3	16.7	45	0.41	N
532	5 36 8.1	-6 26 50	7.0	5119	81	0.16	21.9	17.8	166	0.22	N
533	5 36 8.6	-6 37 35	8.1	2700	59	0.12	27.0	10.0	144	0.28	N
534	5 36 8.9	-6 0 0	7.7	3825	70	0.14	20.2	14.3	-165	0.38	N
535	5 36 9.1	-5 23 14	9.0	14400	135	0.27	30.7	25.6	179	0.65	N
536	5 36 9.1	-5 36 52	7.6	2475	56	0.11	17.9	9.2	-140	0.49	N
537	5 36 9.1	-5 41 17	7.7	2813	60	0.12	20.8	7.5	99	0.46	N
538	5 36 9.2	-6 15 51	8.1	16706	146	0.29	40.6	26.6	81	0.33	N
539	5 36 9.6	-5 21 10	10.3	5288	82	0.16	24.6	14.2	69	0.40	N

Table 3: Continued

ID	RA (J2000)	Dec (J2000)	v_{LSR} (km s ⁻¹)	A (arcsec ²)	$2R_{\text{core}}$ (arcsec)	$2R_{\text{core}}$ (pc)	a_{major} (arcsec)	a_{minor} (arcsec)	PA (deg)	dV_{core} (km s ⁻¹)	YSO
540	5 36 10.0	-6 33 57	7.8	13781	132	0.27	45.2	21.9	71	0.61	N
541	5 36 10.1	-6 26 52	8.7	4613	77	0.15	26.4	14.5	175	0.27	N
542	5 36 10.4	-6 19 56	9.1	3094	63	0.13	22.3	13.1	61	0.20	N
543	5 36 10.8	-6 9 26	9.3	6919	94	0.19	33.0	17.3	-162	0.27	N
544	5 36 11.5	-6 23 20	6.3	3206	64	0.13	21.1	11.3	130	0.20	N
545	5 36 12.3	-6 28 35	9.0	2925	61	0.12	18.1	15.7	134	0.24	N
546	5 36 12.9	-6 23 15	6.9	4725	78	0.16	20.6	16.2	78	0.24	N
547	5 36 12.9	-6 29 60	6.8	9394	109	0.22	34.7	20.7	138	0.35	N
548	5 36 14.2	-6 46 58	8.0	14344	135	0.27	49.4	18.0	112	0.33	N
549	5 36 14.3	-6 17 22	9.4	3319	65	0.13	20.1	16.0	61	0.19	N
550	5 36 14.9	-5 53 58	8.7	5963	87	0.17	25.9	14.8	74	0.58	N
551	5 36 15.2	-6 35 38	8.8	3375	66	0.13	19.6	11.5	85	0.18	N
552	5 36 15.8	-6 44 34	9.3	4838	78	0.16	19.5	17.7	168	0.36	N
553	5 36 15.9	-6 31 51	7.8	2250	54	0.11	13.9	10.2	119	0.17	N
554	5 36 15.9	-6 37 55	8.6	12825	128	0.26	43.8	18.6	64	0.37	N
555	5 36 16.1	-6 34 39	7.1	2869	60	0.12	19.7	9.7	56	0.32	N
556	5 36 16.3	-6 36 37	6.6	1350	41	0.08	9.6	8.0	147	0.18	N
557	5 36 16.6	-6 42 54	6.6	10913	118	0.24	42.7	20.4	173	0.46	N
558	5 36 17.0	-6 35 39	7.7	3263	64	0.13	16.9	13.4	-144	0.25	N
559	5 36 17.3	-6 48 31	6.5	9956	113	0.23	30.8	24.3	179	0.29	N
560	5 36 17.4	-6 36 47	7.4	3994	71	0.14	18.7	14.3	67	0.41	N
561	5 36 18.0	-6 40 7	6.9	5175	81	0.16	27.0	15.4	101	0.33	N
562	5 36 18.5	-6 5 45	8.4	2250	54	0.11	19.0	9.6	156	0.25	N
563	5 36 18.5	-6 18 18	7.9	2194	53	0.11	20.3	9.3	-154	0.22	N
564	5 36 18.7	-6 45 23	9.0	2588	57	0.12	23.1	8.5	160	0.22	N
565	5 36 19.0	-6 48 8	9.9	2081	51	0.10	17.9	10.0	143	0.30	N
566	5 36 19.4	-6 30 52	7.7	2756	59	0.12	19.2	10.0	148	0.19	N
567	5 36 19.8	-5 52 49	6.9	3206	64	0.13	25.4	17.0	172	0.27	N
568	5 36 20.1	-6 35 25	7.4	2419	55	0.11	16.4	12.2	55	0.19	N
569	5 36 20.3	-6 12 38	8.1	3881	70	0.14	36.9	7.4	59	0.18	N
570	5 36 20.3	-6 30 37	6.7	11475	121	0.24	30.0	25.2	-142	0.36	N
571	5 36 21.0	-6 17 48	8.6	4556	76	0.15	31.4	10.8	97	0.29	N
572	5 36 21.0	-6 20 49	9.7	2475	56	0.11	18.8	11.0	138	0.20	N
573	5 36 21.1	-6 33 19	6.8	5738	85	0.17	38.0	11.5	77	0.41	N
574	5 36 21.6	-6 9 24	8.6	5006	80	0.16	26.8	15.4	179	0.24	N
575	5 36 22.1	-6 35 38	6.9	3488	67	0.13	32.4	9.5	97	0.22	N
576	5 36 22.6	-5 55 38	8.0	6075	88	0.18	27.7	13.9	63	0.36	N
577	5 36 22.6	-6 46 24	10.1	5063	80	0.16	21.0	12.6	120	0.46	N
578	5 36 22.9	-6 19 37	6.1	11869	123	0.25	38.1	25.0	-172	0.33	N
579	5 36 22.9	-6 47 22	6.4	2306	54	0.11	18.5	8.0	100	0.27	N
580	5 36 23.1	-6 43 51	6.8	7481	98	0.20	35.5	26.9	91	0.34	N
581	5 36 23.5	-5 59 35	8.2	3994	71	0.14	22.2	13.8	-163	0.37	N
582	5 36 23.9	-6 24 6	6.7	49444	251	0.50	63.5	51.0	164	0.78	N
583	5 36 25.2	-6 14 28	8.3	4838	78	0.16	34.9	9.4	46	0.37	N
584	5 36 25.4	-6 47 19	8.1	6975	94	0.19	37.4	14.2	74	0.61	N
585	5 36 25.7	-6 44 29	8.7	9844	112	0.22	33.6	18.1	179	0.55	N
586	5 36 25.8	-6 39 42	7.1	5063	80	0.16	20.8	15.5	-180	0.30	N
587	5 36 26.0	-6 7 5	8.3	5231	82	0.16	29.3	13.1	103	0.41	N
588	5 36 26.1	-6 42 6	8.8	5231	82	0.16	36.7	13.7	61	0.29	N

Table 3: Continued

ID	RA (J2000)	Dec (J2000)	v_{LSR} (km s ⁻¹)	A (arcsec ²)	$2R_{\text{core}}$ (arcsec)	$2R_{\text{core}}$ (pc)	a_{major} (arcsec)	a_{minor} (arcsec)	PA (deg)	dV_{core} (km s ⁻¹)	YSO
589	5 36 26.3	-6 15 22	6.5	2306	54	0.11	13.3	11.5	66	0.18	N
590	5 36 26.9	-6 22 0	9.7	2756	59	0.12	15.4	11.6	87	0.33	N
591	5 36 27.0	-6 20 44	8.2	6356	90	0.18	38.5	14.5	161	0.26	N
592	5 36 28.0	-6 29 19	7.1	2194	53	0.11	14.2	11.3	169	0.19	N
593	5 36 28.7	-6 46 36	9.3	1575	45	0.09	11.3	8.9	128	0.20	N
594	5 36 29.5	-6 48 19	6.3	1913	49	0.10	14.1	8.8	123	0.22	N
595	5 36 30.5	-6 10 7	6.6	10013	113	0.23	47.2	21.4	94	0.45	N
596	5 36 30.6	-6 40 26	6.9	3713	69	0.14	23.7	11.9	-163	0.18	N
597	5 36 30.7	-6 21 8	9.8	2475	56	0.11	16.0	13.1	92	0.22	N
598	5 36 30.8	-6 46 40	6.5	2250	54	0.11	19.3	9.2	85	0.21	N
599	5 36 31.1	-6 15 47	8.1	3094	63	0.13	26.8	7.7	-138	0.25	N
600	5 36 31.5	-6 41 8	9.2	2531	57	0.11	21.1	9.3	118	0.20	N
601	5 36 31.7	-6 2 2	8.0	11813	123	0.25	35.5	28.0	72	0.28	N
602	5 36 32.1	-6 33 1	7.3	3825	70	0.14	24.0	13.3	52	0.30	N
603	5 36 32.1	-6 35 45	7.5	8325	103	0.21	55.6	17.1	99	0.16	N
604	5 36 32.7	-6 39 31	8.8	2925	61	0.12	21.3	12.6	165	0.28	N
605	5 36 33.1	-6 26 32	7.2	3319	65	0.13	20.3	12.0	-168	0.21	N
606	5 36 33.7	-6 20 45	8.5	6581	92	0.18	27.9	16.9	81	0.48	N
607	5 36 33.7	-6 22 9	9.5	4556	76	0.15	24.5	13.5	87	0.19	N
608	5 36 34.0	-6 23 48	9.4	1856	49	0.10	12.8	9.2	-178	0.20	N
609	5 36 34.1	-6 18 47	9.3	2700	59	0.12	19.3	11.3	131	0.19	N
610	5 36 35.1	-6 6 34	6.3	6525	91	0.18	22.7	18.8	-166	0.26	N
611	5 36 35.3	-6 9 34	8.2	7369	97	0.19	28.9	15.3	158	0.28	Y
612	5 36 35.7	-6 19 12	9.9	4781	78	0.16	24.5	21.1	-138	0.25	N
613	5 36 35.8	-6 38 54	7.1	12881	128	0.26	45.4	21.3	47	0.28	N
614	5 36 36.1	-6 42 5	7.2	1856	49	0.10	20.0	7.2	93	0.20	N
615	5 36 37.0	-6 43 10	7.0	3150	63	0.13	16.7	12.8	48	0.23	N
616	5 36 37.2	-6 38 20	6.1	2250	54	0.11	20.0	9.3	89	0.21	N
617	5 36 37.3	-6 10 48	8.4	3319	65	0.13	19.0	13.7	90	0.16	N
618	5 36 37.3	-6 41 1	7.1	4725	78	0.16	25.4	15.1	61	0.22	Y
619	5 36 37.5	-6 46 39	8.7	3600	68	0.14	17.7	15.3	58	0.34	N
620	5 36 37.6	-6 3 45	8.3	2813	60	0.12	21.0	9.6	59	0.29	Y
621	5 36 37.8	-6 48 41	7.8	3206	64	0.13	29.1	14.6	137	0.17	N
622	5 36 38.0	-6 39 54	8.9	5681	85	0.17	49.7	17.3	54	0.25	N
623	5 36 38.5	-6 13 34	8.2	16763	146	0.29	49.4	24.0	-145	0.40	N
624	5 36 38.5	-6 35 28	6.0	5175	81	0.16	34.4	15.5	73	0.32	N
625	5 36 38.5	-6 43 50	8.2	4219	73	0.15	35.4	11.6	-138	0.24	N
626	5 36 39.2	-6 30 38	8.2	3825	70	0.14	30.0	14.4	-161	0.28	N
627	5 36 39.7	-6 34 54	6.6	1856	49	0.10	18.2	8.2	97	0.19	N
628	5 36 39.9	-6 40 52	8.4	1631	46	0.09	11.8	10.2	94	0.18	N
629	5 36 40.1	-6 13 38	6.2	29588	194	0.39	71.4	32.2	177	0.23	N
630	5 36 41.0	-6 22 44	8.6	1688	46	0.09	17.8	6.8	-167	0.21	N
631	5 36 41.9	-6 26 37	5.9	1631	46	0.09	16.9	8.9	-156	0.24	N
632	5 36 42.4	-6 18 20	8.7	11081	119	0.24	51.2	21.1	63	0.23	N
633	5 36 42.5	-6 41 15	7.3	3994	71	0.14	25.8	11.8	70	0.22	N
634	5 36 42.6	-6 20 33	7.5	2250	54	0.11	14.1	10.3	169	0.23	Y
635	5 36 42.8	-6 1 39	7.2	4781	78	0.16	46.3	17.3	112	0.20	N
636	5 36 42.9	-6 1 57	8.0	3263	64	0.13	18.9	14.3	85	0.12	N
637	5 36 43.3	-6 46 35	7.3	3994	71	0.14	20.8	16.4	143	0.16	N

Table 3: Continued

ID	RA (J2000)	Dec (J2000)	v_{LSR} (km s ⁻¹)	A (arcsec ²)	$2R_{\text{core}}$ (arcsec)	$2R_{\text{core}}$ (pc)	a_{major} (arcsec)	a_{minor} (arcsec)	PA (deg)	dV_{core} (km s ⁻¹)	YSO
638	5 36 43.7	-6 21 25	8.7	4500	76	0.15	23.0	17.1	137	0.30	N
639	5 36 44.5	-6 25 29	9.2	2925	61	0.12	21.1	12.5	-166	0.19	N
640	5 36 44.7	-6 42 53	7.6	2925	61	0.12	17.1	10.7	70	0.30	N
641	5 36 44.8	-6 35 46	7.4	3544	67	0.13	21.2	11.4	-141	0.24	N
642	5 36 44.8	-6 44 15	7.4	6694	92	0.19	29.1	13.8	61	0.45	N
643	5 36 45.0	-6 30 11	7.3	2475	56	0.11	16.3	9.7	73	0.47	N
644	5 36 45.2	-6 6 21	8.4	8550	104	0.21	38.0	19.6	-151	0.23	N
645	5 36 45.2	-6 24 9	8.1	1519	44	0.09	16.6	6.7	93	0.20	N
646	5 36 45.6	-6 17 48	5.8	9731	111	0.22	37.7	19.3	-144	0.31	N
647	5 36 46.0	-6 5 28	6.3	15469	140	0.28	33.0	31.3	104	0.52	N
648	5 36 46.1	-6 21 22	8.0	4388	75	0.15	18.1	14.6	110	0.35	N
649	5 36 46.1	-6 31 10	6.8	4613	77	0.15	24.4	12.5	161	0.34	N
650	5 36 46.2	-6 15 22	8.4	4106	72	0.15	18.1	13.9	99	0.31	N
651	5 36 46.7	-6 33 29	7.5	8044	101	0.20	66.9	21.1	96	0.37	N
652	5 36 46.8	-6 25 26	8.1	3150	63	0.13	20.8	9.3	45	0.31	N
653	5 36 47.6	-6 15 57	5.6	12825	128	0.26	43.9	26.9	52	0.37	N
654	5 36 47.6	-6 19 50	6.2	13613	132	0.26	40.0	27.0	147	0.29	N
655	5 36 47.8	-6 28 36	6.1	9844	112	0.22	48.4	15.8	49	0.41	N
656	5 36 48.1	-6 26 11	9.5	6525	91	0.18	33.8	18.7	128	0.48	N
657	5 36 48.2	-6 19 31	7.7	2925	61	0.12	24.2	9.2	67	0.20	N
658	5 36 48.9	-6 35 15	6.4	3600	68	0.14	21.5	15.7	139	0.17	N
659	5 36 49.4	-6 23 0	8.8	5906	87	0.17	29.4	14.5	141	0.27	N
660	5 36 49.5	-6 2 34	8.4	5850	86	0.17	44.6	19.9	83	0.37	N
661	5 36 49.9	-6 21 20	8.8	3206	64	0.13	17.3	14.8	60	0.19	Y
662	5 36 50.0	-6 39 52	7.0	4388	75	0.15	27.1	10.0	63	0.30	N
663	5 36 50.1	-6 28 51	7.4	7425	97	0.20	34.0	13.3	-140	0.37	N
664	5 36 52.8	-6 41 7	7.1	3938	71	0.14	22.3	13.2	107	0.38	N
665	5 36 53.3	-6 32 24	5.6	10350	115	0.23	40.1	17.7	102	0.37	N
666	5 36 53.5	-6 17 16	9.1	3544	67	0.13	20.8	13.4	68	0.28	N
667	5 36 53.8	-6 18 1	5.7	5625	85	0.17	25.8	18.6	71	0.28	N
668	5 36 54.1	-6 33 47	8.7	7425	97	0.20	32.8	16.6	92	0.51	N
669	5 36 55.1	-6 34 51	5.7	3488	67	0.13	17.2	12.2	-152	0.39	N
670	5 36 55.3	-6 19 17	9.3	3038	62	0.12	20.6	12.5	123	0.20	N
671	5 36 55.6	-6 34 29	6.5	1575	45	0.09	12.7	8.8	-178	0.24	N
672	5 36 55.7	-6 31 52	6.9	7594	98	0.20	44.4	17.2	70	0.24	N
673	5 36 56.0	-6 22 37	8.5	6469	91	0.18	24.6	17.0	53	0.28	N
674	5 36 57.2	-6 35 20	11.5	2588	57	0.12	18.3	11.2	134	0.30	N
675	5 36 57.4	-6 41 14	12.0	2531	57	0.11	19.1	10.0	165	0.24	N
676	5 36 57.5	-6 40 48	6.3	2869	60	0.12	16.1	10.9	49	0.21	N
677	5 36 57.7	-6 15 52	6.7	4106	72	0.15	25.2	16.5	100	0.27	N
678	5 36 58.5	-6 36 24	7.4	2700	59	0.12	15.8	10.9	106	0.34	N
679	5 36 59.3	-6 19 1	5.7	5906	87	0.17	34.3	21.6	-155	0.28	N
680	5 36 59.6	-6 29 0	9.7	3375	66	0.13	38.0	11.8	53	0.20	N
681	5 36 59.7	-6 20 31	9.7	2250	54	0.11	22.5	11.3	141	0.27	N
682	5 37 0.2	-6 39 2	6.2	3713	69	0.14	36.4	8.4	78	0.31	N
683	5 37 0.3	-6 24 44	8.6	9844	112	0.22	45.9	22.6	88	0.33	N
684	5 37 0.6	-6 24 58	9.5	3544	67	0.13	25.2	12.7	162	0.37	N
685	5 37 0.6	-6 37 5	6.0	3544	67	0.13	15.2	14.1	47	0.30	N
686	5 37 1.8	-6 35 23	6.5	5400	83	0.17	24.3	16.7	-160	0.34	N

Table 3: Continued

ID	RA (J2000)	Dec (J2000)	v_{LSR} (km s ⁻¹)	A (arcsec ²)	$2R_{\text{core}}$ (arcsec)	$2R_{\text{core}}$ (pc)	a_{major} (arcsec)	a_{minor} (arcsec)	PA (deg)	dV_{core} (km s ⁻¹)	YSO
687	5 37 2.3	-6 39 5	7.2	3319	65	0.13	32.2	10.2	108	0.14	N
688	5 37 3.4	-6 20 16	9.2	7144	95	0.19	28.4	16.5	159	0.63	N
689	5 37 3.7	-6 17 54	5.5	5456	83	0.17	27.9	17.7	-151	0.30	N
690	5 37 4.1	-6 34 13	8.1	2306	54	0.11	15.6	10.8	72	0.25	N
691	5 37 5.5	-6 23 43	9.0	5063	80	0.16	23.2	12.5	78	0.50	Y
692	5 37 6.0	-6 35 41	6.2	2700	59	0.12	16.0	11.8	-157	0.26	N
693	5 37 6.9	-6 27 22	9.0	4106	72	0.15	28.2	12.2	-150	0.17	N
694	5 37 7.1	-6 36 58	8.7	3319	65	0.13	21.8	14.4	140	0.25	N
695	5 37 8.5	-6 26 2	8.5	8269	103	0.21	31.1	26.2	138	0.26	N
696	5 37 8.5	-6 28 18	9.4	5738	85	0.17	21.7	18.4	159	0.46	N
697	5 37 8.9	-6 44 40	7.6	8100	102	0.20	54.2	19.3	63	0.42	N
698	5 37 9.1	-6 36 13	5.9	3319	65	0.13	17.5	12.3	142	0.32	N
699	5 37 9.9	-6 38 41	8.6	4838	78	0.16	40.8	12.8	-161	0.34	N
700	5 37 10.8	-6 31 20	9.0	3881	70	0.14	27.2	10.6	88	0.27	N
701	5 37 11.5	-6 41 43	6.5	2588	57	0.12	17.5	11.9	109	0.29	N
702	5 37 11.8	-6 31 57	9.5	2813	60	0.12	19.7	11.1	88	0.22	N
703	5 37 12.3	-6 39 29	7.3	3825	70	0.14	25.2	10.1	-148	0.28	N
704	5 37 13.9	-6 27 39	8.8	6131	88	0.18	32.6	18.8	76	0.42	N
705	5 37 14.3	-6 46 47	7.2	2925	61	0.12	17.6	12.9	-147	0.22	N
706	5 37 14.8	-6 27 19	5.8	11869	123	0.25	40.3	20.0	122	0.42	N
707	5 37 14.8	-6 33 9	7.1	1913	49	0.10	15.0	9.4	-163	0.18	Y
708	5 37 15.5	-6 19 36	5.5	1406	42	0.08	14.2	6.0	145	0.21	Y
709	5 37 15.7	-6 18 53	5.8	4275	74	0.15	31.0	14.3	49	0.26	N
710	5 37 15.8	-6 36 18	6.7	3881	70	0.14	25.7	15.8	-166	0.21	N
711	5 37 15.8	-6 36 19	7.5	5681	85	0.17	24.7	17.5	81	0.44	N
712	5 37 16.1	-6 30 11	6.2	5231	82	0.16	27.5	17.4	-151	0.20	N
713	5 37 16.3	-6 34 33	8.7	5569	84	0.17	37.8	14.1	64	0.27	Y
714	5 37 16.3	-6 46 28	7.8	7594	98	0.20	32.9	21.1	85	0.45	N
715	5 37 17.5	-6 30 0	4.4	3544	67	0.13	26.1	11.1	83	0.39	N
716	5 37 17.5	-6 33 23	9.4	4500	76	0.15	25.3	15.5	-178	0.27	N
717	5 37 18.1	-6 40 18	7.6	3488	67	0.13	17.4	12.8	-167	0.22	N
718	5 37 18.6	-6 46 13	7.1	2419	55	0.11	18.8	12.0	112	0.18	N
719	5 37 19.0	-6 44 4	6.6	2981	62	0.12	19.7	11.5	155	0.19	N
720	5 37 19.1	-6 37 16	6.1	5006	80	0.16	41.3	16.6	102	0.16	N
721	5 37 20.2	-6 44 19	6.1	4444	75	0.15	23.4	16.6	156	0.19	N
722	5 37 20.5	-6 34 60	5.9	3263	64	0.13	28.3	15.4	119	0.37	N
723	5 37 21.8	-6 36 33	9.0	8325	103	0.21	32.5	21.6	-138	0.69	N
724	5 37 22.2	-6 47 43	8.0	6075	88	0.18	21.1	17.0	108	0.35	N
725	5 37 22.5	-6 36 51	5.7	10519	116	0.23	35.6	19.9	138	0.39	N
726	5 37 22.9	-6 41 43	7.3	8888	106	0.21	33.7	19.9	143	0.47	N
727	5 37 22.9	-6 45 32	7.9	6356	90	0.18	23.4	22.0	-161	0.30	N
728	5 37 25.0	-6 47 4	6.9	5006	80	0.16	22.2	20.1	68	0.26	N
729	5 37 26.8	-6 43 54	7.7	6638	92	0.18	38.6	15.3	174	0.27	N
730	5 37 27.3	-6 39 7	5.8	4331	74	0.15	25.2	12.3	56	0.18	N
731	5 37 27.6	-6 44 32	10.5	3263	64	0.13	15.8	11.6	88	0.41	N
732	5 37 28.9	-6 39 5	6.3	5963	87	0.17	25.6	16.0	89	0.42	N
733	5 37 29.7	-6 44 48	6.2	11588	121	0.24	32.7	25.4	50	0.44	N
734	5 37 30.4	-6 42 3	5.4	2250	54	0.11	17.2	9.2	164	0.19	N
735	5 37 31.1	-6 34 59	6.2	3881	70	0.14	23.2	15.4	80	0.24	N

Table 3: Continued

ID	RA (J2000)	Dec (J2000)	v_{LSR} (km s ⁻¹)	A (arcsec ²)	$2R_{\text{core}}$ (arcsec)	$2R_{\text{core}}$ (pc)	a_{major} (arcsec)	a_{minor} (arcsec)	PA (deg)	dV_{core} (km s ⁻¹)	YSO
736	5 37 33.8	-6 36 51	6.0	9675	111	0.22	33.5	20.8	-169	0.30	N
737	5 37 36.8	-6 45 59	6.2	2869	60	0.12	22.3	10.6	53	0.21	N
738	5 37 37.5	-6 34 40	6.0	5906	87	0.17	30.7	14.8	117	0.25	N
739	5 37 38.2	-6 45 16	8.8	2869	60	0.12	19.7	13.1	127	0.23	N
740	5 37 38.5	-6 42 59	5.5	6188	89	0.18	27.1	14.7	-165	0.36	N
741	5 37 41.2	-6 36 48	5.9	6525	91	0.18	31.9	17.5	82	0.25	N
742	5 37 42.8	-6 44 21	8.3	4444	75	0.15	30.7	13.9	106	0.21	N
743	5 37 43.3	-6 45 29	6.4	4163	73	0.15	27.1	12.6	-140	0.42	N
744	5 37 45.4	-6 39 24	6.3	2250	54	0.11	16.8	10.3	146	0.19	N
745	5 37 45.9	-6 42 32	6.4	5794	86	0.17	30.6	21.2	-164	0.48	N
746	5 37 47.2	-6 40 41	5.2	3263	64	0.13	35.2	8.6	121	0.19	N

Table 4: Properties of Identified Cores (2)

ID	$T_{\text{mb}}^{\text{peak}}$ (K)	$T_{\text{mb}}^{\text{total}}$ (K)	M_{core} (M_{\odot})	$M_{\text{vir}}/M_{\text{core}}$	\bar{n} (10^4 cm^{-3})	\bar{T}_{ex} (K)	$\bar{N}_{\text{C}^{18}\text{O}}$ (10^{15} cm^{-2})	$\bar{X}_{\text{C}^{18}\text{O}}$ (10^{-7})
1	1.7	183.0	0.7	0.7	0.5	20.3	0.5	2.8
2	2.9	154.2	0.2	0.5	0.3	21.9	1.5	7.5
3	1.5	84.4	0.2	0.3	0.4	21.9	1.0	4.9
4	3.5	522.1	0.6	0.4	0.5	23.5	2.7	7.1
5	1.4	66.9	0.3	0.4	0.5	14.1	0.9	7.8
6	2.9	687.8	1.7	0.3	0.7	23.6	1.5	3.6
7	1.9	115.6	0.3	0.5	0.5	25.2	1.4	3.6
8	1.6	89.0	0.6	0.1	0.9	28.8	1.3	5.2
9	3.3	236.4	0.2	0.6	0.6	23.6	2.7	6.7
10	2.8	460.8	0.8	0.5	0.5	23.7	1.9	3.8
11	2.7	157.7	0.1	0.5	0.4	24.5	3.0	8.6
12	4.1	798.0	0.7	0.4	0.4	23.2	3.5	7.4
13	2.0	318.6	0.5	3.3	0.5	30.3	2.0	5.0
14	1.6	68.7	0.1	1.9	0.2	24.7	3.0	8.5
15	1.8	297.0	0.9	0.5	0.5	26.0	1.7	4.2
16	5.0	609.6	1.3	0.1	1.6	28.8	4.5	4.6
17	5.1	849.1	1.1	0.2	1.1	25.1	3.8	5.2
18	3.5	378.9	0.5	0.3	0.6	27.2	2.9	6.6
19	1.9	1908.1	6.3	0.7	0.3	27.0	1.4	5.6
20	4.8	1624.0	3.4	0.2	1.0	24.7	4.6	3.6
21	4.0	225.5	0.5	0.2	1.2	25.2	3.4	3.1
22	2.5	274.5	0.3	0.8	0.5	26.3	2.4	6.2
23	2.0	195.2	0.4	0.7	0.7	25.9	3.2	5.8
24	1.4	97.9	0.2	0.4	0.2	23.6	2.6	3.3
25	3.0	940.7	1.5	0.4	0.3	34.2	4.6	5.6
26	2.5	190.1	0.4	0.4	0.8	26.8	3.2	4.8
27	3.7	663.9	1.2	0.4	0.7	23.3	3.1	3.8
28	1.9	262.9	0.5	1.7	0.2	25.2	2.6	6.3
29	1.6	179.7	0.5	0.7	0.3	25.3	1.7	4.1
30	1.4	67.6	0.1	0.4	0.2	25.3	2.1	4.0
31	1.5	258.6	1.2	0.7	0.5	25.8	1.1	4.9
32	2.2	238.8	0.3	0.6	0.4	25.1	3.5	7.7
33	2.2	239.4	0.5	0.5	0.4	26.4	2.3	5.4
34	1.5	404.5	1.8	0.4	0.3	25.2	1.1	5.8
35	1.6	135.7	0.3	0.3	0.2	23.8	3.4	3.8
36	2.1	106.1	0.3	0.4	0.6	24.2	1.6	3.6
37	2.4	179.4	0.3	0.4	0.5	25.4	2.2	5.5
38	5.2	1404.9	2.8	0.2	1.2	24.5	4.0	3.6
39	2.0	83.0	0.2	0.4	0.7	23.6	1.7	3.8
40	2.6	362.6	0.7	0.6	0.4	24.1	2.3	4.3
41	1.4	198.1	1.0	0.3	0.6	32.9	1.2	5.1
42	2.4	207.5	0.5	0.3	0.9	24.4	2.4	3.3
43	2.1	292.9	0.7	0.4	0.5	35.2	3.0	4.7
44	2.6	201.8	0.3	0.4	0.8	25.8	2.2	5.0
45	1.6	150.7	1.0	0.4	0.8	21.1	1.1	3.3
46	2.9	863.5	2.1	0.4	0.5	21.3	1.6	3.6
47	3.9	1731.5	4.2	0.7	1.2	24.0	4.2	3.1
48	1.8	568.4	1.4	0.9	0.3	27.6	1.9	6.2
49	2.5	530.6	0.8	0.4	0.4	26.5	2.6	5.7

Table 4: Continued

ID	$T_{\text{mb}}^{\text{peak}}$ (K)	$T_{\text{mb}}^{\text{total}}$ (K)	M_{core} (M_{\odot})	$M_{\text{vir}}/M_{\text{core}}$	\bar{n} (10^4 cm^{-3})	\bar{T}_{ex} (K)	$\bar{N}_{\text{C}^{18}\text{O}}$ (10^{15} cm^{-2})	$\bar{X}_{\text{C}^{18}\text{O}}$ (10^{-7})
50	1.7	407.3	2.0	0.1	0.6	23.6	0.6	1.9
51	1.4	157.2	0.6	0.4	0.3	27.1	2.0	5.4
52	1.6	52.2	0.1	0.3	0.5	25.2	2.8	7.7
53	2.6	233.5	0.4	0.6	0.8	21.8	2.5	4.5
54	1.6	358.2	1.4	0.7	0.6	22.9	1.1	4.8
55	1.5	276.9	1.1	0.4	0.5	27.0	1.7	4.6
56	2.7	101.1	0.1	1.3	1.2	24.3	2.6	5.2
57	1.6	113.7	0.3	0.4	0.4	26.9	1.6	5.9
58	2.3	475.8	1.1	0.6	0.5	34.0	2.6	6.9
59	4.1	406.1	0.8	0.3	1.5	24.7	4.4	4.4
60	1.9	161.7	0.4	0.3	0.3	44.7	3.1	8.1
61	4.8	314.1	0.6	0.1	1.4	28.1	4.7	5.0
62	2.8	432.6	0.9	0.2	0.8	23.9	1.9	3.8
63	3.4	323.7	0.6	0.2	0.9	20.1	2.1	3.9
64	4.1	1198.5	1.8	0.7	0.8	26.8	4.4	5.2
65	3.1	220.7	0.5	0.7	1.2	24.5	3.7	3.1
66	2.5	387.9	1.6	0.2	0.6	15.8	0.6	1.9
67	1.8	96.7	0.5	0.2	0.9	26.5	1.8	5.1
68	2.1	211.9	0.6	0.3	0.5	39.3	2.8	8.1
69	3.0	157.5	0.3	0.2	0.9	35.4	3.5	5.2
70	1.4	53.5	0.2	0.3	0.4	46.4	3.2	7.7
71	1.4	313.2	1.1	1.6	0.4	46.5	2.8	7.8
72	1.9	260.3	0.7	2.2	0.4	31.6	2.1	9.2
73	1.6	87.6	0.2	1.2	0.4	24.8	3.6	3.2
74	1.6	331.0	2.1	0.2	0.6	22.6	0.6	1.8
75	4.1	452.3	1.0	0.2	0.9	25.7	3.5	4.0
76	1.4	182.3	1.1	0.3	0.6	32.7	1.5	6.4
77	1.4	52.7	0.2	0.2	0.7	23.2	1.5	2.9
78	4.2	586.3	1.3	0.1	1.0	22.5	3.6	3.4
79	2.9	1620.3	5.1	0.2	0.4	27.5	1.5	4.6
80	1.7	483.1	1.3	0.6	0.2	36.3	1.9	7.6
81	2.1	554.5	0.8	1.8	0.3	38.7	4.1	7.6
82	1.5	272.2	0.8	1.0	0.5	27.7	2.0	6.0
83	2.9	1121.5	1.2	1.0	0.4	31.6	3.4	8.0
84	3.3	252.8	0.4	0.2	0.7	25.1	2.6	4.3
85	3.8	770.2	1.8	0.3	1.6	25.3	4.9	3.6
86	2.4	365.3	0.6	1.7	0.2	28.2	2.9	6.4
87	3.2	171.8	0.3	0.3	0.6	27.7	2.9	6.6
88	2.1	673.8	1.7	0.9	0.4	42.4	2.3	7.2
89	1.5	59.7	0.1	2.8	0.1	31.9	3.6	10.1
90	3.7	371.7	0.7	0.2	0.9	27.1	5.2	3.8
91	3.1	179.6	0.3	0.4	1.1	27.0	4.4	4.2
92	3.1	298.9	0.7	0.3	0.9	28.9	4.3	3.4
93	2.3	594.1	0.8	1.0	0.2	44.6	4.3	12.5
94	2.6	417.8	0.4	1.4	0.3	32.6	3.9	9.0
95	3.7	1224.9	1.6	0.8	0.7	29.4	3.5	6.3
96	2.1	166.9	0.5	0.3	0.5	29.4	2.3	6.2
97	3.7	208.2	0.3	0.3	0.8	31.6	5.3	6.2
98	3.9	1790.1	4.0	0.8	0.9	31.8	4.8	4.8

Table 4: Continued

ID	$T_{\text{mb}}^{\text{peak}}$ (K)	$T_{\text{mb}}^{\text{total}}$ (K)	M_{core} (M_{\odot})	$M_{\text{vir}}/M_{\text{core}}$	\bar{n} (10^4 cm^{-3})	\bar{T}_{ex} (K)	$\bar{N}_{\text{C}^{18}\text{O}}$ (10^{15} cm^{-2})	$\bar{X}_{\text{C}^{18}\text{O}}$ (10^{-7})
99	2.5	505.5	0.7	0.9	0.5	38.2	3.5	8.2
100	1.8	303.5	0.9	0.6	0.5	24.6	2.4	4.5
101	2.5	997.0	1.3	1.6	0.2	36.9	2.6	11.4
102	1.4	62.5	0.1	3.1	0.2	33.1	5.1	9.4
103	1.4	100.8	0.4	0.8	0.4	24.8	0.4	2.2
104	4.0	162.1	0.5	0.1	2.6	28.0	6.1	3.4
105	1.3	67.8	0.3	0.3	0.7	48.8	3.9	11.1
106	1.5	87.0	0.2	0.5	0.3	8.8	0.4	3.5
107	3.1	176.1	0.3	0.3	1.1	31.4	10.2	4.6
108	1.9	86.0	0.2	0.5	0.6	16.2	1.0	2.8
109	3.7	582.7	0.7	0.3	0.5	32.3	5.1	8.6
110	4.3	619.9	1.2	0.1	1.2	29.4	7.3	4.2
111	1.5	79.4	0.2	1.3	0.5	8.9	0.6	4.2
112	2.4	387.2	1.0	1.7	0.3	27.5	3.6	5.1
113	1.5	61.4	0.3	0.5	0.6	55.4	2.6	10.8
114	2.1	521.1	1.1	1.5	0.4	31.4	1.9	9.3
115	2.8	154.4	0.2	0.2	0.6	38.3	3.9	8.5
116	1.8	40.8	0.1	0.4	0.6	22.0	1.8	8.9
117	2.9	158.8	0.3	0.4	1.1	33.3	4.5	6.6
118	5.7	870.6	1.6	0.2	1.5	31.4	10.6	4.4
119	1.5	155.0	0.3	0.7	0.2	28.2	3.8	5.0
120	3.3	670.6	1.0	0.7	0.6	31.5	4.0	8.1
121	1.4	93.3	0.2	1.0	0.4	27.8	4.2	5.4
122	1.4	107.5	0.6	0.2	0.6	12.4	0.4	2.0
123	1.5	545.1	1.9	0.6	0.3	33.0	2.0	6.9
124	5.4	1178.4	2.7	0.3	2.1	42.3	7.5	5.5
125	3.5	445.3	0.7	0.7	0.6	49.9	5.3	8.5
126	4.8	2096.3	4.0	0.5	0.9	31.1	5.7	6.0
127	2.3	399.7	1.4	0.6	0.5	30.8	2.0	6.9
128	3.5	492.2	0.8	0.8	0.6	33.9	4.4	7.1
129	3.4	243.7	0.4	0.2	1.1	35.8	7.8	6.3
130	2.1	933.5	2.0	2.4	0.2	44.6	5.3	10.9
131	2.3	508.7	0.8	0.8	0.4	29.6	4.5	6.7
132	4.3	396.4	0.7	0.7	2.1	32.1	12.3	4.6
133	2.4	647.7	1.1	0.4	0.3	38.6	2.5	9.8
134	3.7	295.3	0.5	0.4	1.2	40.8	5.8	6.6
135	3.9	144.5	0.2	0.5	1.6	38.5	8.9	7.4
136	2.7	126.6	0.2	1.1	0.7	42.6	5.1	8.8
137	1.5	138.3	0.2	1.2	0.2	34.0	5.2	8.6
138	1.8	238.0	0.5	0.9	0.2	40.0	5.1	7.8
139	4.8	346.1	1.0	0.1	1.8	36.6	11.2	3.9
140	6.1	1741.9	3.1	0.3	1.0	35.7	15.2	4.9
141	2.3	627.2	0.8	1.0	0.4	41.8	4.6	12.7
142	4.5	702.0	1.8	0.2	1.9	42.9	6.4	4.8
143	2.7	358.6	0.4	0.5	0.3	40.0	4.1	13.0
144	5.1	245.8	0.4	0.3	1.8	37.7	19.6	5.2
145	3.0	499.6	0.7	1.6	0.4	45.3	5.7	13.3
146	2.7	391.3	0.6	1.0	0.6	35.8	6.6	7.7
147	1.7	239.4	1.3	0.3	0.7	27.8	1.8	2.7

Table 4: Continued

ID	$T_{\text{mb}}^{\text{peak}}$ (K)	$T_{\text{mb}}^{\text{total}}$ (K)	M_{core} (M_{\odot})	$M_{\text{vir}}/M_{\text{core}}$	\bar{n} (10^4 cm^{-3})	\bar{T}_{ex} (K)	$\bar{N}_{\text{C}^{18}\text{O}}$ (10^{15} cm^{-2})	$\bar{X}_{\text{C}^{18}\text{O}}$ (10^{-7})
148	3.3	391.5	0.6	0.7	0.6	34.9	9.5	6.2
149	1.4	144.1	0.2	2.2	0.3	44.1	7.2	9.3
150	3.5	108.0	0.5	0.1	4.2	36.7	12.6	2.1
151	6.0	1545.1	2.7	0.2	1.4	39.9	15.7	5.2
152	4.1	1243.8	2.2	0.1	0.7	38.6	14.9	5.2
153	1.3	93.6	0.2	0.6	0.2	43.2	4.8	6.7
154	2.8	162.3	0.7	0.1	1.4	26.8	2.6	2.7
155	1.5	75.7	0.2	3.1	0.2	32.5	2.8	10.0
156	4.3	411.8	0.5	0.4	1.0	30.0	9.5	6.1
157	4.2	737.6	1.4	0.2	0.8	38.3	15.2	4.9
158	4.6	251.5	0.3	0.3	2.0	49.6	15.0	9.1
159	2.3	171.5	0.2	0.8	0.3	31.8	8.8	6.3
160	2.4	186.6	0.3	1.0	0.4	46.4	3.8	9.3
161	5.1	982.0	1.7	0.1	0.8	50.9	6.7	6.5
162	2.8	193.0	0.7	0.3	1.2	22.4	2.3	2.4
163	2.4	175.7	0.4	0.2	0.7	41.5	6.8	5.8
164	1.5	82.8	0.8	0.1	1.4	18.0	0.7	1.3
165	5.2	1626.8	2.4	0.2	1.1	36.1	10.6	6.3
166	2.5	840.7	1.2	0.8	0.2	43.7	4.4	9.9
167	4.0	443.9	0.9	0.3	1.0	46.2	6.5	6.8
168	4.6	409.6	0.9	0.5	7.8	55.9	16.8	6.1
169	4.8	685.6	0.9	0.3	1.3	30.8	9.3	6.1
170	1.3	75.2	0.1	0.6	0.1	38.1	11.2	6.9
171	5.2	481.2	1.1	0.1	2.1	41.0	13.8	4.5
172	4.6	352.6	0.5	0.2	0.9	34.6	9.2	6.6
173	1.6	149.4	0.3	1.4	0.6	43.3	6.3	11.4
174	2.5	332.6	1.5	0.2	1.1	17.8	1.5	2.1
175	2.3	145.0	0.2	0.6	0.4	34.2	8.8	6.4
176	2.4	525.9	1.1	1.6	0.9	51.3	8.1	7.4
177	1.8	50.8	0.1	0.4	0.6	27.5	2.1	3.4
178	3.0	1187.6	1.9	1.2	0.6	43.0	5.7	8.3
179	2.0	158.8	0.3	0.5	0.3	42.3	4.4	8.0
180	1.4	102.5	0.5	0.6	0.6	24.3	2.4	3.5
181	2.1	78.3	0.1	0.6	0.4	39.8	10.4	7.4
182	4.3	983.2	1.2	0.7	1.1	38.7	10.4	8.6
183	4.6	1008.3	1.0	0.9	1.1	42.2	10.1	10.1
184	2.3	224.5	0.9	0.5	1.3	19.0	2.2	2.1
185	1.7	1190.5	4.6	0.5	0.3	40.1	4.6	8.2
186	7.6	12034.9	22.2	0.2	0.9	48.2	16.0	7.0
187	5.3	1524.2	3.7	0.3	1.3	31.0	8.5	4.3
188	3.8	962.6	1.2	0.5	0.3	40.2	4.1	7.1
189	1.6	68.7	0.2	0.6	0.5	39.5	5.1	10.7
190	1.6	722.9	2.0	0.8	0.3	37.0	5.9	6.0
191	2.2	198.0	0.3	1.5	0.2	44.2	4.5	7.8
192	2.7	548.0	0.7	0.7	0.3	43.0	4.5	7.2
193	1.6	49.9	0.1	1.0	0.3	64.0	5.7	8.7
194	2.0	152.4	0.4	0.9	1.0	59.4	12.5	7.9
195	2.6	1386.4	2.0	1.6	0.5	46.6	10.4	10.4
196	2.3	117.1	0.1	1.3	0.1	12.3	0.6	2.6

Table 4: Continued

ID	$T_{\text{mb}}^{\text{peak}}$ (K)	$T_{\text{mb}}^{\text{total}}$ (K)	M_{core} (M_{\odot})	$M_{\text{vir}}/M_{\text{core}}$	\bar{n} (10^4 cm^{-3})	\bar{T}_{ex} (K)	$\bar{N}_{\text{C}^{18}\text{O}}$ (10^{15} cm^{-2})	$\bar{X}_{\text{C}^{18}\text{O}}$ (10^{-7})
197	3.3	429.9	0.5	0.5	0.6	45.2	10.7	8.7
198	2.5	884.2	2.2	1.4	1.1	62.7	13.5	7.7
199	5.3	326.5	1.0	0.1	2.9	47.2	14.8	3.6
200	1.6	287.2	1.3	1.0	0.5	19.2	1.8	2.8
201	2.3	282.6	0.8	1.4	0.9	61.2	14.4	7.1
202	2.2	207.8	0.2	1.5	0.2	46.0	4.5	10.9
203	5.0	491.4	0.7	0.2	1.5	45.3	10.6	6.1
204	2.9	286.0	0.4	1.3	0.3	40.4	4.8	5.4
205	1.9	129.7	0.1	3.8	0.1	8.0	0.2	2.3
206	2.0	187.2	0.8	0.2	1.4	18.0	2.8	1.9
207	3.4	763.7	2.0	0.2	0.8	18.4	2.1	2.3
208	2.7	245.8	0.2	0.5	0.2	44.7	4.4	8.7
209	2.9	261.8	0.8	0.1	0.6	18.8	2.8	2.2
210	2.1	236.9	0.7	0.5	0.7	18.2	2.0	2.9
211	3.8	311.3	0.3	0.6	0.6	50.7	9.3	13.9
212	1.6	348.9	1.8	0.6	0.6	34.1	3.2	6.4
213	2.7	209.8	0.7	0.7	2.2	62.5	15.6	5.3
214	1.5	275.1	2.0	0.6	0.5	19.5	1.3	2.5
215	2.8	711.1	1.4	0.3	0.6	21.3	3.4	3.3
216	2.5	184.9	0.4	0.2	0.7	38.8	3.8	6.8
217	2.3	122.6	0.2	0.5	0.3	73.2	12.0	7.2
218	1.6	223.4	0.6	1.1	0.6	39.6	5.3	7.7
219	2.4	95.6	0.2	1.5	0.4	66.4	10.8	7.1
220	5.6	5680.3	11.0	0.1	0.7	28.9	7.6	4.3
221	4.2	1517.1	1.4	0.7	0.4	50.9	12.2	14.0
222	1.7	404.9	0.4	2.5	0.2	47.6	7.5	13.3
223	3.6	245.9	1.3	0.1	2.7	37.4	6.4	2.5
224	2.9	76.1	0.1	0.8	0.4	41.6	3.4	5.7
225	2.2	297.1	1.0	0.5	0.7	17.7	1.8	2.3
226	3.3	481.0	1.2	0.4	1.3	20.2	3.5	3.1
227	3.8	208.4	0.2	0.7	0.3	41.7	7.3	6.4
228	2.0	368.6	0.7	0.6	0.4	23.1	5.0	3.8
229	3.1	347.2	0.8	0.6	0.7	18.5	2.5	2.7
230	3.7	1311.6	2.4	0.7	0.7	23.5	4.9	4.0
231	6.3	3235.4	7.4	0.2	2.0	48.7	17.8	5.6
232	4.7	1522.9	2.1	0.4	1.0	54.3	13.6	10.0
233	3.0	112.5	0.1	1.1	0.2	40.3	3.9	6.7
234	4.1	1706.5	2.3	0.9	1.4	40.5	10.9	8.5
235	2.9	482.1	0.8	0.6	1.0	42.3	7.2	8.2
236	2.6	110.8	0.1	2.9	0.2	39.4	4.0	7.5
237	3.4	492.0	0.8	0.6	1.3	51.0	13.7	8.8
238	3.7	4396.8	18.2	0.2	1.1	20.2	3.2	1.8
239	4.5	533.2	0.3	1.7	0.3	49.1	7.6	9.9
240	3.1	155.8	0.1	0.9	0.1	45.1	1.8	4.5
241	2.5	214.5	0.0	19.4	0.0	7.1	0.5	5.2
242	4.1	386.7	0.7	0.2	1.1	29.7	9.1	4.8
243	3.4	202.8	0.1	1.3	0.3	46.1	7.6	11.8
244	2.7	166.7	0.4	0.6	0.6	18.1	2.2	2.9
245	2.8	917.1	2.5	0.3	0.8	31.0	4.4	4.1

Table 4: Continued

ID	$T_{\text{mb}}^{\text{peak}}$ (K)	$T_{\text{mb}}^{\text{total}}$ (K)	M_{core} (M_{\odot})	$M_{\text{vir}}/M_{\text{core}}$	\bar{n} (10^4 cm^{-3})	\bar{T}_{ex} (K)	$\bar{N}_{\text{C}^{18}\text{O}}$ (10^{15} cm^{-2})	$\bar{X}_{\text{C}^{18}\text{O}}$ (10^{-7})
246	3.5	196.8	0.2	0.8	0.2	42.0	15.6	6.2
247	3.0	246.8	0.5	0.7	0.9	59.9	19.5	8.1
248	8.4	1730.8	2.6	0.3	2.3	49.4	17.5	6.3
249	1.4	127.7	0.5	0.4	0.3	20.1	1.6	3.0
250	3.0	223.2	0.1	2.3	0.1	49.8	8.3	11.3
251	2.0	343.8	0.3	4.5	0.3	51.8	9.2	13.2
252	2.2	231.0	1.0	0.2	0.8	20.0	1.2	3.1
253	4.6	481.6	3.2	0.1	11.2	105.4	69.1	4.0
254	5.4	832.1	1.8	0.4	5.0	104.3	48.0	11.4
255	1.9	55.9	0.0	1.6	0.2	48.4	-0.6	-1.3
256	5.3	545.0	4.1	0.2	37.4	106.6	77.0	3.2
257	5.1	1153.2	6.8	0.2	19.9	109.7	66.1	4.6
258	4.6	1089.4	1.5	0.1	0.6	29.9	8.4	5.8
259	1.6	60.2	0.1	0.6	0.4	19.5	2.2	2.9
260	1.5	165.9	0.7	0.3	0.5	20.4	1.3	2.4
261	2.7	266.8	0.4	0.9	0.2	41.9	16.7	5.5
262	4.0	633.3	1.9	0.1	1.0	20.8	3.1	2.6
263	2.0	307.2	0.4	2.1	0.4	33.9	6.4	8.0
264	4.5	388.2	0.9	0.1	2.0	33.2	10.7	4.0
265	1.9	120.3	0.2	1.8	0.4	55.8	10.0	10.3
266	4.9	357.4	0.3	0.8	0.5	40.7	11.7	7.8
267	2.3	408.3	1.9	0.3	0.8	18.7	1.3	2.3
268	5.4	512.8	0.4	0.8	0.6	40.5	12.5	7.9
269	3.7	917.5	1.7	0.3	1.0	61.1	14.2	8.6
270	5.0	1609.5	2.4	0.3	1.8	51.8	14.1	8.6
271	4.1	946.5	1.5	0.3	0.6	30.8	8.5	5.2
272	7.1	566.5	1.1	0.3	3.0	41.5	23.6	5.2
273	5.6	399.8	0.4	0.5	0.6	39.6	10.8	9.5
274	6.9	2697.3	24.4	0.1	18.8	106.4	47.9	3.2
275	5.2	584.6	1.4	0.4	3.8	112.8	43.8	10.9
276	4.3	548.5	0.9	0.3	1.5	59.6	14.9	8.8
277	4.7	2797.4	4.9	0.4	1.1	51.2	8.8	9.1
278	2.3	429.4	0.9	0.5	0.3	25.4	3.3	4.8
279	5.5	442.0	3.6	0.1	13.1	87.1	36.7	2.8
280	1.5	187.1	1.1	0.2	0.5	32.2	0.6	3.2
281	1.9	370.9	0.8	0.4	0.2	34.1	8.5	4.7
282	2.7	301.4	0.4	0.4	0.4	27.6	5.8	6.3
283	1.6	65.7	0.5	0.4	1.2	19.6	0.8	1.7
284	5.8	320.0	0.9	0.2	4.3	40.1	13.7	3.7
285	5.4	779.3	1.5	0.2	1.3	53.5	11.6	7.8
286	7.8	1732.4	8.4	0.0	6.5	43.3	21.6	3.3
287	3.3	227.7	0.4	0.5	1.6	39.9	17.4	5.1
288	2.8	822.4	1.5	0.3	0.3	35.2	2.0	8.1
289	2.9	855.9	3.5	0.2	0.5	19.6	1.5	2.8
290	5.3	502.6	2.2	0.2	10.4	81.1	36.4	4.3
291	2.3	126.7	0.2	0.4	0.6	64.7	13.0	12.4
292	3.8	443.2	0.5	1.0	0.9	53.6	11.6	12.7
293	1.7	188.7	0.5	0.8	0.3	22.1	2.2	4.4
294	1.8	92.7	0.2	0.4	0.3	23.1	2.8	6.0

Table 4: Continued

ID	$T_{\text{mb}}^{\text{peak}}$ (K)	$T_{\text{mb}}^{\text{total}}$ (K)	M_{core} (M_{\odot})	$M_{\text{vir}}/M_{\text{core}}$	\bar{n} (10^4 cm^{-3})	\bar{T}_{ex} (K)	$\bar{N}_{\text{C}^{18}\text{O}}$ (10^{15} cm^{-2})	$\bar{X}_{\text{C}^{18}\text{O}}$ (10^{-7})
295	1.4	90.0	0.8	0.5	0.9	28.4	1.8	6.3
296	1.5	237.3	0.9	0.5	0.3	18.5	1.3	2.4
297	1.6	56.8	0.2	0.4	1.1	34.5	2.9	5.5
298	2.2	88.2	0.5	0.2	3.0	22.5	1.9	1.6
299	5.6	934.5	2.1	0.3	2.3	58.4	17.7	7.1
300	5.4	1444.7	3.3	0.2	1.8	45.4	14.0	5.3
301	1.7	152.9	0.3	1.1	0.3	22.9	2.7	5.6
302	5.2	3006.9	4.1	0.4	0.9	28.6	8.7	6.1
303	1.6	89.9	0.2	1.4	0.2	22.8	2.4	4.7
304	2.0	134.3	0.8	0.4	1.2	20.9	1.4	1.4
305	1.7	46.4	0.1	1.8	0.3	23.1	3.3	6.5
306	1.6	48.4	0.1	0.8	0.2	29.3	8.8	6.3
307	2.9	231.1	0.6	0.5	2.3	113.7	20.3	10.8
308	4.0	670.6	2.0	0.2	1.8	64.7	13.7	7.6
309	1.5	71.3	0.4	0.4	0.9	87.7	12.0	8.0
310	3.5	301.3	0.5	0.3	0.9	33.2	5.9	7.3
311	1.7	131.0	0.5	0.7	0.6	26.5	1.7	4.6
312	1.9	127.3	0.3	0.5	0.4	34.1	3.4	7.4
313	1.4	142.1	0.9	0.4	0.8	81.4	8.0	8.5
314	3.5	341.4	1.8	0.1	2.4	72.3	13.8	4.1
315	1.4	69.4	0.2	0.5	0.3	101.9	15.8	12.0
316	1.9	126.8	0.4	0.5	1.0	18.1	1.5	2.2
317	3.3	784.1	1.6	0.3	0.8	30.3	6.7	4.2
318	1.5	61.1	0.3	0.3	0.5	9.0	0.4	3.2
319	2.7	569.2	1.2	0.5	0.5	33.5	1.2	3.6
320	1.7	76.3	0.1	0.8	0.4	28.4	4.2	5.3
321	2.2	1072.9	1.7	0.6	0.2	28.2	6.5	4.8
322	4.9	212.3	1.2	0.1	6.5	40.0	8.3	1.6
323	2.2	155.9	0.7	0.7	1.6	62.4	8.2	5.2
324	3.7	184.1	0.5	0.2	1.3	21.9	4.9	2.5
325	6.2	4252.5	7.3	0.2	0.8	25.7	5.5	4.5
326	2.5	548.5	1.3	0.6	0.6	29.1	3.5	4.5
327	2.2	89.2	0.4	0.2	1.9	61.7	8.4	5.0
328	2.8	935.5	1.7	0.4	0.3	27.6	5.8	4.3
329	1.5	53.5	0.1	1.2	0.2	30.1	4.5	5.5
330	1.9	244.4	0.7	0.4	0.5	32.2	1.4	5.1
331	3.1	859.3	2.0	1.3	1.1	88.9	13.5	10.9
332	1.4	86.0	0.2	0.4	0.2	63.1	5.0	10.1
333	2.5	181.5	0.3	0.4	0.6	31.1	2.2	5.9
334	1.4	58.0	0.6	0.1	1.5	24.8	1.4	3.9
335	6.2	928.9	4.9	0.0	4.4	46.0	12.2	2.8
336	1.5	101.8	0.5	0.3	1.1	26.0	1.8	4.1
337	3.6	612.4	0.9	0.4	1.0	29.3	6.9	5.5
338	4.7	410.4	0.7	0.1	1.1	31.8	3.5	4.2
339	4.6	589.6	1.6	0.1	2.1	57.6	13.9	5.7
340	1.4	186.2	1.2	0.1	0.6	23.9	1.0	4.3
341	1.6	114.0	0.9	0.1	0.9	65.8	4.5	6.2
342	7.6	2621.6	5.6	0.2	2.8	47.8	14.4	6.2
343	2.9	203.8	0.5	0.2	1.2	23.0	4.4	1.9

Table 4: Continued

ID	$T_{\text{mb}}^{\text{peak}}$ (K)	$T_{\text{mb}}^{\text{total}}$ (K)	M_{core} (M_{\odot})	$M_{\text{vir}}/M_{\text{core}}$	\bar{n} (10^4 cm^{-3})	\bar{T}_{ex} (K)	$\bar{N}_{\text{C}^{18}\text{O}}$ (10^{15} cm^{-2})	$\bar{X}_{\text{C}^{18}\text{O}}$ (10^{-7})
344	1.9	117.0	0.6	0.2	0.6	25.9	1.8	5.0
345	3.4	404.2	1.1	0.3	0.7	25.1	2.7	3.6
346	6.1	1090.3	2.2	0.1	1.5	35.5	7.5	4.5
347	1.7	105.2	0.4	0.3	0.4	46.7	1.8	6.6
348	5.0	254.3	0.5	0.3	2.6	38.2	9.1	5.1
349	1.8	59.7	0.3	0.3	0.5	23.6	0.9	3.4
350	2.8	436.9	1.4	0.3	0.6	34.9	3.0	4.9
351	1.8	364.3	1.4	1.6	0.7	62.0	8.7	6.8
352	3.0	907.5	1.5	0.4	0.5	26.2	4.8	4.7
353	1.5	80.8	0.5	0.4	0.8	30.9	0.6	2.8
354	2.7	135.1	0.2	1.0	0.6	23.7	2.7	5.1
355	3.4	670.6	1.2	0.5	0.5	27.7	3.9	4.6
356	4.2	781.7	2.1	0.2	1.7	60.8	11.7	5.4
357	1.9	156.7	0.3	0.6	0.3	33.3	1.2	5.1
358	4.3	355.1	1.1	0.1	1.3	24.2	3.5	2.0
359	3.7	602.1	1.4	0.2	1.1	57.5	8.6	5.6
360	6.1	487.4	1.2	0.3	3.8	50.7	16.9	5.3
361	1.7	219.3	0.4	3.4	0.4	40.5	6.8	7.3
362	3.5	221.0	0.3	0.5	0.5	32.7	7.6	6.0
363	1.9	305.3	0.6	0.4	0.3	27.1	3.9	4.8
364	1.3	80.9	0.2	0.5	0.4	48.6	3.4	11.0
365	1.4	56.1	0.1	1.1	0.2	25.9	2.8	4.7
366	1.9	376.1	1.3	1.2	0.7	59.3	8.0	7.5
367	1.4	121.6	0.5	0.7	0.3	60.0	7.4	7.2
368	5.1	394.1	0.8	0.1	2.2	42.9	8.5	5.1
369	1.5	37.3	0.1	1.0	0.4	32.4	9.4	5.1
370	2.4	171.9	0.3	0.3	0.3	32.1	5.2	7.2
371	1.7	164.3	0.9	0.7	0.6	23.3	1.5	5.1
372	1.8	152.9	0.4	0.3	0.4	23.5	2.4	3.1
373	1.5	71.7	0.1	1.0	0.3	28.0	4.3	5.9
374	1.6	104.5	0.5	0.2	0.7	56.9	4.2	5.9
375	1.9	124.5	0.7	0.1	0.6	32.1	1.7	3.6
376	1.6	64.3	0.1	0.6	0.3	29.7	5.1	6.9
377	1.5	100.8	0.5	0.3	0.5	54.0	6.0	6.4
378	3.5	233.0	0.4	0.3	0.9	32.3	9.3	5.1
379	1.4	79.6	0.3	0.3	0.4	25.7	1.3	6.4
380	2.7	287.8	0.6	0.1	0.6	25.4	2.4	3.8
381	1.7	117.2	0.4	0.5	0.4	24.0	1.4	6.1
382	3.2	397.9	0.8	0.3	1.1	47.4	8.8	6.7
383	1.7	105.3	0.3	0.5	0.4	51.8	4.5	7.9
384	3.0	401.6	0.6	1.4	0.9	56.1	9.6	9.8
385	1.5	52.6	0.2	0.4	0.6	24.6	1.3	6.7
386	1.7	79.1	0.3	0.3	0.5	36.5	3.0	5.7
387	2.4	168.9	0.2	1.7	0.5	56.7	5.7	12.5
388	1.5	72.0	0.7	0.3	1.2	49.7	2.4	3.1
389	1.5	98.9	0.2	0.4	0.2	36.6	4.2	5.6
390	3.1	385.0	1.0	0.2	0.9	37.1	4.1	5.1
391	2.7	457.1	0.7	0.5	0.4	33.4	8.2	6.0
392	2.4	739.6	1.5	0.3	0.4	30.1	3.9	5.3

Table 4: Continued

ID	$T_{\text{mb}}^{\text{peak}}$ (K)	$T_{\text{mb}}^{\text{total}}$ (K)	M_{core} (M_{\odot})	$M_{\text{vir}}/M_{\text{core}}$	\bar{n} (10^4 cm^{-3})	\bar{T}_{ex} (K)	$\bar{N}_{\text{C}^{18}\text{O}}$ (10^{15} cm^{-2})	$\bar{X}_{\text{C}^{18}\text{O}}$ (10^{-7})
393	1.3	46.2	0.2	0.3	0.5	22.6	0.8	4.5
394	1.6	70.8	0.3	0.4	0.5	39.0	2.8	5.2
395	1.7	154.7	0.3	0.8	0.2	31.5	2.8	11.5
396	1.7	104.7	0.3	1.4	1.0	54.1	3.3	4.7
397	2.6	168.6	0.4	0.6	0.7	27.7	3.4	4.0
398	1.6	64.3	0.3	0.3	0.7	54.3	2.3	4.9
399	2.8	334.2	0.5	0.4	0.3	27.9	5.3	5.2
400	2.2	79.7	0.1	1.2	0.3	34.7	4.8	11.7
401	3.4	345.4	0.6	0.5	0.6	30.0	7.4	4.9
402	4.8	571.8	1.0	0.3	2.3	50.8	12.6	7.1
403	1.8	327.7	0.7	0.6	0.3	26.9	3.2	4.1
404	1.9	187.0	0.5	0.4	0.4	48.9	1.9	3.2
405	4.7	560.4	0.8	0.3	0.6	34.3	4.8	6.2
406	1.5	166.3	1.0	0.2	0.4	35.8	2.0	9.2
407	3.4	450.1	0.7	0.3	0.5	29.4	7.5	5.3
408	1.5	179.8	0.7	0.6	0.3	19.8	0.9	6.6
409	2.8	137.5	0.3	0.2	1.1	29.8	3.5	4.7
410	2.9	204.3	0.3	0.9	0.9	54.4	8.1	9.8
411	3.7	529.9	1.0	0.2	0.8	38.3	5.0	6.5
412	2.1	156.1	0.5	0.3	0.6	33.5	1.4	3.7
413	3.8	318.2	0.4	0.3	1.0	39.1	5.1	7.3
414	1.7	201.9	0.6	0.5	0.5	23.6	1.9	5.9
415	1.8	115.5	0.2	2.1	0.2	38.3	2.2	10.0
416	2.2	203.7	0.4	0.8	0.3	25.1	4.6	4.2
417	2.1	128.2	0.4	1.0	1.3	49.0	4.3	4.0
418	2.4	821.7	1.9	0.4	0.5	32.9	6.5	4.1
419	1.9	118.9	0.3	0.3	0.5	32.3	2.0	9.4
420	3.1	167.7	0.3	0.2	1.4	39.9	8.7	5.8
421	2.6	305.6	0.6	0.5	0.4	33.0	7.9	4.9
422	1.6	68.7	0.2	0.3	0.5	34.9	3.6	4.9
423	1.7	152.6	0.4	1.6	0.5	49.5	3.0	5.9
424	3.0	297.8	0.6	0.4	0.5	25.6	4.6	4.2
425	1.9	171.0	0.4	0.9	0.2	35.9	2.0	9.2
426	2.5	242.0	0.8	0.2	0.7	36.3	3.9	6.3
427	1.9	72.5	0.2	0.5	0.4	53.8	7.9	6.1
428	1.9	167.5	0.5	0.4	0.6	36.0	4.3	6.3
429	3.1	513.8	1.2	0.2	0.7	33.1	6.4	4.3
430	2.9	559.0	1.6	0.8	1.1	53.6	5.8	4.9
431	3.1	482.5	0.6	0.4	0.2	31.1	3.0	7.4
432	1.9	83.8	0.3	0.2	0.5	49.3	4.3	4.3
433	1.7	158.8	0.2	1.8	0.2	31.7	2.5	10.2
434	1.9	73.4	0.1	0.7	0.4	34.0	2.5	10.8
435	2.4	146.4	0.3	0.5	0.5	48.0	4.1	8.1
436	4.6	1064.3	2.4	0.3	1.2	29.2	6.7	3.8
437	1.7	118.8	0.6	0.1	0.6	44.4	2.2	4.9
438	2.5	258.1	0.3	2.2	0.3	27.9	1.6	6.7
439	1.5	79.9	0.3	0.3	0.4	29.5	1.4	7.1
440	1.6	187.2	0.6	0.3	0.3	23.1	1.3	6.5
441	2.0	121.8	0.4	0.6	0.7	30.9	4.2	4.4

Table 4: Continued

ID	$T_{\text{mb}}^{\text{peak}}$ (K)	$T_{\text{mb}}^{\text{total}}$ (K)	M_{core} (M_{\odot})	$M_{\text{vir}}/M_{\text{core}}$	\bar{n} (10^4 cm^{-3})	\bar{T}_{ex} (K)	$\bar{N}_{\text{C}^{18}\text{O}}$ (10^{15} cm^{-2})	$\bar{X}_{\text{C}^{18}\text{O}}$ (10^{-7})
442	2.2	222.4	0.4	0.9	0.6	32.1	2.6	6.2
443	2.2	471.8	1.3	0.8	0.8	46.4	4.3	6.6
444	2.5	360.1	0.9	0.2	0.6	34.1	3.8	5.7
445	5.5	4741.7	5.1	0.3	0.4	30.8	5.4	8.5
446	2.2	112.2	0.5	0.4	1.6	58.6	5.1	5.6
447	2.2	468.2	0.8	0.4	0.3	33.5	3.1	8.2
448	2.6	1205.8	1.7	0.5	0.2	35.2	5.9	7.0
449	1.6	64.6	0.1	0.3	0.2	25.8	2.1	9.5
450	2.6	134.9	0.1	0.7	0.3	38.0	5.0	12.3
451	4.2	346.0	0.5	0.2	0.8	33.8	5.1	6.2
452	1.6	74.8	0.6	0.2	1.1	44.3	3.0	4.9
453	1.7	76.3	0.4	0.3	0.6	18.2	0.7	4.7
454	4.0	925.6	1.7	0.3	1.0	30.5	6.7	4.4
455	1.5	124.7	0.2	0.8	0.2	20.2	0.9	4.9
456	1.4	51.9	0.5	0.1	1.0	49.5	2.7	6.2
457	1.4	72.0	0.4	0.4	0.7	22.6	0.7	3.2
458	1.6	108.0	0.9	0.2	1.1	46.0	2.5	4.5
459	2.1	329.5	0.8	0.8	0.5	49.4	5.3	7.2
460	1.9	251.0	0.7	0.5	0.6	37.8	3.0	6.6
461	1.5	274.6	0.8	1.5	0.3	49.1	4.4	7.1
462	3.2	284.8	0.4	0.3	0.4	29.9	2.6	6.5
463	1.8	56.0	0.1	0.8	0.3	30.7	2.0	5.2
464	2.9	134.6	0.3	0.1	0.8	26.9	2.3	3.6
465	4.8	3143.7	4.5	0.1	0.5	32.4	5.9	7.6
466	1.9	137.7	0.7	0.8	0.7	21.6	1.2	4.6
467	3.6	2124.0	6.6	0.3	0.7	41.9	3.0	4.4
468	3.1	457.3	0.6	0.5	0.2	33.2	6.7	8.0
469	5.1	1074.2	1.2	0.3	0.7	35.9	8.1	9.1
470	3.9	394.5	1.0	0.4	1.1	34.4	6.3	4.1
471	1.5	98.4	0.5	0.3	0.6	37.4	1.5	4.8
472	1.6	79.3	0.3	0.7	0.3	27.5	2.1	4.2
473	1.5	429.5	0.7	0.7	0.1	31.4	3.4	6.5
474	1.5	71.2	0.1	3.7	0.1	32.9	5.1	9.6
475	2.4	244.3	0.4	0.8	0.4	33.7	3.5	8.8
476	1.6	55.3	0.1	2.2	0.1	32.4	4.7	9.5
477	3.5	499.9	0.8	0.7	0.6	38.0	7.4	7.5
478	1.7	139.3	0.4	1.6	0.4	27.5	1.8	4.7
479	2.9	6553.0	22.6	0.1	0.3	46.4	2.8	5.5
480	1.4	55.4	0.1	0.9	0.2	33.4	3.7	9.2
481	1.6	99.0	0.2	3.2	0.1	20.8	1.0	3.7
482	1.5	74.3	1.1	0.1	1.2	42.6	0.9	2.1
483	1.7	145.9	0.3	0.3	0.2	31.1	2.2	7.6
484	1.6	105.5	1.1	0.4	0.9	42.9	1.7	5.7
485	4.6	1476.5	1.7	0.4	0.4	32.2	6.1	7.8
486	1.8	301.8	0.9	0.7	0.4	27.3	1.1	3.5
487	4.1	475.5	0.6	0.2	0.6	32.4	7.3	7.0
488	1.9	402.0	0.6	0.7	0.2	37.1	4.7	9.4
489	4.0	266.9	0.2	0.4	0.6	35.7	7.3	10.3
490	1.5	45.3	0.1	0.5	0.7	45.8	3.0	7.6

Table 4: Continued

ID	$T_{\text{mb}}^{\text{peak}}$ (K)	$T_{\text{mb}}^{\text{total}}$ (K)	M_{core} (M_{\odot})	$M_{\text{vir}}/M_{\text{core}}$	\bar{n} (10^4 cm^{-3})	\bar{T}_{ex} (K)	$\bar{N}_{\text{C}^{18}\text{O}}$ (10^{15} cm^{-2})	$\bar{X}_{\text{C}^{18}\text{O}}$ (10^{-7})
491	1.5	102.1	0.2	2.0	0.3	33.0	3.6	10.9
492	2.8	479.7	0.5	0.4	0.2	32.3	4.3	8.4
493	1.7	114.4	0.2	0.5	0.2	32.1	4.1	9.0
494	2.5	221.9	0.2	0.9	0.2	32.8	4.3	9.0
495	1.5	145.8	0.6	0.5	0.4	48.1	3.1	9.0
496	1.8	67.6	0.4	0.2	0.7	30.1	1.2	4.1
497	1.6	58.9	0.2	0.3	0.6	31.1	1.2	4.2
498	1.5	170.7	1.2	0.4	0.7	45.5	2.3	5.7
499	1.8	69.6	0.1	1.0	0.3	35.7	3.7	8.6
500	2.7	529.2	0.6	0.7	0.2	36.0	4.6	10.3
501	4.6	522.4	0.5	0.3	0.5	37.5	8.7	9.8
502	3.4	748.7	1.0	0.7	0.6	34.4	6.5	6.2
503	1.8	119.3	0.1	2.5	0.2	31.7	4.7	9.5
504	1.4	89.4	0.7	0.2	0.6	28.7	1.2	4.6
505	1.5	98.2	0.7	0.5	0.8	38.9	1.7	6.2
506	4.0	253.8	0.3	0.5	1.1	32.1	6.5	5.8
507	2.1	63.1	0.1	1.1	0.2	35.9	7.8	7.8
508	2.2	234.3	0.2	2.2	0.2	34.2	7.2	12.4
509	1.6	558.1	2.8	1.6	0.5	38.1	1.8	4.0
510	1.6	136.3	0.2	0.5	0.1	30.5	5.2	8.6
511	1.7	84.1	0.2	0.5	0.3	31.3	3.2	8.5
512	1.6	401.9	2.2	0.6	0.5	39.6	0.7	2.5
513	1.4	43.8	0.1	1.0	0.2	31.2	4.4	5.6
514	2.7	396.7	0.4	0.7	0.2	30.4	4.8	9.3
515	4.4	1311.4	1.7	0.1	0.4	30.9	5.5	6.7
516	1.8	88.1	0.2	0.7	0.4	32.6	2.0	5.3
517	2.2	179.2	0.3	0.5	0.3	34.9	3.2	6.6
518	1.6	181.1	0.3	1.6	0.2	30.7	3.4	8.6
519	1.9	185.6	0.7	0.2	0.8	39.9	2.0	4.6
520	2.7	748.7	0.9	0.4	0.3	34.9	4.1	9.1
521	2.9	229.7	0.5	0.2	0.7	34.1	2.0	4.4
522	4.7	2500.5	4.1	0.4	0.5	33.1	6.7	5.3
523	1.9	293.3	0.5	1.1	0.3	35.0	4.5	7.7
524	3.3	164.9	0.2	0.4	0.5	33.7	7.1	8.9
525	1.8	93.1	0.2	0.6	0.3	30.7	3.2	8.0
526	1.7	136.6	0.2	1.2	0.1	29.3	3.8	8.9
527	1.9	143.6	0.3	1.7	0.4	31.8	3.2	7.9
528	1.6	58.6	0.1	0.6	0.2	33.2	4.6	9.0
529	3.8	391.4	0.5	0.3	0.6	30.1	6.7	5.8
530	1.6	83.7	0.1	3.2	0.2	39.1	6.1	13.2
531	1.7	259.2	1.4	0.4	0.6	36.8	0.7	1.6
532	2.2	233.1	0.2	0.7	0.2	39.3	6.1	13.0
533	1.6	68.4	0.1	1.3	0.3	32.7	2.6	7.7
534	1.5	110.4	0.8	0.5	1.0	32.7	0.8	3.2
535	2.3	126.5	0.4	1.3	0.7	35.5	2.0	4.9
536	1.6	85.7	0.5	1.1	1.1	36.6	1.9	4.3
537	2.0	879.9	4.8	0.5	0.8	44.4	2.9	5.6
538	3.7	1951.3	2.5	0.2	0.3	33.2	5.1	7.3
539	1.5	187.4	0.8	0.6	0.6	44.8	2.6	6.3

Table 4: Continued

ID	$T_{\text{mb}}^{\text{peak}}$ (K)	$T_{\text{mb}}^{\text{total}}$ (K)	M_{core} (M_{\odot})	$M_{\text{vir}}/M_{\text{core}}$	\bar{n} (10^4 cm^{-3})	\bar{T}_{ex} (K)	$\bar{N}_{\text{C}^{18}\text{O}}$ (10^{15} cm^{-2})	$\bar{X}_{\text{C}^{18}\text{O}}$ (10^{-7})
540	3.1	1360.0	1.9	1.0	0.3	36.7	5.7	8.6
541	1.6	144.2	0.1	1.5	0.1	39.0	7.0	12.2
542	1.4	64.5	0.2	0.4	0.4	27.3	2.0	5.3
543	1.7	226.3	0.6	0.4	0.3	38.5	3.2	6.0
544	4.1	312.8	0.4	0.2	0.6	32.1	11.1	6.5
545	1.5	69.2	0.1	2.0	0.1	33.5	5.5	12.9
546	3.2	863.6	0.8	0.6	0.3	31.3	5.5	10.4
547	4.4	558.1	0.7	0.2	0.7	30.8	10.8	6.3
548	5.5	2515.7	4.2	0.1	0.7	27.7	8.4	4.6
549	1.4	67.4	0.1	0.7	0.2	26.5	4.1	9.7
550	1.7	224.2	0.8	1.4	0.5	20.3	0.8	3.3
551	2.6	175.4	0.2	0.3	0.3	35.1	3.5	6.8
552	4.3	692.0	0.9	0.4	0.8	27.5	8.3	5.7
553	4.3	1604.1	2.4	0.3	0.5	33.4	3.8	6.7
554	3.4	211.6	0.3	0.2	0.8	28.5	5.3	5.6
555	2.4	210.0	0.3	0.9	0.5	30.8	4.4	7.5
556	1.7	40.3	0.0	1.1	0.3	32.6	4.3	8.7
557	1.9	435.7	0.7	1.4	0.2	34.2	4.6	6.7
558	2.3	201.8	0.3	0.6	0.4	32.8	3.8	6.9
559	4.0	998.3	2.2	0.2	0.6	22.8	5.7	3.3
560	2.3	288.7	0.3	1.3	0.4	32.1	3.8	7.8
561	2.8	293.4	0.4	0.9	0.3	30.5	3.4	7.7
562	1.7	62.5	0.1	0.7	0.4	25.3	2.4	4.8
563	1.5	62.4	0.3	0.5	0.7	34.6	1.7	8.6
564	4.4	315.1	0.6	0.2	1.3	27.9	10.7	4.7
565	2.7	120.4	0.3	0.6	0.8	21.9	5.7	2.9
566	3.1	221.5	0.3	0.3	0.5	23.9	5.4	5.9
567	1.4	85.2	0.3	0.6	0.4	13.2	0.4	3.5
568	2.6	160.9	0.2	0.3	0.5	26.3	3.4	6.3
569	3.6	1305.5	1.7	0.3	0.4	24.7	4.7	6.0
570	4.7	509.1	1.0	0.1	1.3	37.2	10.0	5.0
571	1.5	63.6	0.1	0.9	0.2	32.4	6.5	5.8
572	2.3	216.4	0.4	0.6	0.4	26.1	2.7	5.3
573	3.1	430.7	0.7	0.7	0.5	23.7	2.9	4.0
574	2.9	277.8	0.4	0.5	0.3	36.5	3.5	10.6
575	3.1	282.4	0.5	0.2	0.7	25.4	3.3	4.7
576	5.2	1290.4	4.7	0.1	3.8	27.2	9.4	2.3
577	5.1	906.9	3.2	0.1	1.9	32.6	3.5	2.7
578	2.6	188.9	0.4	0.3	1.2	26.5	6.8	3.5
579	2.2	491.0	1.1	0.4	0.3	27.6	3.9	5.2
580	1.7	238.5	0.4	1.1	0.2	31.8	7.0	6.7
581	2.1	190.8	0.4	1.0	0.4	32.3	1.7	5.4
582	6.7	20067.2	42.0	0.1	1.1	29.9	11.8	4.8
583	4.9	913.5	2.6	0.2	2.3	32.8	9.1	3.3
584	2.2	394.2	0.9	1.5	0.5	27.0	6.7	3.5
585	5.2	1981.4	4.2	0.3	1.2	29.3	8.2	4.6
586	2.1	279.0	0.6	0.4	0.5	36.5	3.0	6.7
587	4.5	566.9	0.7	0.7	0.5	35.1	5.1	8.4
588	3.8	518.2	0.7	0.4	0.5	34.3	5.1	8.4

Table 4: Continued

ID	$T_{\text{mb}}^{\text{peak}}$ (K)	$T_{\text{mb}}^{\text{total}}$ (K)	M_{core} (M_{\odot})	$M_{\text{vir}}/M_{\text{core}}$	\bar{n} (10^4 cm^{-3})	\bar{T}_{ex} (K)	$\bar{N}_{\text{C}^{18}\text{O}}$ (10^{15} cm^{-2})	$\bar{X}_{\text{C}^{18}\text{O}}$ (10^{-7})
589	1.5	56.6	0.1	0.8	0.2	31.0	6.8	5.9
590	2.0	157.6	0.2	1.1	0.5	32.1	9.7	5.9
591	2.5	356.8	0.6	0.4	0.3	28.4	6.5	5.6
592	2.5	112.0	0.1	0.6	0.4	26.5	2.8	7.8
593	2.0	80.9	0.1	0.5	0.7	25.6	7.3	4.1
594	3.2	192.2	0.3	0.3	1.1	23.1	4.9	5.3
595	2.1	315.4	0.4	2.3	0.1	34.0	4.0	9.4
596	1.8	118.0	0.2	0.4	0.3	33.6	3.7	7.4
597	3.3	211.3	0.3	0.3	0.8	29.5	6.2	5.9
598	3.2	148.2	0.2	0.4	0.6	25.2	5.6	5.0
599	4.9	449.9	1.0	0.1	1.7	29.5	7.6	3.6
600	1.6	59.0	0.1	0.8	0.3	31.8	2.9	6.3
601	7.0	2400.6	6.4	0.1	1.4	31.7	6.6	3.7
602	1.6	159.0	0.5	0.2	0.2	24.7	1.1	5.5
603	1.5	114.8	0.4	0.6	0.5	25.5	1.2	5.5
604	2.4	175.7	0.3	0.7	0.5	34.6	3.5	6.3
605	4.2	374.8	0.8	0.1	1.2	26.8	8.9	3.5
606	3.6	433.3	0.5	0.2	0.5	28.1	7.3	6.8
607	2.8	486.2	0.7	1.2	0.4	28.6	5.6	6.3
608	2.0	74.1	0.1	1.1	0.2	27.2	8.5	8.1
609	1.7	69.7	0.1	0.6	0.3	24.9	4.1	5.9
610	3.2	543.8	0.6	0.4	0.4	29.8	4.5	6.0
611	5.6	1241.1	1.8	0.2	0.8	29.9	3.9	5.3
612	1.4	129.1	0.3	0.6	0.3	24.3	3.2	4.6
613	3.2	1059.4	3.0	0.1	0.6	31.5	3.1	3.9
614	2.0	87.1	0.2	0.3	0.8	31.0	2.4	5.6
615	2.1	128.7	0.3	0.4	0.5	31.1	2.6	6.3
616	1.4	56.0	0.2	0.5	0.5	29.5	2.6	4.0
617	3.1	281.4	0.6	0.2	0.5	32.8	2.1	4.1
618	3.7	327.8	0.5	0.1	0.7	29.2	4.8	6.3
619	1.7	121.6	0.4	0.7	0.6	26.9	1.5	3.6
620	4.9	429.7	1.2	0.2	2.3	38.0	5.3	3.0
621	1.4	64.0	0.4	0.2	0.6	23.8	1.0	3.3
622	2.6	308.8	0.7	0.3	0.5	32.1	3.0	3.9
623	1.5	94.6	0.3	0.5	0.4	29.1	2.3	6.2
624	1.5	108.8	0.4	0.8	0.3	22.8	0.8	3.4
625	5.7	3572.1	4.6	0.2	0.6	29.5	6.3	6.2
626	1.4	76.2	0.1	1.5	0.2	27.5	2.4	7.3
627	1.4	43.8	0.1	0.8	0.3	25.4	2.1	7.0
628	1.8	61.6	0.1	0.7	0.4	31.9	2.9	6.7
629	3.1	1693.2	2.2	0.2	0.1	29.8	5.3	6.3
630	2.8	99.1	0.2	0.4	0.8	25.6	4.3	4.5
631	3.7	146.5	0.8	0.1	3.4	27.3	7.5	1.5
632	3.7	897.1	1.5	0.2	0.4	25.9	4.5	4.8
633	2.3	184.9	0.3	0.4	0.4	33.5	3.1	6.8
634	2.7	132.9	0.3	0.4	0.7	29.0	4.3	5.8
635	1.4	98.8	0.3	0.4	0.3	23.5	1.5	5.2
636	1.9	74.2	0.3	0.1	0.5	23.7	0.8	3.2
637	1.9	140.2	0.3	0.2	0.3	25.4	2.2	7.5

Table 4: Continued

ID	$T_{\text{mb}}^{\text{peak}}$ (K)	$T_{\text{mb}}^{\text{total}}$ (K)	M_{core} (M_{\odot})	$M_{\text{vir}}/M_{\text{core}}$	\bar{n} (10^4 cm^{-3})	\bar{T}_{ex} (K)	$\bar{N}_{\text{C}^{18}\text{O}}$ (10^{15} cm^{-2})	$\bar{X}_{\text{C}^{18}\text{O}}$ (10^{-7})
638	3.3	442.3	0.7	0.4	0.7	27.5	5.7	5.7
639	1.8	70.2	0.1	0.8	0.2	25.3	5.3	4.5
640	1.9	126.7	0.3	0.6	0.6	34.6	2.1	6.0
641	2.4	340.7	0.8	0.9	0.4	30.2	2.0	5.5
642	3.3	350.1	0.4	0.3	0.6	25.4	3.3	7.1
643	2.4	172.4	0.2	1.9	0.6	24.9	4.0	5.8
644	3.5	178.5	0.3	0.2	1.5	23.4	4.3	3.6
645	4.9	1043.8	1.7	0.1	0.6	29.8	4.3	5.0
646	2.0	350.3	0.5	0.9	0.1	24.1	3.5	5.0
647	1.8	590.3	0.9	1.5	0.1	31.6	3.9	6.5
648	3.8	467.3	0.8	0.4	0.7	25.0	4.2	5.1
649	3.0	306.4	0.5	0.7	0.5	29.0	5.4	4.9
650	5.0	774.0	0.9	0.3	1.0	28.7	5.7	5.5
651	3.3	527.1	1.0	0.5	0.4	25.8	3.2	5.4
652	3.6	405.6	0.6	0.4	1.0	25.6	4.8	4.5
653	2.0	535.2	0.8	0.5	0.1	26.4	3.8	5.2
654	2.0	412.7	0.6	1.2	0.1	27.6	4.5	5.2
655	4.0	1174.2	2.6	0.3	0.8	26.4	7.0	3.3
656	1.7	156.0	0.3	2.8	0.2	27.2	5.4	4.5
657	1.6	80.5	0.1	0.9	0.2	25.4	3.8	5.8
658	1.5	74.5	0.2	0.3	0.3	28.5	2.9	5.7
659	3.7	622.2	1.1	0.2	0.7	22.9	4.2	4.5
660	1.4	127.8	0.6	0.7	0.4	19.1	0.6	4.3
661	3.3	251.3	0.4	0.2	0.6	29.0	5.2	4.9
662	2.6	272.4	0.4	0.6	0.4	26.0	1.5	5.2
663	4.0	826.2	1.8	0.3	0.8	26.1	7.2	3.4
664	1.9	199.1	0.3	1.2	0.4	26.5	1.7	6.3
665	2.1	602.2	1.2	0.5	0.3	25.1	3.6	4.8
666	2.2	149.9	0.2	0.9	0.3	25.6	4.0	6.2
667	1.8	209.9	0.3	0.8	0.2	23.7	3.3	5.7
668	1.9	302.9	0.6	1.6	0.3	26.6	3.7	6.2
669	2.6	263.7	0.6	0.6	0.8	25.5	4.0	4.4
670	2.4	144.9	0.3	0.3	0.5	24.7	2.3	4.4
671	2.0	57.8	0.1	0.7	0.7	25.0	3.9	4.4
672	2.3	319.9	0.9	0.2	0.4	24.3	3.2	3.9
673	2.4	374.2	1.1	0.2	0.6	23.5	1.9	2.7
674	1.4	61.8	0.1	1.3	0.3	25.3	3.9	3.5
675	1.5	59.3	0.1	0.9	0.3	23.0	1.8	5.9
676	2.1	123.0	0.3	0.4	0.5	23.7	2.4	6.0
677	1.5	85.8	0.3	0.6	0.3	25.3	1.1	3.6
678	2.1	132.4	0.4	0.7	0.8	23.4	2.7	2.5
679	2.1	207.5	0.6	0.4	0.4	23.3	1.6	3.3
680	1.4	90.2	0.4	0.2	0.6	22.6	1.5	2.5
681	1.4	42.7	0.1	1.1	0.3	21.1	0.7	2.2
682	3.0	236.7	0.7	0.4	0.8	22.3	3.2	2.4
683	2.3	488.4	1.6	0.3	0.5	24.1	1.5	2.5
684	3.3	484.2	1.9	0.1	2.7	22.2	4.3	1.6
685	1.5	91.6	0.3	1.1	0.4	25.5	1.4	2.3
686	3.7	595.7	1.5	0.2	1.1	25.4	4.9	2.8

Table 4: Continued

ID	$T_{\text{mb}}^{\text{peak}}$ (K)	$T_{\text{mb}}^{\text{total}}$ (K)	M_{core} (M_{\odot})	$M_{\text{vir}}/M_{\text{core}}$	\bar{n} (10^4 cm^{-3})	\bar{T}_{ex} (K)	$\bar{N}_{\text{C}^{18}\text{O}}$ (10^{15} cm^{-2})	$\bar{X}_{\text{C}^{18}\text{O}}$ (10^{-7})
687	1.6	79.1	0.2	0.2	0.3	20.8	2.3	2.5
688	1.7	285.5	0.9	1.6	0.4	20.9	0.8	2.3
689	1.5	136.3	0.8	0.3	0.6	20.9	1.2	4.4
690	1.4	53.0	0.1	1.1	0.3	24.7	2.6	4.4
691	1.7	222.4	0.9	0.8	0.7	20.8	0.6	1.6
692	3.5	232.6	0.6	0.2	1.2	24.4	4.0	2.6
693	2.0	109.3	1.0	0.1	1.1	21.4	1.6	4.0
694	1.4	66.3	0.4	0.4	0.6	20.1	1.7	1.8
695	1.8	160.0	1.4	0.5	0.9	21.2	1.1	2.8
696	1.4	180.8	2.6	0.1	1.0	22.1	0.9	2.1
697	2.2	447.2	1.0	0.7	0.4	21.1	1.9	3.7
698	3.3	326.1	0.9	0.3	1.3	23.4	3.8	3.2
699	1.8	140.8	0.3	1.0	0.3	19.5	2.0	2.7
700	1.8	118.9	0.8	0.2	1.0	22.2	1.2	2.8
701	3.1	198.2	0.6	0.3	1.3	21.9	2.3	3.1
702	1.5	68.5	0.6	0.2	1.2	25.5	1.0	2.3
703	4.0	418.4	0.9	0.2	1.1	20.0	3.7	3.5
704	1.6	188.8	1.0	0.6	0.6	21.8	1.3	3.1
705	2.2	121.7	0.4	0.3	0.8	20.3	2.3	3.3
706	1.6	52.7	0.2	0.3	0.7	22.3	1.8	3.5
707	1.7	392.5	2.5	0.3	0.6	21.4	1.0	2.5
708	1.7	45.6	0.1	0.5	0.8	16.6	0.8	3.7
709	1.4	104.0	0.6	0.3	0.6	18.2	0.3	1.7
710	1.7	168.2	0.7	0.9	0.5	21.4	2.3	3.8
711	1.6	89.2	0.3	0.4	0.4	21.1	2.5	4.1
712	1.5	107.0	0.7	0.2	0.5	19.9	1.0	3.2
713	1.9	269.8	0.8	0.9	0.4	21.9	2.1	3.0
714	2.2	204.6	0.7	0.3	0.5	20.6	1.5	2.9
715	1.5	120.7	0.6	0.4	0.5	20.6	1.0	2.1
716	1.7	80.3	0.4	1.0	0.5	20.4	1.4	4.6
717	3.8	417.3	0.9	0.1	1.2	20.6	1.9	2.4
718	1.9	90.0	0.4	0.2	1.0	22.9	1.2	1.9
719	2.2	136.4	0.4	0.2	0.7	21.9	1.4	2.5
720	1.7	133.8	0.6	0.1	0.5	20.6	1.5	2.6
721	1.9	152.1	0.5	0.2	0.5	22.2	1.3	2.2
722	1.4	75.5	0.4	0.8	0.6	18.8	0.8	1.6
723	1.4	245.4	1.3	1.4	0.5	20.2	1.3	1.7
724	2.2	233.9	0.8	0.5	0.5	25.1	1.1	2.5
725	2.8	612.3	2.6	0.3	0.7	21.0	1.5	2.1
726	1.8	190.6	0.8	0.4	0.4	22.9	0.8	2.1
727	2.3	495.1	1.6	0.5	0.6	20.4	0.9	1.5
728	1.7	112.7	0.7	0.3	0.6	26.0	0.8	2.4
729	1.8	157.5	1.0	0.3	0.5	22.0	1.4	2.8
730	1.8	133.5	0.6	0.2	0.6	20.1	1.0	2.2
731	1.8	106.7	0.4	1.0	0.6	21.2	1.8	3.7
732	1.8	209.5	1.1	0.5	0.7	20.6	1.2	2.4
733	1.8	476.4	2.6	0.4	0.6	20.1	1.2	2.5
734	2.2	110.5	0.5	0.2	1.3	21.1	2.2	2.4
735	1.8	117.8	0.6	0.2	0.8	21.4	1.6	3.0

Table 4: Continued

ID	$T_{\text{mb}}^{\text{peak}}$ (K)	$T_{\text{mb}}^{\text{total}}$ (K)	M_{core} (M_{\odot})	$M_{\text{vir}}/M_{\text{core}}$	\bar{n} (10^4 cm^{-3})	\bar{T}_{ex} (K)	$\bar{N}_{\text{C}^{18}\text{O}}$ (10^{15} cm^{-2})	$\bar{X}_{\text{C}^{18}\text{O}}$ (10^{-7})
736	2.9	527.0	1.7	0.2	0.5	21.8	1.8	2.9
737	1.8	87.5	0.5	0.2	0.9	21.6	0.8	1.8
738	1.7	196.5	1.2	0.2	0.8	22.8	0.2	0.6
739	1.7	57.6	0.3	0.4	0.5	21.1	2.1	5.3
740	2.4	333.9	1.7	0.3	1.0	19.6	1.2	1.9
741	2.9	306.0	0.7	0.3	0.4	24.5	5.1	9.2
742	1.4	101.9	0.7	0.2	0.7	19.4	0.7	1.6
743	1.7	109.3	0.5	0.9	0.6	18.3	1.3	3.2
744	1.9	53.3	0.4	0.2	1.0	19.5	0.5	1.2
745	2.1	148.5	0.9	0.9	0.6	19.8	1.1	2.5
746	1.9	73.0	0.3	0.3	0.5	19.3	0.8	1.4